Antonio Montoro Marín

Nanotechnology-based wearable devices

Final degree thesis
Supervised by Beatriz Prieto Simón & Saeed Bahadorikhalili

Biomedical Engineering Degree

UNIVERSITAT ROVIRA I VIRGILI

Tarragona
2022

Index

1 Summary

The synthesis of biomaterials from porous nanostructured templates, has generated great interest especially for the creation of highly ordered polymeric structures for electronic, mechanical, optical and biochemical applications. In this project, macroporous silicon and porous alumina, two promising materials, will be tested as templates for the fabrication of polymeric nanostructures with the aim of serve as a biosensor able to provide continuous, non-invasive or minimally invasive measurements of key biomarkers in biofluids, such as sweat, tears, saliva, interstitial fluid or blood. For the theoretical part, first, an introduction of the monitoring of key biomarkers in biofluids and nanotechnology-based wearable devices is made. Then, the templated-assisted method is explained followed by the discussion on porous silicon and porous alumina to be used as templates, introducing their fabrication process, history and properties. Finally, the report ends up describing and comparing the polymeric replicas and polymers used. For the experimental part, the materials and equipment used are presented as well as the steps we have followed in the fabrication of the templates and replicas. Finally, the results obtained are presented in the form of scanning electron microscopy (SEM) images and conclusions are drawn.

2 Introduction

First of all, it is necessary to understand what a biomarker is. According to the National Institute of Environmental Health Sciences (NIH), a biomarker is an objective measure that captures what is happening in a cell or an organism at a given moment [1]. This compound, can be found in different body fluids, such as blood, saliva, urine or interstitial fluid. Biomarkers can vary from electrolytes (K^+), to metabolites (glucose), hormones (cortisol), proteins (cytokines) or oligonucleotides (microRNA) [2]. The presence, absence or variation of the concentration of a biomarker, can indicate a physiological disorder, state or risk factors in an organism. This variation of the biomarker can be related to various health conditions such as stress (cortisol) or diabetes (glucose), and this is the reason why the monitoring of a biomarker and therefore the advent of wearable devices capable of doing the above, is so important. The use of these biomarkers by scientists and epidemiologists for both clinical diagnosis and preclinical studies is not new. Currently, the studies related to the monitoring of biomarkers, must be done in dedicated laboratories with large and expensive equipment and qualified personnel. In addition to the above, biomarker analysis is also time consuming and some results may take longer than expected. For this reason, there is currently a high demand in this field for devices capable of providing efficient biomarker analysis in a fast, accurate and inexpensive manner. This is where wearable devices and biosensors come into play, in particular, the ones that are capturing more attention are devices based on micro- and nanotechnologies, since their potential to overcome the sensitivity, miniaturization and cost-effectiveness challenges is really promising. Nanomaterials also acquire great importance here, having shown promising results in different studies due to their unique physicochemical properties derived from their small size, such as their large surface area to volume ratio, thus allowing the immobilization of a large number of biomarkers and offering an increase in the sensitivity of the readout. They have also been shown to have exceptional optical properties, which have been put to practical use in studies related to fluorescence and surface-enhanced Raman scattering (SERS) biosensors. Some examples of the most researched and most interesting nanomaterials in biosensing we have, include metallic nanoparticles, silicon nanowires and carbon materials (nanotubes). Thanks also to the access of new strategies for miniaturization, the integration of transducers at a nano level is possible in biosensors, even if what is needed is a larger component (micro-, macro-), there is the possibility that this component can integrate surfaces or nanostructured materials within multi-scale platforms.

This feature, not only affects in a structural way, but also, at the level of the organism, brings the advantage of reducing the immune response against a foreign body, thus improving the biocompatibility of the biosensor.

2.1 Introduction to nanotechnology-based wearable devices and biosensors

Currently, there are a large number of wearable devices on the market, focused on monitoring different physiological parameters such as heart rate, hours of sleep or physical activity, among many others. But, if we refer to wearable devices capable of detecting parameters at a molecular level, we see that it is still at an early stage and all scientists involved in this field of research seem to agree that wearable biosensing devices are, without a doubt, the next potential frontier to be crossed in wearable technologies for the monitoring of individual and public health. Moreover, due to their good accessibility and affordability, they are proving to be a good alternative not only within a technical field such as personalized medicine from the point of view of patients and doctors, but also in healthy individuals [4]. At this point, we can see how advances in this type of technology are resulting in an approach towards a revolution in healthcare systems and medicine, making them increasingly proactive practices and involving both patients and physicians more and more. Having introduced the above, it is now time to explain the main function of these wearable devices. The purpose of these on-body monitoring devices is to detect and provide continuous information about different physiological parameters or the well-known biomarkers, which will provide us with information related to the patient's condition, from monitoring the evolution of a pathology, to the effectiveness and adherence of a treatment. As previously explained, every possible biomarker is related to a specific health condition, and for nearly every condition there is a method to detect this compound, the problem is that usually the methods are predominantly based on invasive body fluid analysis using standard laboratory techniques. Among these techniques, enzyme-linked immunosorbent assay (ELISA) as immunoassay, and polymerase chain reaction (PCR) as a molecular diagnostic tool, are considered gold standards and have been able to achieve accurate diagnosis in early stages of multiple diseases. Despite this, still exists the problem of time consumption and the need for specialized personnel capable of dealing with the sophisticated and bulky instruments required by the diagnostic method in question. This is why there is a need to replace these conventional devices with wearable devices capable of performing the same or even better functions, in a more efficient and sophisticated way. To achieve this, it is first necessary that these devices have highly selective and sensitive biosensors that can continuously monitor the variation in the levels of the selected biomarker. To achieve that, a typical biosensor integrates two basic functional units: a "bioreceptor" (an enzyme for example), which will be the responsible for the detection and recognition of the targeted analyte, and then a "transducer", which can be electrochemical (the most common and used), optical or mechanical, and will have the function to translate the previous biorecognition event into a useful and understandable signal [40]. As a consequence of this monitoring, a large amount of data will be generated which must be processed and analyzed efficiently to provide a baseline of the health status of the patient or even a population. The combination of biomedical data collection and analytical techniques, will enable individualized monitoring of developing health conditions, assistance to physicians to predict and prevent these health conditions, management of chronic diseases and guidance for therapeutic decisions.

2.2 Monitoring of key biomarkers in biofluids

To achieve global acceptance of the use of these wearable biosensors and to understand how they work in order to obtain adequate results, it is necessary to have a deep knowledge of the biochemical composition of the body fluids from which the biomarkers are intended to

be obtained, such as saliva, blood, sweat or tears. With the ability to continuously and in real time monitor biomarkers related to a user's health and performance, wearable monitoring platforms are able to provide information about biochemical processes dynamically in these biofluids. All this can be achieved in a non-invasive or minimally invasive way, avoiding the sometimes-painful traditional methods of blood sampling, for example, and aiding easy integration into the user's daily life. To achieve this, the wearable device must be in direct contact with the biofluid without causing any discomfort or adverse reaction to the user, making use of advanced materials and smart designs that can provide the necessary flexibility and versatility to the device. In the following, we will show different scenarios in which we can find a relevant application of wearable devices.

2.2.1 Skin wearable biosensors

2.2.1.1 Skin anatomy

The skin is the largest and most accessible organ available in the human body, and it is because of this that most wearable devices are designed to perform their function on the skin. Not only this, but it also coincides with the fact that the biofluids contained in the skin are a rich source of biomarkers. Despite this, the skin is a very complex organ and this is why a great deal of understanding is strictly necessary in order to make the most of these biomarkers. Anatomically, the skin serves as a protective organ of the inner tissue layers against external agents. It also prevents the loss of body fluids, helps regulate body temperature through sweating, serves as a sensory organ, and plays an important role in the production of antimicrobial peptides and vitamin D. It consists of three layers: epidermis, dermis, and hypodermis (Figure 1).

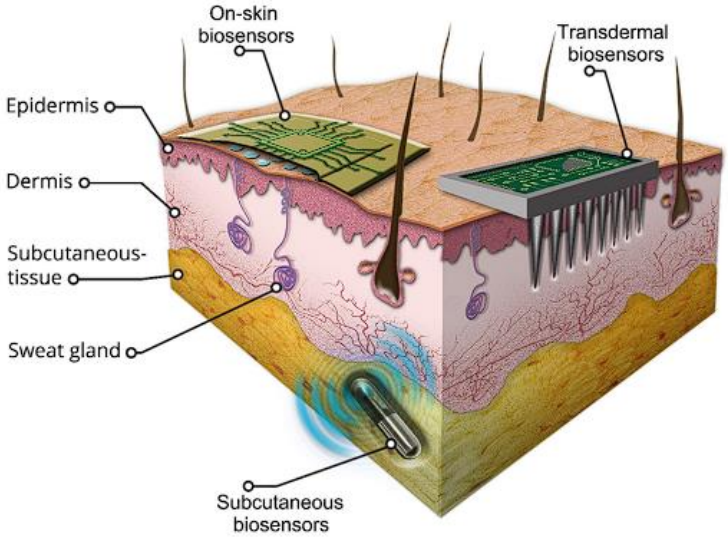

Figure 1: *Diagram of the different layers of the skin as well as some examples of biosensors [19].*

The epidermis, with a thickness of between 50 and 150 μm, is composed of a stratified epithelium that serves as a protective interface to the exterior. It also has several structures attached, such as sweat glands. Its outermost layer is called the stratum corneum (SC) and acts as a hydrophobic barrier to environmental pathogens. Below the epidermis, we find the dermis with a thickness between 500-2000 μm, which in turn, is formed by two distinct regions, one adjacent to the epidermis called the papillary region of the dermis and a lower region called the reticular dermis. The region between the dermis and the epidermis is called the dermoepidermal junction and is a porous membrane that serves as a space for the exchange of fluids and nutrients and as a reservoir for various molecules involved in wound healing. Finally, the deepest layer is called the hypodermis, and is the thickest layer of the skin. In the

space outside the parenchymal cells, blood and lymphatic vessels, we found what is called the interstitial space or interstitium, which is filled with one of the targeted biofluids options during biosensing, which is the interstitial fluid (ISF) [18,19].

2.2.1.2 Accessible fluids for wearable biosensing

Having seen the above, we have that the skin gives us access to three different biofluids: sweat, ISF and blood. Each of these biofluids has its own specific characteristics and components, but together they form a great basis for the detection of a wide and diverse range of biomarkers and biochemical information. In relation to blood, we have that is the most common sampled biofluid for clinical diagnosis and its proteome has been well studied during time. However, since blood only contributes to a 5 % of the skin volume in addition to the fact that the epidermis is an avascular skin region, we will need to reach the capillaries of the dermis, which is the highly vascularized region, along with a small amount of blood from arterioles and venules in an invasive manner for the collection and sampling of blood. In these blood vessels, we not only found blood, but also nutrients. Note that the distinction between capillary blood and systemic blood is very important, since it has been shown that the concentration of some components such as proteins and ions may vary.

Interstitial fluid is another source of biomarkers contributing 45% to the skin volume fraction versus 5% for blood. The ISF plays an important role in the transport of signaling molecules, nutrients and waste between cells, and also carrying antigens and cytokines for immune regulation [44]. Its composition is similar to plasma (93 % approximately) although there are important differences, such as the concentration of proteins which in ISF is lower than in plasma, but with glucose for example, the concentration is identical to the blood in steady-state conditions. These features make ISF an interesting biofluid for the detection of analytes. Nonetheless, there is a major problem, since traditionally the collection of ISF from the human body has been proved to be relatively difficult, and is therefore not the primary choice in most researches.

Finally, sweat is the easiest fluid to access from skin making it very convenient for wearable sensing. It is secreted by the eccrine glands upon stimulation by mainly acetylcholine neurotransmitter. Sweat plays an important role especially during the thermoregulation of the body and pH and electrolyte balance [41]. It also contains a wide range of chemical species including ions such as Ca^{2+}, released by the action of acetylcholine, Na^{+}, Cl^{-} and also metabolites, peptides, hormones (cortisol) and proteins among other important biomarkers useful for the diagnosis and health monitoring [42]. Thanks to this large number of biomarkers that can be found and their relatively easy accessibility, wearable devices and different non-invasive sweat monitoring methods with applications in the field of healthcare, have attracted a great deal of interest. However, in order to analyze this fluid, sweat must be excreted to the outermost part of the skin. The mechanisms of excretion can vary, from physical exercise, thermal heating or stress to chemical stimuli, and it is here where we must pay attention, since depending on the mechanism in which this sweat is excreted, its biochemical composition may vary [43].

As a summary, an illustrative table (Table 1) is attached showing the main biomarkers (ions, proteins, metabolites and hormones) that can be found in the different biofluids accessible through the skin. As an observation, low molecular weight biomarkers, such as ions, metabolites and hormones, are found in similar concentrations in both blood and ISF due to the rapid diffusion of these components through capillaries. However, for higher molecular weights, these capillaries do not act as diffusers but as filters.

Table 1: *Comparison of analytes' concentrations in blood, ISF and sweat [6].*

		Blood	ISF	Sweat
Ions	Na^+	135–145 mM*		10–90 mM [26,27]
	K^+*	3.5–5.5 mM*	Similar to	2–10 mM [27]
	Cl	95–110 mM*	plasma	14–48 mM [28]
	Ca^{2+}	>2.6 mM*		0.37 mM [29]
Metabolites	Glucose*	3.6-6.0 mM*		36-60 μM [32]
	Lactate	0.5–10 mM	Similar to	5.0–20 mM [33]
	Urea*	3.0–7.5 mM*	plasma	13–24 mM [34]
	Cholesterol*	<3.5 mM*		
	Uric acid	0.12-0.45 mM [30]		25-36 μM [34]
	Ascorbic acid	30-80 μM [31]		10-50 μM [35,36]
Hormones	Cortisol	Morning 193–773 nM [37] Afternoon 55–496.6 nM	Similar to plasma	20-500 nM [38]
Proteins	Cytokines	pM to nM	80 % of plasma	<0.1 % of plasma
	Antibodies e.g. IgA	0.4 –16 mg/mL ~262 mg/mL [39]	15-25 % of plasma	0.1–10 ng/mL [40]

* values obtained from Melbourne Pathology biochemical analysis test.

2.2.1.3 Exercise-based wearable sweat biosensors

Due to the elastic nature of the skin and in order to offer the greatest comfort to users during physical activities that require a high degree of mobility, the design of this type of device is based on the use of new biocompatible and stress-resistant materials and sensors. Skin tattoo type platforms are an example of this, through the use of screen-printed flexible electrodes, these devices are in continuous contact with the user's skin offering a comfortable biosensing alternative. In fact, recent studies have been able to demonstrate non-invasive real-time results of different key electrolytes, such as pH or sodium, heavy metals and metabolites present in sweat using these tattoo-based epidermal biosensors. More specifically, the study conducted by (J.W. et al.) [7] presented a proposal for monitoring lactate levels in sweat produced during physical activity in real time and in a non-invasive manner, using an electrochemical epidermal biosensor. Lactate is a compound secreted by local sweat gland metabolism and it is closely related to the physical activity, resulting in an increase of sweat lactate levels during prolonged exercise sessions. Although sweat lactate concentration is not directly related to blood concentration, it is still of interest as a marker of efficiency in athletes, as it indicates the level of physical exertion during exercise.

Another important advance involves the development of multiplexed sweat biosensor platforms with the objective of providing a quantitative analysis of sweat on the basis of a fully integrated patch-based wearable sensor array, as shown in Figure 2.a/2.b/2.c. Another example of this type of multiplexed wearable devices has achieved promising results by merging sweat glucose monitor devices with pH, humidity and temperature sensors in a single device (Figure 2.b).

Leaving electrochemical sensors aside, it is also worth to mention devices based on colorimetric signal transduction techniques, using different dyes for the recognition of analytes in sweat (Figure 2.d). Thanks to the nature of this technique, these devices do not require the sensor to be powered, which is an advantage when it comes to miniaturizing the wearable device, but in exchange for this, the use of extra devices is required in order to analyze this new type of data, such as cameras with color analysis software. In terms of operation, the device consists of a closed microfluidic system collector of sweat that allows the sampling of multiple biomarkers present in the biofluid. This microfluidic monitoring system has also been integrated in studies related to the measurement of fluorescence through a smartphone-based imaging module (Figure 2.e).

Finally, advances have also been made in the detection of biomarkers related to immune responses and hormones, such as the wearable immunosensor created to detect cortisol and interleukin-6 in sweat as a diagnostic method [5].

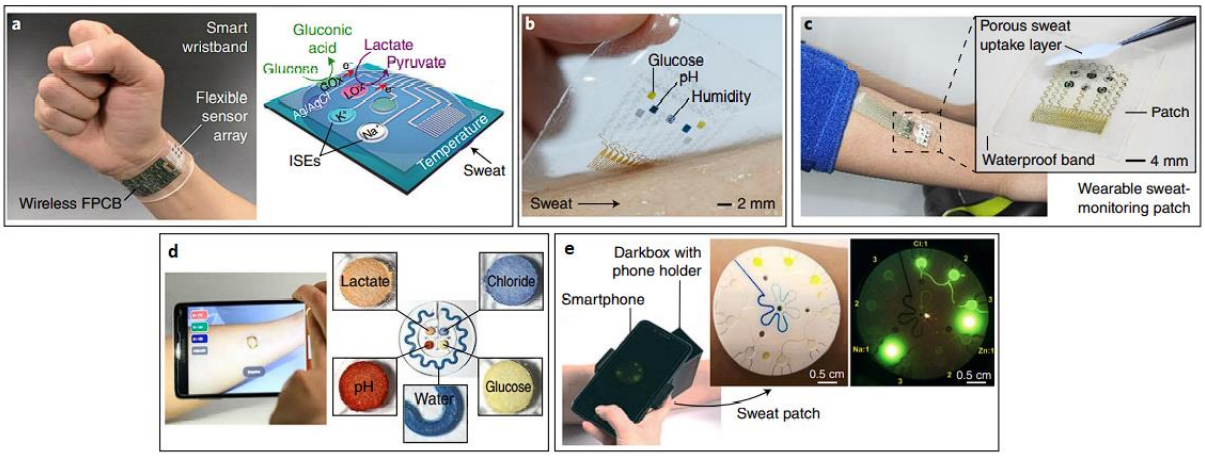

Figure 2: Some sweat biosensor examples. a, *Wearable sensor arrays for multiplexed perspiration analysis applied to wrist. On the right, schematic representation of the sensor [6][20].* ***b,*** *Multiplexed graphene-based sweat sensor array for diabetes monitoring [7].* ***c,*** *Multiplexed wearable sweat-based glucose sensor applied to human forearm during exercise [8].* ***d,*** *Colorimetric microfluidic sweat sampling device with smartphone-based signal analysis [9].* ***E,*** *Fluorometric skin-interfaced microfluidic platform for the detection of chloride, sodium and zinc in sweat [10].*

2.2.2 Ocular wearable biosensors

2.2.2.1 Secretion and composition of tears

Leaving aside the skin, another biofluid with relative potential for monitoring the physiological state of a patient, are tears. As might be expected, the study of biomarkers in tears provides vitally important information for diagnosing ocular diseases. The advantages that this biofluid can offer are generating interest in the field of healthcare and monitoring of physiological parameters. The main of these advantages is the great similarity of biomarkers with respect to blood because of its direct diffusion from this fluid. In addition, it is a much less complex biofluid than blood, so that the diagnosis of ocular diseases can be carried out in a simpler and more effective way.

Human tears, also known as lachrymal fluid, is a substance generated by the lacrimal glands as a protective layer on the surface of the eye allowing optimal functioning of the visual system. As with biofluids from the skin, tears possess potential biomarkers of both low and high molecular weights (proteins, lipids, peptides, electrolytes, ...). In particular, glucose concentration in tears is of interest due to its good correlation with its blood concentration, thanks to the diffusion process mentioned above from the lachrymal artery, on condition that the tear samples are taken without any ocular irritation or stimulation, as the presence of any of these states may alter the relationship [45]. However, not all are advantages, since the sampling of this biofluid presents a series of problems mainly related to the small volume of fluid that can be collected, its easy evaporation and the instability in the production of tears during the day depending on the individual [46]. The method of collection is also a major problem as it is a very sensitive part of the body and difficult to manipulate, so the concentration of biomarkers may vary depending on how the extraction is performed. This is why the accuracy and quality of the results are highly dependent on the collection method, the most commonly used being the Schirmer's strip and a glass capillary tube. Finally, as with sweat, depending on how these tears are generated, their biochemical composition varies, i.e., tears that form a protective layer in the eye, called basal tears, do not have the same characteristics as reflex tears generated from a chemical or mechanical stimulus. It is for this reason that both, present and future studies, should have as one of the main priorities the design of a wearable sensing platform that avoids eye irritation.

2.2.2.2 Tear-based wearable biosensors

There are different devices for tear collection and analysis. One of the most common, is the traditional contact lens fitted with the necessary biosensors, data processing and power supply, which in turn presents the challenge of integrating all these elements into a very sophisticated device. This solution is attractive because the lenses remain in continuous contact with the basal tears without causing any eye irritation, in addition to continuing to provide the necessary oxygenation of the eye enhancing the accuracy of continuous analyte monitoring. In the early days of these wearable devices, their operation was based on an optical measurement of glucose levels in tears. For glucose detection and following the example of contact lenses, at the same time also appeared holographic contact lenses that allowed the quantification of glucose in tears under physiological conditions. Later new contact lenses were developed based on the line of optical sensors, but this time involving the use of photonic crystal materials fused with responsive hydrogels.

Future developments related to the demonstration of electrochemical biosensing allowed to start introducing functional wireless readout chips and sophisticated new power supplies to wearable devices. As a result of these advances, one of the largest companies in the world, Google, in association with the pharmaceutical and biotechnology company Novartis, presented its prototype in the field of metabolite monitoring in the form of a miniature electrochemical transducer integrated with a wireless control chip and an antenna, applied on a soft contact lens platform with the glucose sensor embedded within a hydrogel matrix to non-invasively measure glucose in the surrounding tears (Figure 3.a). Thanks to the power and relevance of this partnership, the release of these devices to the market was believed to be closer and closer, however, since the appearance of this prototype, there have been several delays demonstrating once again the many challenges that still need to be overcome in this area in order to obtain a reliable and accurate platform.

Another development related to contact lenses, involves wireless ocular diagnostics, by combining glucose and ocular pressure contact lens sensor to integrate wireless in vivo glucose monitoring in the eye of a rabbit with in vitro monitoring of ocular pressure using a bovine eyeball (Figure 3.b).

Finally, and leaving aside the devices related to contact lenses, there is also an electrochemical sensor in the form of a spring (Figure 3.c) formed by multiple coiled wire electrodes coated with a protective hydrogel, designed to be implanted in the inferior conjunctival fornix where the biosensor will have constant access to lachrymal fluid, providing continuous tear glucose measurements without causing discomfort to the wearer.

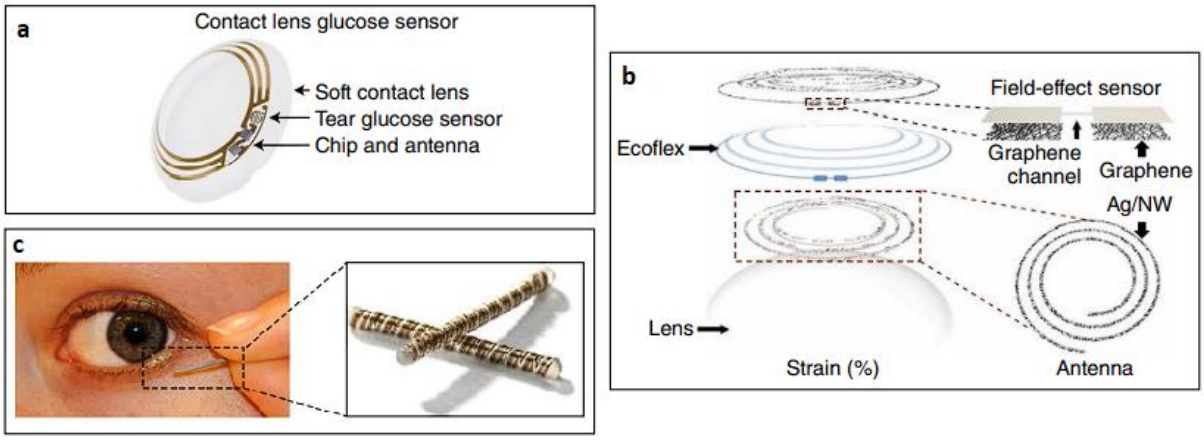

Figure 3: Some optical wearable biosensors examples. a, *Google and Novartis proposed prototype for the measurement of glucose using a contact lens sensor [12].* ***b,*** *Multifunctional wireless wearable smart sensor system incorporated onto a contact lens for monitoring both glucose in tears and intraocular pressure [13].* ***c,*** *NovioSense spring-like electrochemical tear glucose sensor [11].*

2.2.3 Oral-cavity wearable biosensors

2.2.3.1 Secretion and composition of saliva

Saliva as a sampling biofluid has gained relevance in recent years, because many of its biomarkers present come from the bloodstream, making it the "mirror of the human body", offering a non-invasive and cost-efficient view of a patient's health status as an alternative to blood tests. The high protein content in its composition makes it especially interesting in the detection of stress biomarkers and in the detection of diseases.

Saliva is a complex biofluid secreted by a combination of different glands such as the parotid gland, submandibular and sublingual glands, hundreds of minor salivary glands and gingival crevice fluid [21]. Its composition includes metabolites, hormones, ions, enzymes, microorganisms and proteins. Its main functions are to participate in the digestion process, forming the alimentary bolus, serving as lubrication, facilitating the perception of taste and finally acting as an immune aid through the secretion of antimicrobial peptides and immunoglobulins. In addition, since it is a fluid in constant regeneration, it is considered a very good "physiological snapshot", i.e., it is capable of providing instantaneous information on the health status of a patient at a given moment over a prolonged period of time. Although for many years the aforementioned saliva biomarkers have been used extensively in clinical settings, the current trend is towards the development of oral platforms of wearable devices that can benefit from the continuous flow of saliva in the oral cavity. The design of some of these platforms consists in the integration of the biosensor with all the electronic interface in oral devices such as mouthguards or denture-based systems.

2.2.3.2 Saliva-based wearable biosensors

We found the first wearable oral sensor in the 1960s, and consisted of a partial denture in charge of monitoring the chewing process and pH control. Obviously and due to the means available at the time, it was a very rudimentary system to the point of requiring the substitution of several teeth by the sensors.

Nowadays, thanks to technological advances in all scientific and technical fields and to recent studies that have shown good correlation between metabolite levels in saliva and blood, the attractiveness of oral cavity sensor research has increased, in particular the ones related to wearable mouthguard platforms. As an example, we have the device presented by Kim *et al.* [17,22], which developed a mouthguard-based salivary metabolite electrochemical biosensor through integration of screen-printed enzymatic electrodes. This device is based on the knowledge that salivary lactate correlates well with blood lactate which can be used to diagnose physical stress and performance. Knowing this, the platform is aimed to electrochemically detect lactate in saliva. J.K., J.W. *et al.* [14], also developed a mouthguard-based uric acid biosensor, as we can see in Figure 4.a, incorporating miniaturized instrumentation electronics such as a microcontroller, potentiostat and even a Bluetooth low energy (BLE) transceiver for the monitoring of the biomarker.

More sophisticated oral biosensor devices have implemented the advantage of miniaturization by turning them into detachable cavity sensors capable of measuring salivary glucose levels in a mouthguard platform designed to fit over the user's teeth. Despite its small size, this prototype (Figure 4.c) [15] also integrates a wireless data transmitter enabling the telemetric measurement of salivary glucose. As previously mentioned, there is a good correlation between blood glucose levels and glucose levels in saliva due to the diffusion and active transport of substances present in the blood to the salivary gland. This fact provides a non-invasive diagnostic alternative in diseases such as diabetes, where salivary glucose levels produced by the salivary glands may be increased by hormonal changes.

Finally, another wearable sensor based on an oral-cavity platform worth to mention, has been demonstrated for the first time in an in-mouth operation with a human subject (Figure 4.b) [16]. The tooth-mounted sensor that can be seen in the image, was made from biocompatible materials such as porous silk and hydrogels and it is capable of perform a monitoring of several food properties during ingestion, such as salinity, sugars, pH, among others.

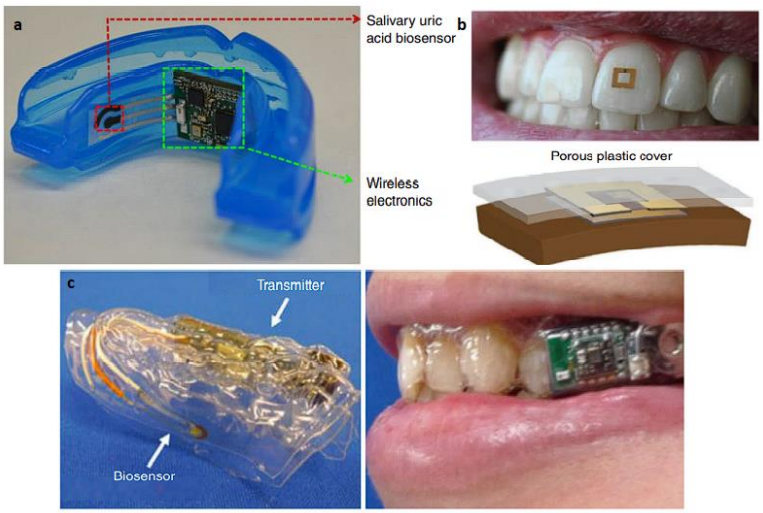

Figure 4: Saliva-based biosensors. a, *Mouthguard-based wearable salivary uric acid biosensing platform [14].* ***b,*** *Radio frequency trilayer tooth-mounted sensor for wireless monitoring of food consumption [16].* ***c,*** *Mouthguard-based sensor or glucose monitoring in saliva [15].*

In general, saliva could be a good alternative for tracking some biomarkers such as glucose, however, future work has to pay attention to minimize sample contamination from other components of saliva and food debris ensuring the safety and reliability of the device.

2.3 Porous silicon as a template for polymeric replicas

Porous silicon (pSi) is a promising porous material that, thanks to its properties, has generated a lot of interest especially as a sensing platform for the detection of different components. Nonetheless, in this project, macroporous silicon (macropSi) has been used as a template for the fabrication of polymeric nanostructures with the aim to serve as a platform capable of detecting biomarkers in bodily fluids. This is possible thanks to the control that we can exercise over the pore size, film thickness and porosity of these materials, that will allow us to modify at will the dimensions and characteristics of the manufactured polymeric nanostructures.

2.3.1 Introduction to porous silicon

PSi is a nanostructured material with hollow cavities (pores), similar to the surface we might see on a sponge. In a matter of years, it has become one of the most studied nanomaterials and its properties have made it the focus of attention for a wide range of applications ranging from its use in batteries and fuel cells to drug delivery and diagnostics even recently, fields related to cosmetics and nutrition have also benefited from the characteristics of this material [26].

Its manufacturing process also proves to be an advantage, as it is a relatively cheap and simple procedure. Since it is a material with very tunable structural, mechanical, optical, electrical, physicochemical and other properties, its fabrication can be carried out through different methods depending on the structure and properties desired for the final material.

2.3.2 History of porous silicon

This nanomaterial was discovered accidentally in the mid-1950s by two engineers called Arthur Uhlir Jr. and Ingeborg Uhlir at Bell Laboratories [10]. At that time, the Uhlirs were trying to develop a method for shaping and polishing silicon and germanium wafers, when unexpectedly and after several attempts using mixtures of HF with other solvents, they observed that under specific conditions of current and solvent composition, the silicon wafer did not dissolve uniformly but began to form a series of fine holes in the same directions of the wafer.

Despite being a major potential discovery, at the time it was simply reported in a laboratory technical note and subsequently ignored until the 1970s and 1980s, when a great deal of interest in pSi emerged due to its high surface area, which was proved to be useful in spectroscopy studies, as a precursor to the generation of thick oxide layers on silicon and as a dielectric layer in capacitance-based chemical sensors.

In the late 1980s, quantum confinement and room-temperature photoluminescence effects were discovered by two research groups working independently formed by Leigh Canham in the first group, and Ulrich Goesele and Volker Lehmann in the second group. Basically, what they achieved was to make the electrochemically etched material's pore walls thinner under almost 5 nm, resulting in a material able to glow with a red-orange color when illuminated with ultraviolet light. According to the quantum confinement relation, this resulting color can be translated into the material's energy being significantly larger than the bandgap energy for bulk silicon, which occurs in the infrared region of the spectrum.

With the above discovery, there was an explosion of optical studies focused on creating Si-based optoelectronic devices. Decades later, we find ourselves at a point where, in addition to this optical property discovered in silicon, multiple other properties are being exploited in a wide range of applications, making it a powerful area of research [23].

2.3.3 Properties of porous silicon

Commonly, porous materials are classified according to their pore dimensions, and pSi is no exception. The pSi structures that present pores of dimensions smaller than 2 nm and larger than 50 nm are called microporous and macroporous silicon, respectively; those that are between the two previous sizes are called mesoporous silicon. Because of the wide variety of pore sizes, shape, orientation and distribution that can be obtained, the morphology of the material is the least quantifiable characteristic it possesses (Figure 5). As a result, we can endow pSi with different sets of properties and use it in different fields.

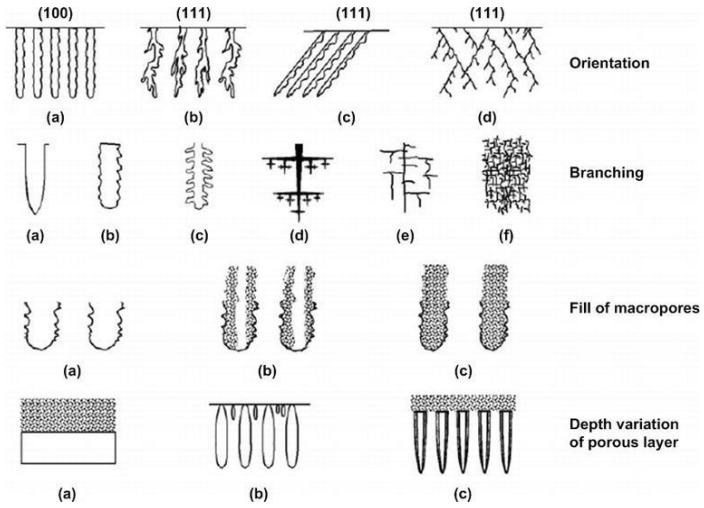

Figure 5: *Morphological characteristics of pSi [26]*

For example, we can opt for a silicon wafer design focused on modifying properties such as porosity, density, surface area or pore diameter, or else focus on optical properties (such as color, reflectivity) for the application of pSi in optoelectronics working as a LED, or perhaps exploit electrical properties (dielectric constant), biochemical properties (medical biodegradability), among many others [26].

2.3.4 Porous silicon fabrication

Since the discovery of pSi in 1956, more than 20 methods have been devised for the fabrication of these porous nanostructures. This set of methods can be classified into two categories: top-down, where monocrystalline silicon clusters are removed from the wafer to reveal small porous cavities, and bottom-up, where these clusters are grouped in such a way that forming a crystalline form, leaves empty spaces behind. Because of this large number of procedures, the manufacturing method that will be discussed below will correspond to the one used during my stay in the laboratory, and that is the **anodization** process. This can be defined as an electrolytic passivation process used to increase the thickness of the natural oxide layer on the surface of the semiconductor.

Its name is given by the role of the material subjected to this process, silicon in our case, since it acts as the anode in the electrolytic cell. With the help of this cell, we induce the formation of a porous structure in silicon by immersing it in a concentration of HF electrolyte which leads an electrochemical attack on the silicon, using silicon as the anode and a platinum filament as the cathode. Subsequently, by applying a constant current to the cell, we achieve a corrosion of the silicon surface, modifying its microstructure. The fact that the applied current is constant helps us to achieve a more homogeneous porous layer.

2.3.4.1 Anodization parameters

As previously mentioned, one of the great advantages of pSi is the great tunability of its properties, which can be controlled by modifying and combining the following anodizing parameters:

1. Current: Its modification allows us to play with the morphology and size of the pores.
2. Etching time: Along with current, it is the parameter with which we have played the most in order to obtain the desired pores. It is closely related to the pore thickness.
3. HF concentration: It is the liquid medium that will allow the electrochemical attack on the silicon, forming the pores.
4. Number of anodization steps: With this parameter we refer to the number of times that the anodization process has been performed on the same silicon sample. Later, in the methodologies section, we will observe that during the fabrication of our macropSi samples, we have played with the way of performing the anodization process, sometimes the sample has been subjected to one step, other times using two steps with different current densities, different times, etc. This results in a variation in the homogeneity of the pores.

There are other parameters such as temperature, lighting, humidity, etc., but the above are the ones taken into account in this project.

2.3.5 Porous silicon stabilization

Once the anodizing process is finished and the final pSi sample has the desired characteristics, a stabilization process is necessary to avoid the degradation of the pSi surface when in contact with air. The most common stabilization technique, and the one we have used, is thermal oxidation. With this procedure, hydride-terminated pSi is converted to SiO_2

and can be finally used as a template. Another less common technique, but which we have also applied, is to oxidize the sample by mixing sulfuric acid and hydrogen peroxide, forming a solution commonly known as piranha solution [35].

2.4 Porous anodic aluminum oxide as a template for polymeric replicas

Similar to pSi, porous anodic aluminum oxide (pAAO), is also being taken into consideration in recent years and is being used in a wide range of applications, the main one being its use in biosensing due to its unique optical properties, its ease of fabrication, large surface area, and tunable properties. In addition, and related to its application in this project, this material is also being used as a mold for the fabrication of polymeric nanostructures, thanks to its highly ordered porous structure.

2.4.1 Introduction to porous anodic aluminum oxide

As a main feature of pAAO, we find a highly ordered and homogeneous honeycomb nanopore surface. This structure is formed by a grouping of hexagonal elements with cylindrical pores inside that extend perpendicular to the surface of the underlying Al substrate. As we can see in the figure below (Figure 6), the geometrical structure of pAAO is characterized by the pore diameter (d_p), the distance between the centers of the different cylindrical pores (d_i), the pore length (l_p) and finally the wall and barrier layer thickness.

These parameters, as with pSi, can be modified at will, depending on the anodization parameters we use: voltage, electrolyte composition, time, etc., also impacting on the percentage of surface porosity.

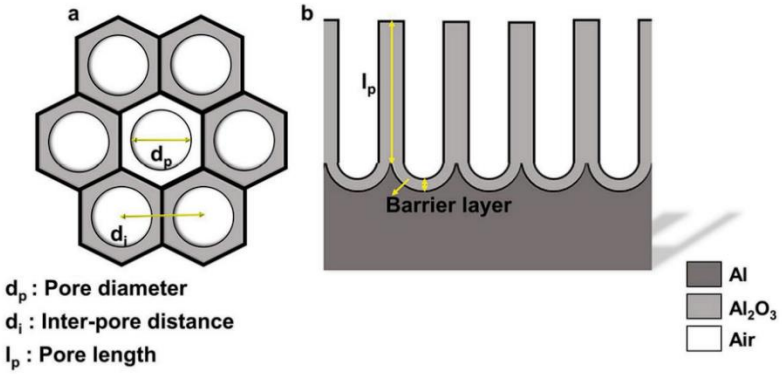

Figure 6: *Porous anodic aluminum oxide characteristics*

2.4.2 History of porous anodic aluminum oxide

The origins of metal anodizing date back to 1923, as a technique for the prevention of corrosion of duralumin, a metal used for the manufacture of seaplane parts. In these beginnings, the technique was based on the use of chromic acid and was called the Bengough-Stuart process in honor of its discoverer. This procedure, although somewhat outdated, is still used today.

Years later, in 1927, Gower and O'Brien patented an improvement in the previous anodizing process, using in this case a new mixture of sulfuric acid, being this solution the most used nowadays as anodizing electrolyte [36].

In the 1930s, the porous nature of anodic alumina was discovered and later, in the 1950s-1970s, it was further investigated. But it was not until 1974, when the scientist Alan W. Smith, patented the use of different acids (chromic, sulfuric, oxalic and phosphoric), for the fabrication of anodic aluminum oxide [38].

Finally, in 1995 one of the major breakthroughs came from Masuda and Fukuda, who discovered a two-step replication process for the fabrication of self-ordered pAAO structure with highly ordered pores [37]. This fact has served as the basis for the vast majority of studies related to this material, being also one of the most cited works by scientists' communities in this field.

2.4.3 Properties of porous anodic aluminum oxide

PAAO has several innate properties. A very important one is its inert chemical composition that allows its use in physiological conditions without damaging the useful life of what could be a potential biosensor. Like pSi and thanks to its porosity, it possesses a large surface area and high aspect ratio allowing the immobilization of a large number of bioreceptors and enhancing the sensitivity of the readouts. Its nanometric structure is also an advantage when detecting biomarkers in very complex media, due to its good filtering capacity of large molecules that can generate an interference effect in the results. All of the above, together with its innate biocompatibility, make it a perfect material especially in its use as a biosensor. We also found unique optical properties, including reflectivity, transmittance, chemiluminescence and photoluminescence (which is strongly related with the electrolyte used during the anodization), in addition to innate electrochemical, thermal and mechanical characteristics [3].

2.4.4 Porous anodic aluminum oxide fabrication

In order to obtain an ordered pore structure, it is necessary to perform a treatment called electropolishing prior to anodizing the Al sample [39]. This technique consists of the electrolytic removal of metal in a highly ionic solution through the application of an electric potential and current. A mixture of perchloric acid and ethanol is commonly used creating the need for a dedicated space with fume hoods and continuous cooling systems. As a result of the above process, a surface with a characteristic brightness is obtained, ready to undergo the anodizing process.

The anodization process is similar to that of pSi. The aluminum acts as the anode, and a piece of platinum as the cathode. These elements are contained in the anodization cell and immersed in an electrolyte or acid solution, which is provided with a voltage by a power supply that connects the positive pole to the anode and the negative pole to the cathode. At this point, an electrolysis process takes place where redox reactions occur simultaneously at the electrodes. On the one hand, the anode is oxidized by the anions of the electrolyte generating a layer of anodic oxide, also called alumina, on the surface of the metal. On the other hand, the negative cathode fed with electrons serves to reduce the concentration of cations.

As a result of the above process, a pAAO structure is obtained on the aluminum sample. In addition to the above, I would like to add that in our case and for our application, once this structure was obtained, the pAAO sample was subjected in some occasions to a phosphoric acid (H_3PO_4) solution to widen the size of the pores [3].

2.4.4.1 Anodization parameters

As we know, the pAAO geometry depends on the conditions used in the process explained above, such as the electrolyte used, anodization time, temperature, voltage and the pretreatment of the aluminum.

While the type of electrolyte influences the homogeneity in the pAAO pores, the applied voltage has a linear relationship with the pore spacing, in the same way that the voltage together with the anodization time controls the pore thickness. Temperature also plays an important role since it has been shown that pore growth is slower at lower temperatures. In

relation to the current, despite being constant, it always begins to decrease after long periods of anodization time, also influencing the rate of pore growth [31].

Finally, another condition we have already discussed, which is necessary for the formation of ordered pore matrices, is the annealing of the aluminum sheets before anodizing. This is done in order to increase the grain size and eliminate mechanical stresses in the metal substrate. It is well known that the organized pAAO structure can only be obtained when the pores start to form from a very clean and smooth aluminum surface, which is why the pre-anodizing process called electrochemical polishing is a very necessary condition [39].

2.5 Methods for polymeric replica fabrication

Thanks to the previous sections, we have been able to see how materials such as silicon and aluminum can be electrochemically modified to give them the function of a template. The question to be solved here is, how can we obtain a microstructured material from these templates? For this reason, in this section we will present a series of techniques used to obtain both micro- and nanostructures, focusing in the final part on the template assisted-technique which will be the method chosen for our project. We will see that thanks to this technique, a great variety of materials can be modified and endowed with specific microstructures. In our case, these materials will be polymers.

These fabrication methods can be classified as "top-down", where we find our chosen template-assisted technique, and "bottom-up", where a large number of techniques widely used in this field are collected, such as lithography and self-assembly strategies. The following is a brief explanation of the techniques mentioned above, together with others that have not yet appeared but are also of great relevance.

- **Lithography:** Within this topic, several techniques have been studied such as photolithography or electron beam lithography. In a nutshell, lithography is a complex technique that converts a design layout on a mask into the structure on a substrate. We found an example of this in serial writing charged particles (electron or ion) [50]
- **Electrospinning:** This technique was created mainly for the fabrication of ultrathin polymer layers. By this technique, polymer nanofibers can be generated from the use of electrical forces. Electrospinning occurs when the electrical forces at the surface of a polymer solution or melt, overcome the surface tension and cause an electrically charged jet to be ejected. When the jet dries or solidifies, an electrically charged fiber remains. [49]
- **Self-assembly:** Defined as the spontaneous organization of two or more components into larger aggregates using covalent and/or noncovalent bonds. [48]

Finally, the method of great importance to us will be explained in more detail in a separate section.

2.5.1 Template assisted-technique

This procedure consists of the infiltration of a specific material into a set of cavities with well-defined contours, receiving the name of template. Subsequently, the infiltrated material will be removed, thus obtaining the inverse replica of the template. This technique does not require very sophisticated equipment and can be carried out with a wide range of materials such as polymers, semiconductors, metals and oxides (the latter two can be electrodeposited into the template).

In our case, the materials used for the infiltration will be a series of polymers, due to their promising applications and their great versatility, while the materials that will adopt the

role of template will be porous anodic aluminum oxide (pAAO) and macroporous silicon (macropSi). Of all the existing ways to infiltrate the biomaterial into the cavities, we will opt for depositing a polymer mixture into the template and allowing it to polymerize, adopting the shape of the pores.

The process to follow would be something similar to what we see in the attached image (Figure 7):

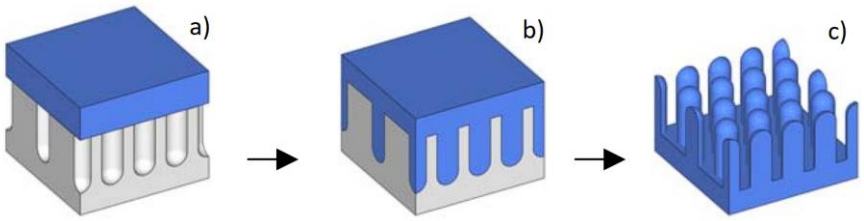

Figure 7: *Polymer infiltration process using a porous template*

As we can see, in the first step (Figure 7.a) the polymer is poured onto the template. Then, because of the high surface energy of the template compared to the polymer, a thin layer of material fills the totality of the pore (Figure 7.b). With this, it only remains to wait for the polymerization process to take place inside the pores to finally remove the template and obtain the polymeric replica with the microstructures adopted from the porous material (Figure 7.c).

In this way, we have that the characteristics of these structures obtained can be highly customized and will be given by the procedure and the parameters that we use during the fabrication of the template. In our case, since we are dealing with macropSi and pAAO, these characteristics can be highly modifiable.

2.5.1.1 Removal of the template

Related to the above, once we have applied the template-assisted technique on our polymer, the next step will be to remove this template to obtain as a final result what we are interested in, which is the replica. For this, different decisions can be taken.

The most common technique is the removal of the template by chemical dissolution of various acids. It should be noted that not all the templates will dissolve with the same acid concentrations. In the case of pAAO templates, a mixture of hydrochloric acid (HCl) and copper chloride ($CuCl_2$) is commonly used for the dissolution of the aluminum, along with a phosphoric acid (H_3PO_4) solution in order to remove the remaining alumina.

In the case of macropSi, there are several options for chemical dissolution. The most widely used among all the works [34] uses a mixture of dimethyl sulfoxide (DMSO), 48 % hydrofluoric acid (HF) and ethanol (C_2H_5OH) in a 4:1:1 v/v ratio. Solutions made from nitric acid (HNO_3) and HF in different concentrations can also be used with caution as they are very aggressive solutions at high concentrations and can damage the replica.

Leaving aside the chemical dissolution method, there is another widely used technique that allows manual removal of the replica from the template without the need to dissolve the template, avoiding the use of hazardous acidic solutions. This method relies on template silanization using 1H,1H,2H,2H-perfluorooctyltrichlorosilane. This compound is widely used to silanize the porous silicon template, and introduces an anti-adhesive layer against the polymer.

3 Working hypotheses and objectives

Once the previous theoretical concepts have been introduced, I will go on to explain the practical part of the project, where the previous concepts will be brought to reality with the help of the different instruments and equipment in the laboratory with the aim of developing a polymeric platform made from porous templates suitable for biosensing. It is at this point that I would like to emphasize something very important, and that is that the biosensing platform that we intend to obtain, is related to its use on **SKIN**, and related with the biomarker monitoring in **SWEAT**. If all goes according to plan, perhaps the methods used in the laboratory for this project, could be used for future biosensing projects focused on other biofluids.

As it has already been mentioned on many occasions, the evolution that wearable devices have undergone has led to one of their main applications being related to their clinical use in the follow-up of patients with risk conditions. To ensure timely intervention in the early stages of these conditions, continuous and real-time monitoring is required in this type of devices, in addition to the biocompatibility and comfort they must have in order to be in contact with the biofluid in question for long periods of time without causing any adverse reaction to the user.

During my stay in the laboratory, we were able to study two types of platforms:

- **Polymeric replicas** made of styrene, polystyrene and PDMS from **macropSi templates**. The possibility to fine-tune the morphological features of pSi should have let us play with a huge variety of polymeric configurations.
- **Polymeric replicas** made of styrene, polystyrene and PDMS from **pAAO templates**. The highly self-ordered honeycomb structure of the pAAO, should have allowed us to obtain very homogeneous and ordered polymeric nanostructures.

With this, we want to study how depending on the anodization parameters used, we obtain different pSi/pAAO template configurations, with very different pore characteristics, and, consequently, we deliver a wide range of polymeric replicas with different nanostructures. From here, we should be able to find the optimal configuration to obtain polymeric replicas with the most appropriate and efficient characteristics to be used for biomarker detection.

According to our expectations, thanks to the high customization of both pSi and pAAO, we should be able to create polymeric nano- micropillars of adequate thickness and sufficient inter-pillar distance to allow the continuous contact with the skin and the immobilization of an adequate number of bioreceptors for accurate measurements.

Therefore, our objective will be to **study the advantages and disadvantages of various polymeric replicas depending on the type of template and polymer used, compare their structures and perform a study of their characteristics to see if they could be used in biomarker tracking applications in sweat in an efficient and correct way**.

Our proposed hypotheses are:

1. **We can obtain stable and functional polymeric replicas from the use of macropSi and pAAO as templates.**
2. **We may be able to obtain suitable templates, and thus suitable replicas, by playing with the anodizing parameters and subjecting them to an optimization process.**

3. **We will be able to understand how the anodizing parameters affect the characteristics of the templates.**

4 Methodology

4.1 Variables and resources

4.1.1 Chemicals

In relation to the chemicals and solutions used during the anodizing process, we have the following:

Template fabrication

- Solution 1 (HF1): Used during the first step of the anodization process. Composed by 20 mL of 48% HF and 150 mL of dimethylformamide (DMF). Proportion 1:7.5.
- Solution 2 (HF2): Used during the second step of the anodization process. Composed by 15 mL of 40% HF and 150 mL of DMF. Proportion 1:10.
- Washing solution: Used for a previous washing of the silicon wafers. Composed by a mixture of 10 mL of 48% HF and 100 mL of deionized water (DI)
- Ethanol: Used for cleaning the samples after the anodization is done to remove the remaining acid.
- Deionized water (DI): Also used for cleaning samples and remaining acid.
- Phosphoric acid (H_3PO_4): Used for pore widening and for the removal of alumina.
- Oxalic acid

Template removal

- For pAAO templates: A mixture of hydrochloric acid (HCl) and copper chloride ($CuCl_2$) for the removal of the aluminum part of templates along with phosphoric acid (H_3PO_4) to completely remove the alumina layer of the polymer and expose the micropillars.
- For pSi templates:
    - 40 % nitric acid (HNO_3) and 60 % HF
    - 20 % nitric acid (HNO_3), 30 % HF at 48%, and 50 % EtOH
    - DMSO/48% HF/EtOH in the proportions 4:1:1
    - 2 M NaOH in 9:1 mixture of H_2O/EtOH.
    - Perfluorooctyltrichloro-silane: It is not related to the chemical dissolution of the template, but it was indeed used to allow the manual removal of the replica from the template.

Polymeric replica fabrication

- PDMS: Made of a mixture of liquid silicon elastomer and silicon elastomer curing agent (Sylgard 184 (Dow Corning) in a proportion of 10:1 (1 g of silicon elastomer and 0.1 g of the curing agent, in our case)
- Polystyrene: Using a mixture of 200 mg polystyrene and 800 mg of Toluene acting as polystyrene's solvent.
- Styrene: Mixture of 1.15 mL of styrene and 28 mg of an initiator called Azobis.

4.1.2 Equipment

4.1.2.1 Macroporous silicon setup

This section shows the set of equipment used during the fabrication of macropSi templates from p-type (boron doped) silicon wafers, following the procedure established by the Department of Electronic, Electric and Automatic Engineering at Rovira i Virgili University. In Figure 8, we can see an overview of all the devices used. We find a computer (a) to control the current and the anodization time, by using a program called TSP Debug (Test Script Builder). We also have a source-meter model Keithley 2611A (b), which acts as a multimeter and a power source for the anodization cell (e) at the same time. Finally, (c) is a motor that enables de stirrer to spin, and the fume hood (d) to avoid toxic fumes and work safely.

In Figure 9, a close-up picture of the anodizing cell used in the laboratory is shown, along with a schematic image of the elements that make it up.

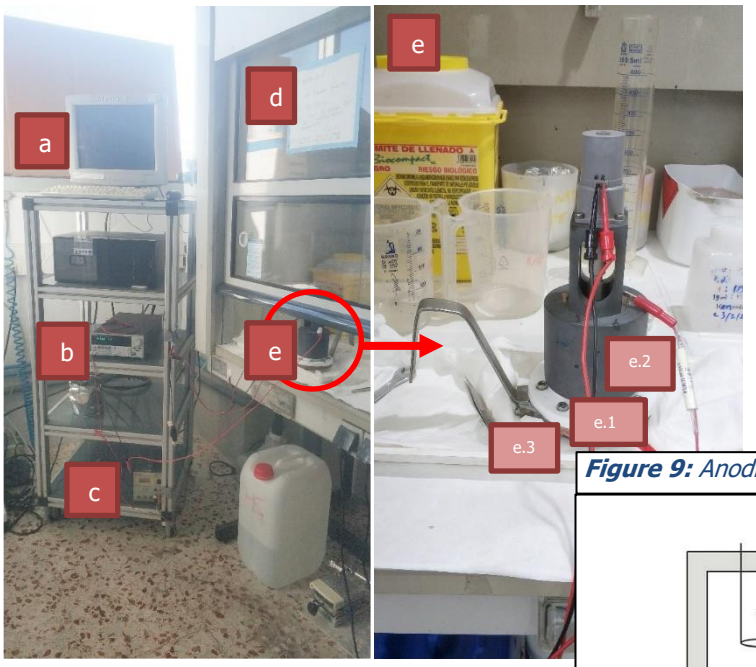

Figure 8: *General view of the macroporous silicon setup*

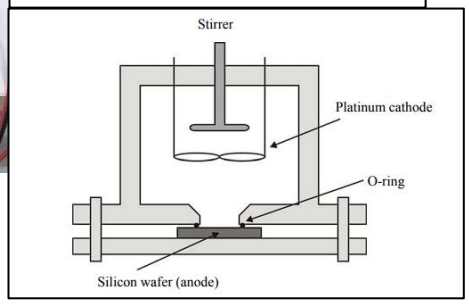

Figure 9: *Anodization cell*

This "home-made" device can be considered the most important part of the fabrication system as it is where the electrochemical process and the formation of the pores take part. It is made of Teflon as it is a material highly resistant to HF, even at high concentrations. The main body consists of a white cylindrical vessel (e.1), which will contain the electrolyte and facilitate its exchange in the different steps of the process. At the bottom of this vessel, we find a circular hole that determines the contact surface between the electrolyte and the silicon wafer. Speaking of the silicon wafer, this acts as the anode and is located between the space formed between the cylindrical container and the copper disk (e.3) that closes the cell. In order to seal this structure and avoid HF leakage, we use a silicon O-ring placed on the wafer fitting the hole of the cylinder. Finally, the part of the container that remains in the air, is closed with the stirrer (e.2), a mechanical device that rotates continuously thanks to the action of a motor connected to the top terminals. The structure of the stirrer has also embedded a filament of platinum, acting as the cathode.

4.1.2.2 Porous anodic aluminum oxide setup

I would like to mention that both in this section and in 4.2.2 Porous alumina fabrication, it may be noted that it does not contain as much detailed information as the macropSi sections. This is because in the case of silicon, I was 100% involved in its fabrication and research, for the alumina instead, the person in charge of its fabrication was a fellow researcher from the lab named Deepanshu Verma whom I would like to thank for his help during the development of this project. Once these templates were fabricated, I received them and proceeded with the fabrication and analysis of the polymeric replicas with all that this implies.

Now I will proceed with the explanation of the setup for the fabrication of the porous alumina. The equipment that we can find in this setup, would be something like the image below (Figure 10).

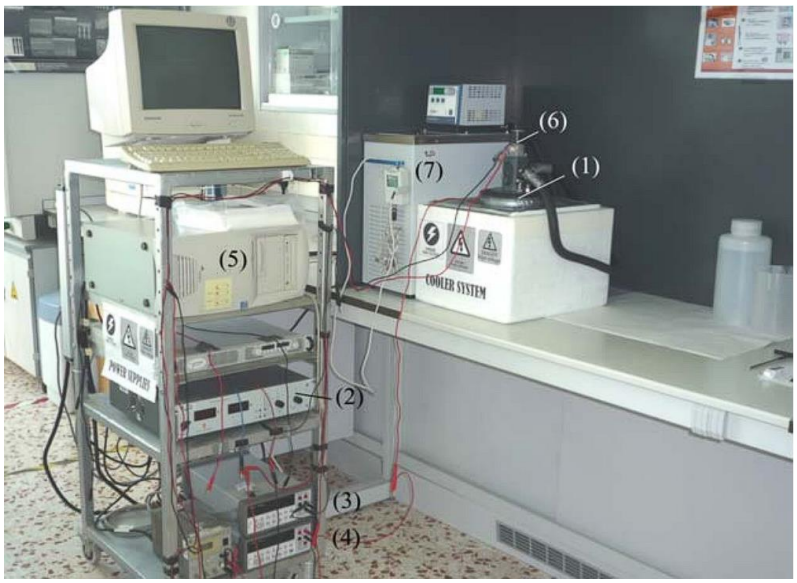

Figure 10: *Setup similar to what we would find in our lab for porous alumina fabrication*

Figure 10 shows the electrochemical cell (1) inside the cooler system, a power supply (2), (3,4) are two multimeters to measure actual current and voltage, in (5) we got the computer with the Test Builder Script program also used for macropSi fabrication, the stirrer and the motor (6) and finally a new device respect to silicon fabrication which is a temperature controller (7). Temperature control and cooling systems will have a major role in this procedure, due to the sub-zero temperatures to which the aluminum sample must be subjected during the first and second anodization processes.

4.1.2.3 Vacuum-based polymer infiltration

The next step after the fabrication of the templates, is the deposition of the polymer on the surface of these samples. During this step, the infiltration of bubbles between the polymer and the porous surface could occur, preventing the polymer from completely filling the porous cavities and not acquiring the proper microstructures. In order to avoid this, a configuration similar to the one shown in Figure 11 was used.

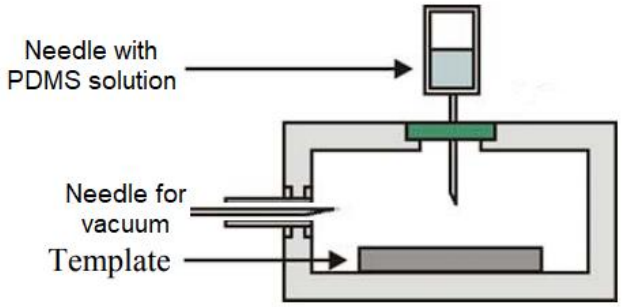

Figure 11: *"Home-made" vacuum system*

We placed the porous template inside a hermetically sealed container. Before closing the container, two needles were inserted and fixed by the pressure exerted by the lid. One of these needles was used to form the vacuum while the other one was used to infiltrate the polymer on the surface of the template.

4.1.2.4 SEM and gold sputtering equip

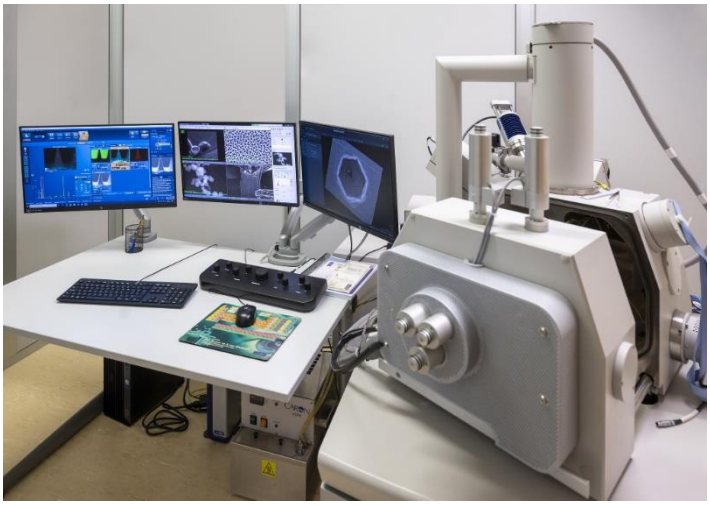

Figure 12: *The Quanta 600 from FEI company. Environmental scanning electron microscopy (ESEM) with X-ray microanalysis located in the SRCIT*

The method used for the analysis and visualization of the microstructures of the polymeric replicas was the scanning electron microscope (SEM). SEM can be defined as *a type of electron microscope that produces images of a sample by scanning the surface with a focused beam of electrons. The electrons interact with atoms in the sample, producing various signals that contain information about the surface topography and composition of the sample* [28]. In addition, this microscope has two modes of operation: low-vacuum and high-vacuum. The traditional mode of operation and the one with the best results and highest resolution obtained is in high vacuum. In our case, we will use the microscope of the SRCIT facility called Quanta 600 from FEI company. To analyze samples via SEM, their surface has to be conductive, something that does not happen naturally with polymers, and thus they have to be covered with a specific metal such as gold. This is why polymeric replicas have to undergo a previous process called **gold sputtering**.

The gold sputtering is carried out by a device provided again by SRCIT, called Q150T Plus. The Q150T Plus is optimized for use with a turbomolecular pump, which gives a lower vacuum down to 5 x 10^{-5} mbar. This enables the sputtering of oxidizing metals, which have a lower grain size suitable for high-resolution imaging [29]. As previously mentioned, we will use a sputtering made of a thin layer of gold.

Figure 13: *Q150T Plus, sputtering machine*

4.1.2.5 Complementary equipment

Finally, during the experiments other equipment was used, such as high temperature ovens, where the polymerization was carried out, refrigerators, ovens for the thermal oxidation of the templates, a vacuum chamber to avoid oxidation of the templates in contact with the air, and other typical laboratory materials of minor relevance such as tweezers, containers, etc.

4.2 Experimental process

4.2.1 Macroporous silicon template fabrication

In this section, we describe the step-by-step methodology carried out in the laboratory in order to fabricate macropSi.

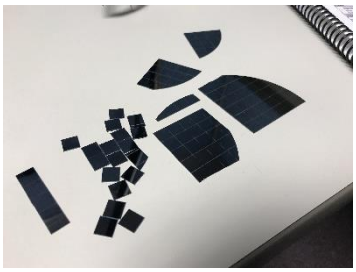

Figure 14: *Silicon wafers cut*

1. Boron-doped silicon wafers were cut in squares of around 25 x 25 mm, which is the measure that fits almost perfectly according to our Teflon made anodization cell. After this, the samples undergo chemical washing. First, samples are immersed in a 5% solution of HF (48%) in EtOH for 2 min and then cleaned with DI water for 3 min, and finally dried under the flow of nitrogen.
2. Once the silicon samples are clean, the anodizing cell is prepared. Carbon sandpaper was used to clean the copper disk and get rid of all the possible impurities remaining from previous anodizations. A cleaning with ethanol is needed to remove the copper oxide dust generated. A piece of high purity aluminum foil as used between the silicon samples and the copper disk in order to increase the contact surface of the silicon wafer with the copper disk.
3. Before mounting the anodizing cell, we have to choose a suitable silicon O-ring that fits perfectly in the hole and thus determines the anodizing surface, in order to avoid possible leakage of the electrolyte solution.
4. The cell was assembled By placing the silicon sample centered in the hole at the bottom of the Teflon cylinder, with the shiny surface facing up. The cut piece of aluminum goes on the bottom of the silicon wafer in contact with the copper disk. After that, the copper disk and the cylindrical container are screwed together.
5. Once the cell is sealed, the electrolyte was added. During the first anodization, HF1 solution was used, which was prepared in the composition of HF (48%)/DMF in a

1:7.5 ratio. In the case of a second anodization, the previous solution is removed and exchanged for the HF2 solution, composed by HF at 40% and DMF in a proportion 1:10. Then, cell's stirred was ran . In relation to the connections (Figure 15), the stirrer is connected to a motor (1), and the platinum wire (black terminal (2)) and the copper disk (red terminal (3)) are connected to the power supply.

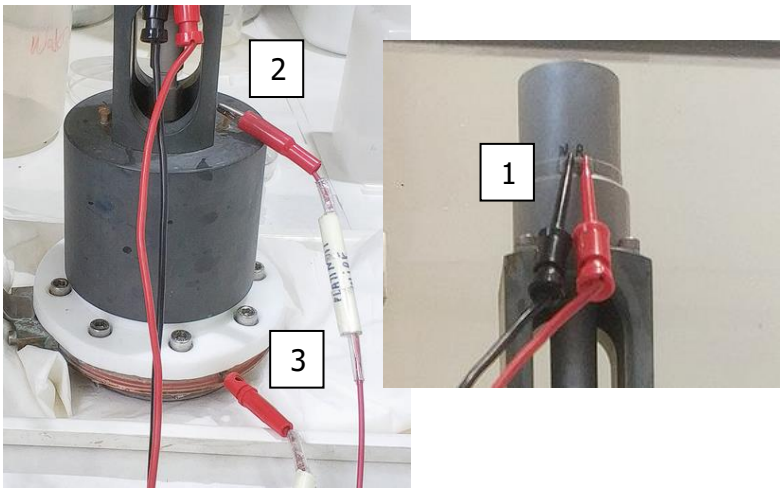

Figure 15: *Connections of the anodization cell*

6. In the next step, we have to go to the computer and through the TSB program, set the time and current of the anodization. This is where most of the work is done. During the fabrication, we tested different parameter settings, which can be seen in the following tables (Table 2):

Table 2: *In these tables, we observe 3 different sets of macropSi samples where we have used different anodization parameters*

SET

	1st Anod Current (mA)	Time 1 (h)	2on Anod Current (mA)	Time 2 (min)
Sample 1	2	1	x	x
Sample 2	2	1	3 and 4	4 and 4
Sample 3	2	1	3 and 4	2 and 2
Sample 4	2	1	4	4
Sample 5	2	1	5	4

SET

	1st Anod Current (mA)	Time 1 (min)	2on Anod Current (mA)	Time 2 (min)
Sample 1	2	15	x	x
Sample 2	2	30	x	x
Sample 3	3	15	x	x
Sample 4	3	30	X	X
Sample 5	3	15	4	4
Sample 6	3	30	4	4

SET

	1st Anod Current (mA)	Time 1 (min)	2on Anod Current (mA)	Time 2 (min)
Sample 1	3	45	x	x
Sample 2	3	37	x	x
Sample 3	3	37	4	2
Sample 4	3	45	4	2

The significant factors that affect the structure of the fabricated macroporous silicon, including current densities, anodization times and the number of anodizations performed were optimized. At the beginning, we decided to perform a first fixed anodization on all samples with currents of 2 mA for 1 h, while with the second anodization, we played with currents of 4 and 5 mA for 4 min, and second split anodizations with initial currents of 3 mA that were increased to 4 mA when the set time was reached. In the later samples, it can be seen the specific times and currents used in order to find the optimum parameters that would result in the porous characteristics suitable for our application.

7. Once the anodization process is completed, we disassemble the cell and extract the sample. If everything has gone according to plan, we should not observe any HF residue on the copper disk and the sample should look similar to the image shown in Figure 16. To clean the acid residues, we use ethanol and dry with N_2.

Figure 16: *Anodized silicon wafer*

8. As a final step, the samples are oxidized by thermal oxidation in air at high temperatures, or by using piranha solution.

9. (Extra step): We have previously mentioned the existence of a technique that allows to manually peel the replica from the template. It is at this point that the technique can be applied. To do so, we create a vacuum configuration similar to the one shown in Figure 17, to allow vapor-phase silanization. We introduce the template together with a vial filled with perfluorooctyltrichloro-silane. Due to the pressure exerted inside the container, the silane evaporates and precipitates on the template. Thanks to this step, the macropSi surface acquires high hydrophobicity, helping the future polymer deposited on it to be easily removed. I would also like to add that this hydrophobicity was successfully tested by contact angle measurement on our templates.

Figure 17: *Coating of the macropSi surface with a layer of perfluorooctyltrichloro-silane*

4.2.2 Porous anodic aluminum oxide template fabrication

Here there is the step-by-step methodology followed to fabricate pAAO templates.

1. As mentioned in the theoretical section 2.5 porous anodic aluminum oxide as a template for polymeric replicas, the first step of this fabrication consists of electropolishing the surface of the ultra-pure aluminum foil previously cut in squares similar to silicon samples. Electropolishing is done using a 4:1 solution (v/v) of ethanol (C_2H_5OH) and perchloric acid ($HClO_4$) at a voltage of 20 V during 6 min under controlled temperature of 5 ºC. During this process, a constant stirring rate of 300 rpm with alternated direction every minute, is also performed.

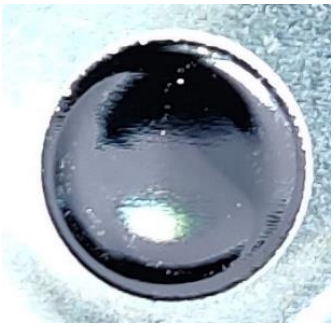

Figure 18: *Electropolished aluminum [32]*

2. Once the electropolishing process is finished, first anodization takes place using a solution of 1 wt% phosphoric acid (H_3PO_4) (water and ethanol). The process starts with the following parameters under constant stirring:
    a. Temperature of -7 ºC
    b. An initial voltage of 175 V for 3 h. This induces the formation of a protective oxide layer preventing the burning of the sample at the beginning of the anodization. After 3 h, the potential is ramped at 0.001 V/s to 195 V. A final voltage of 195 V is applied for 20 h.

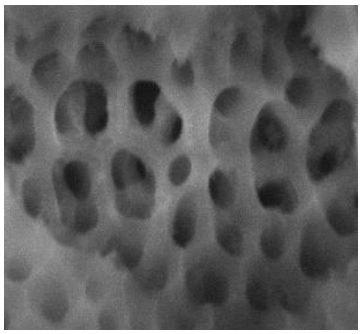

Figure 19: *First anodization [32]*

3. After the first anodization, a wet chemical etching step is performed in order to completely remove the NAA layer. A solution consisting of an acid mixture of chromium oxide (CrO_3 > 99.0%, Emsure) and H_3PO_4 is used. This step is performed for 2 h at a temperature of 70 ºC with constant stirring.

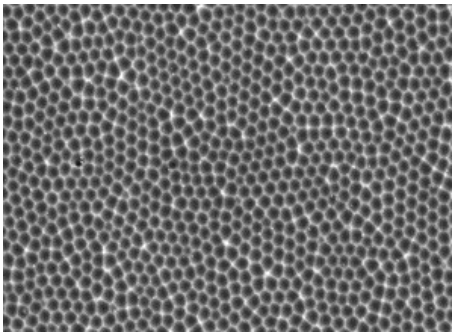

Figure 20: *Wet chemical etching results [32]*

4. Finally, the second anodization is performed using again a solution of 1 wt% Phosphoric acid (H_3PO_4) (water and ethanol). In this case, the parameters and conditions used are the following:
    a. An anodization potential of 195 V at a temperature of -7.5 ºC
    b. The total charge employed in this second anodization step is of 13.15 C per sample where the area of a sample exposed to the electrolyte is 3.52 cm^2 (2.63 C charge for 1 µm growth on 1 sample). The total charge is 52.6 C
    c. The thickness of the resulting porous film is 5 µm

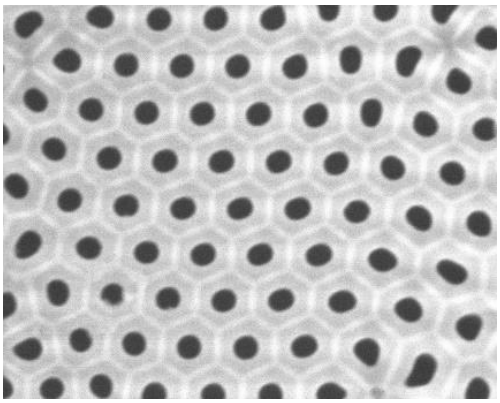

Figure 21: *Second anodization [32]*

4.2.3 Polymeric replicas fabrication

Once we have the templates made, the next step is to build the polymeric replicas. First, the polymer has to be prepared.

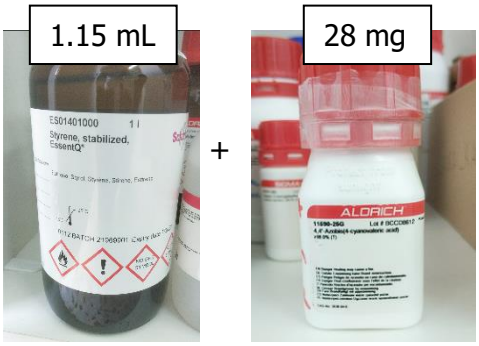

Figure 22: *Styrene on the left, azobis initiator on the right*

In the case of styrene and with the help of a pipet, we will have to deposit in a vial 1.15 mL of stabilized styrene, and with the help of a precision balance, we will add 28 mg of Azobis initiator that will allow the polymerization of the styrene.

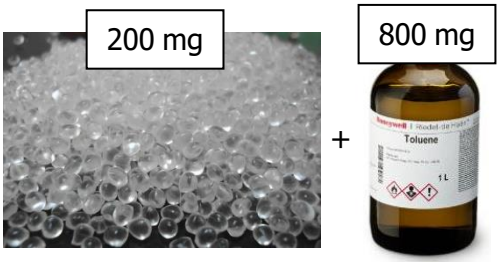

Figure 23: *Raw polystyrene on the left, toluene solvent on the right*

For the polystyrene, the steps are basically the same, but using 200 mg of polystyrene and 800 mg of Toluene which will act as solvent.

Figure 24: *Silicon elastomer on the left, its curing agent on the right*

Finally, with the PDMS, a viscous solution is formed from the mixture of 1 g of silicone elastomer and 0.1 g of curing agent.

Once we have the polymers, we have to mount the templates in cells similar to the anodizing cells. We use an O-ring of a suitable thickness so that at the time of pouring the polymer on the template, we can create a layer of several millimeters. This procedure is carried out in a vacuum configuration, as explained in the section *4.1.2.3 Vacuum-based polymer infiltration.* After adding the polymer on the surface of the template, we proceed to put it in the oven. In the case of PDMS, a temperature of 110 ºC for 3 h is enough to polymerize, for polystyrene 110 ºC for 5 min and styrene at 90º C overnight [34]. Despite the above conditions, in relation to the time, we had that in our experience was not sufficient for polymerization. That is why in most cases we opted to leave the samples for a whole day and periodically checking that the polymerization process has come to an end.

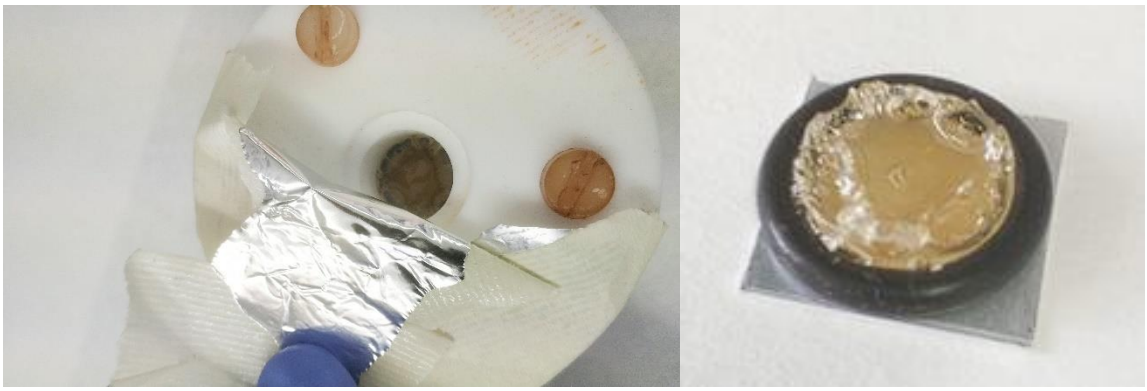

Figure 25: *On the left, cell containing a styrene replica after polymerization in the oven. Some bubbles can be seen, but just in the surface we are not interested in. On the right, close-up view of the polymeric replica once removed from the cell.*

Once the polymerization process is finished, we remove the sample from the cell and proceed to dissolve the template to obtain only the replica. According to section 2*.3.1 Removal of the template,* if the template has been subjected to the perfluorooctyltrichloro-silane step, it will be only necessary to manually pull the replica to separate it from the template. Otherwise, the sample will have to undergo a chemical treatment. For pAAO templates, we used hydrochloric acid (HCl) and copper chloride ($CuCl_2$) solution. As we can see in Figure 26, when the sample is introduced into the solution, the aluminum in the template begins to dissolve. We simply have to wait until visually no aluminum remains in the sample.

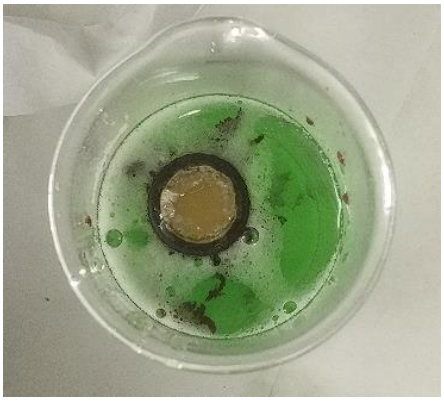

Figure 26: *Alumina template being dissolved in HCl + $CuCl_2$ solution*

Once the aluminum has been completely removed, the polymer is immersed in phosphoric acid (H_3PO_4) at 35 ºC for approximately half an hour (it can be also carried out at room temperature but will take longer). We also introduce a sample containing an alumina membrane, just to serve us as a guide, because when we see that this membrane starts to disappear, we know that the alumina layer of our replica is also dissolving. With this step, we eliminate the alumina layer allowing us to see later in the SEM the microstructures formed in the polymer (Figure 27). This last step was carried out after not being able to observe the microstructures in the first polymeric replicas implying that a layer of alumina was still present covering the microstructures.

Figure 27: *Polymeric replica immersed in phosphoric acid (H_3PO_4) at 35 ºC aprox.*

Figure 28 shows the final results after the above processes.

Figure 28: *Final replica made of styrene*

4.2.4 Sample preparation for SEM

With the polymeric replica already fabricated, we have to prepare our sample for its later observation in the SEM. In order to visualize the sample in the high-vacuum mode of the SEM, we first have to perform gold sputtering on the replica using the Q150T Plus. In our case, a gold sputtering at 30 mA for 180 s is enough, resulting in a deposition of around 30 nm layer of gold (Figure 29). After this, the replica is ready for SEM imaging.

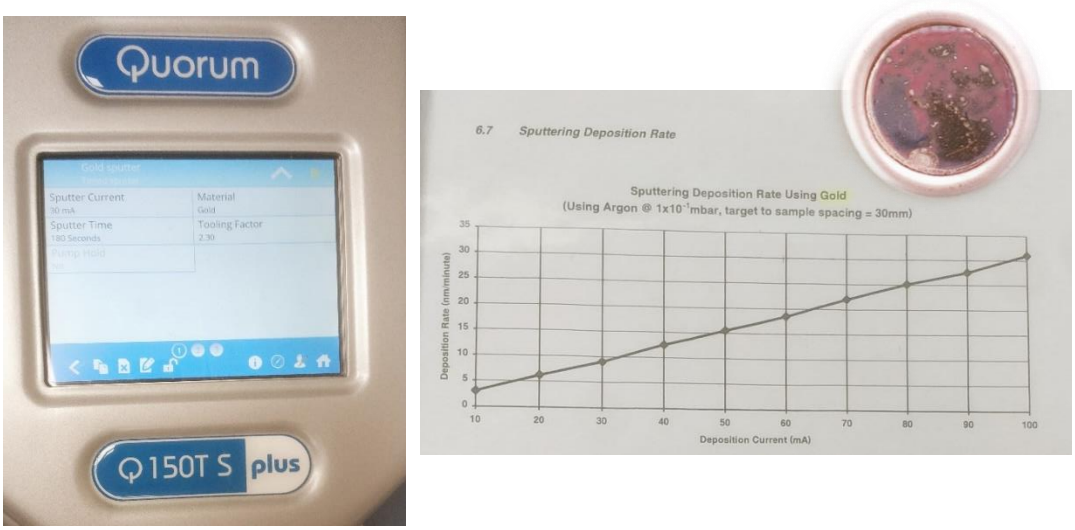

Figure 29: *On the left, parameters used for our gold sputtering. On the right, sputtering deposition rate of gold. Top-left, polymeric replica after gold sputtering ready for the SEM.*

4.2.5 SEM observation

All the control as well as the modification of microscope parameters, zoom, focus, etc., is done through a computer and a command table. Before introducing the samples into the SEM chamber, we must make sure that they have a flat and stable surface. In the case of the polymeric replicas where the area to be observed is the surface there is no problem, but when it comes to observe the cross-section of the macropSi samples, we have to resort to the holders shown in Figure 30. As a note, when we want to obtain results from the cross-section of a template, we have to split it in half, and submit the inner profile to a new gold sputtering.

Figure 30: *Holder used for cross-section examination.*

After introducing the templates into the sample chamber of the SEM, we seal it and wait until the pressure inside is adequate. After this and through the use of a specific software for the microscope control, we move the sample plate to the position where our sample is located. We raise the platform that holds the sample until it is at an adequate and safe distance from the detectors (10 mm approx.). After this, we project a beam of electrons on the sample obtaining a first blurred image. Now we simply have to find the right focus using the control panel where we find the macro-micrometer wheels for the focus, as well as the zoom wheels for the control of the image stigmatism. Once a sharp image is obtained, we can take measurements and save the images. The final images were acquired using two SEM imaging techniques: Backscattered-Electron Detector (BSED) Imaging, where the electrons detected are originated after elastic interactions between the beam and the sample, and the ETD (The Everhart–Thornley detector) technique or SE (Secondary Electrons), where the detected electrons are originated from the atoms of the sample. Depending on the technique used, we are able to appreciate different types of information of the sample. With BSED we have a better distinction between materials with different atomic numbers (higher atomic numbers result in a brightest image), while ETD can provide more detailed surface information.

5 Results and discussion

5.1 SEM results

In this section, first, macropSi templates images will be shown, followed by the replica results obtained. In order to see all the images from all the samples fabricated see section *8. Annex*.

SET A

Sample 4: 1st anodization at 2 mA – 1 h
2nd anodization at 4 mA – 4 min

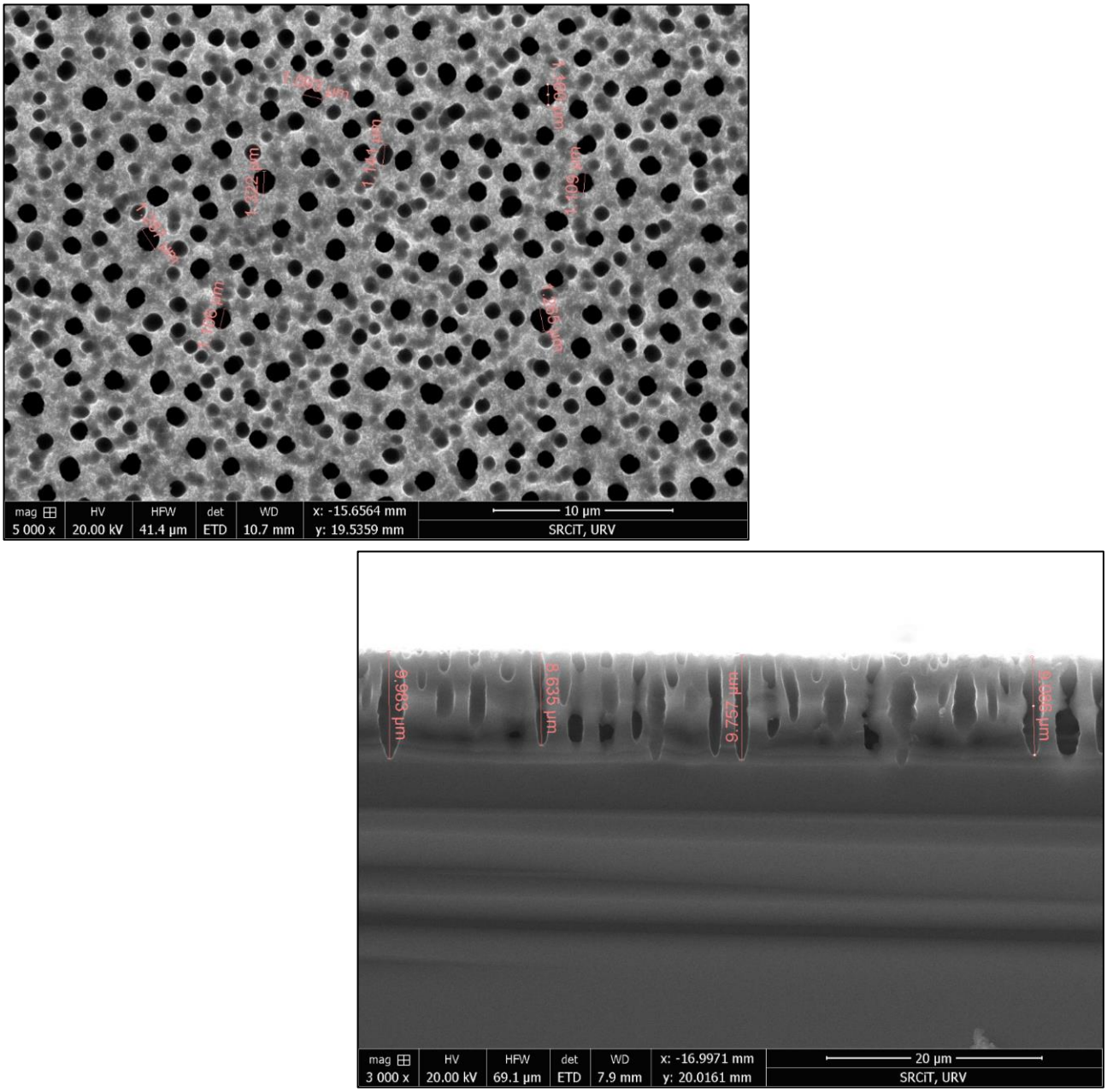

Figure 31: *SEM images of Set A / Sample 4 macropSi template. First image, top view with measurements using ETD mode. Second image, close up view of the cross-section with measurements using ETD mode.*

SET B

Sample 6: 1st anodization at 3 mA – 30 min
2nd anodization at 4 mA – 4 min

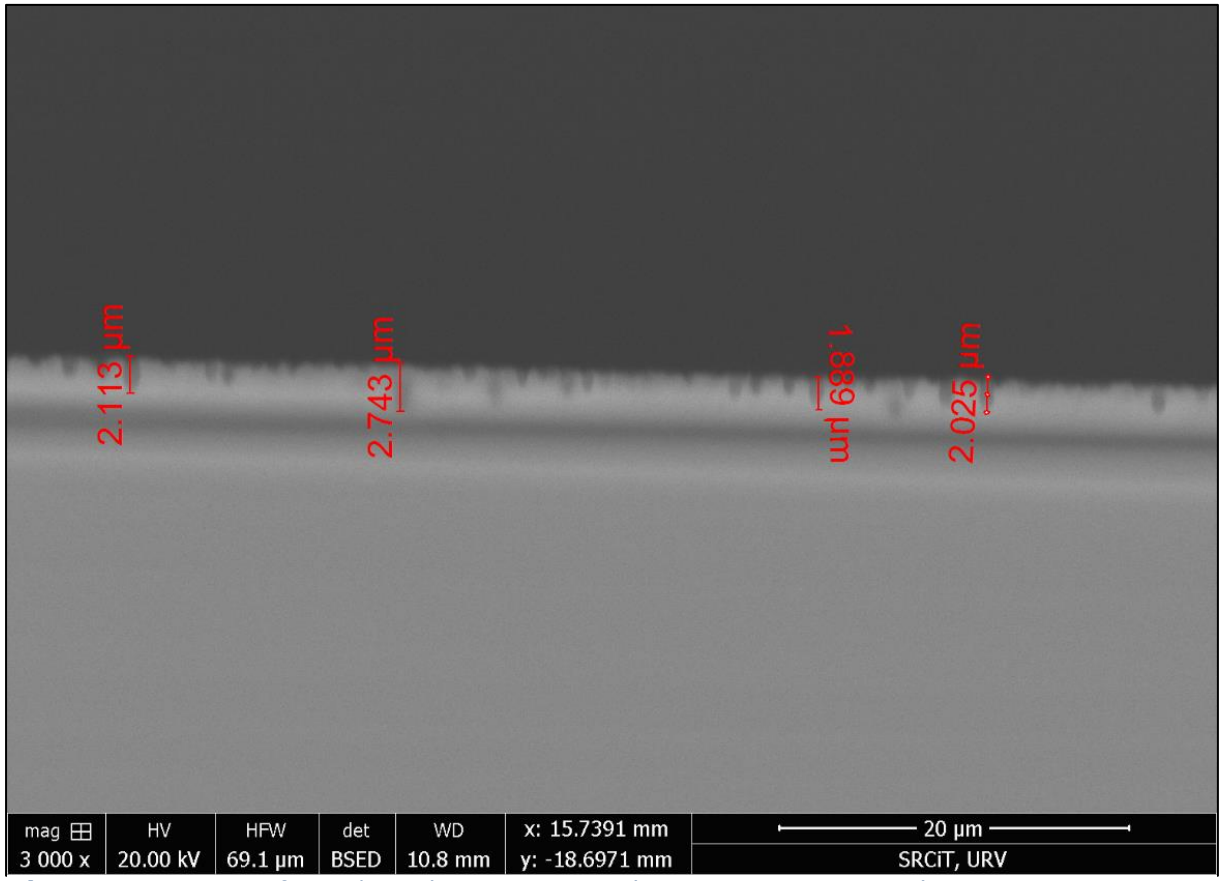

Figure 32: *SEM image of Set B / Sample 6 macropSi template. Cross-section view with measurements using BSED mode*

SET C

Sample 4: 1st anodization at 3 mA – 45 min
2nd anodization at 4 mA – 2 min

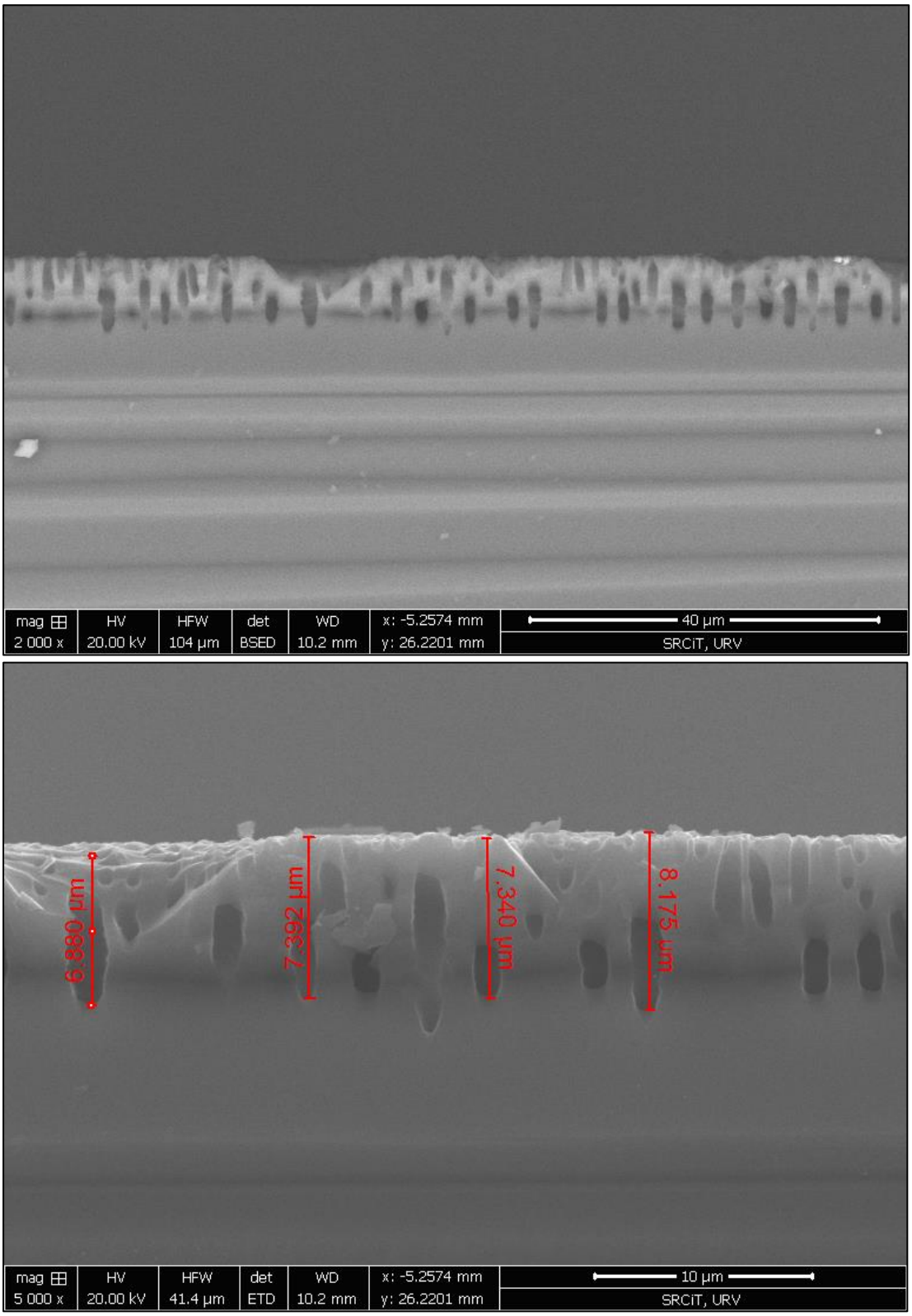

Figure 33: *SEM image of Set C / Sample 4 macropSi silicon template. First image, general cross-section view using BSED mode. Second image, close up view of the cross-section with measurements using ETD mode.*

REPLICA RESULTS

BEST STYRENE replica made from **POROUS ALUMINA TEMPLATE** (350 nm size / 7 µm depth)

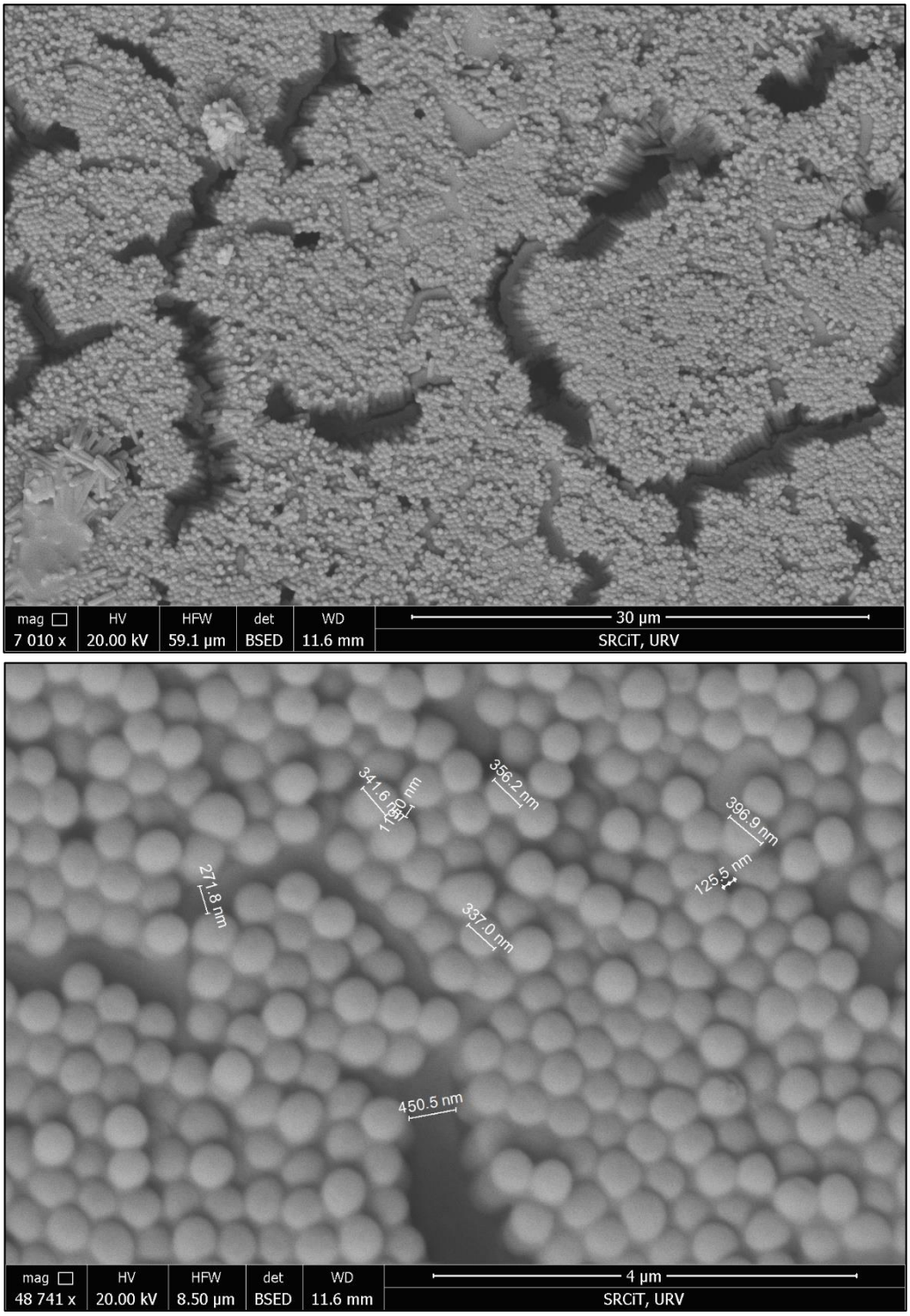

Figure 34: *SEM image of a polymeric replica made of STYRENE from NAA_7µm(thickness)_350nm(size) template. First image, general top view of the microstructures using BSED mode. Second image, close up top view of the micropillars with measurements using BSED mode.*

BEST POLYSTYRENE replica made from **POROUS ALUMINA TEMPLATE** (350 nm size / 7 µm depth)

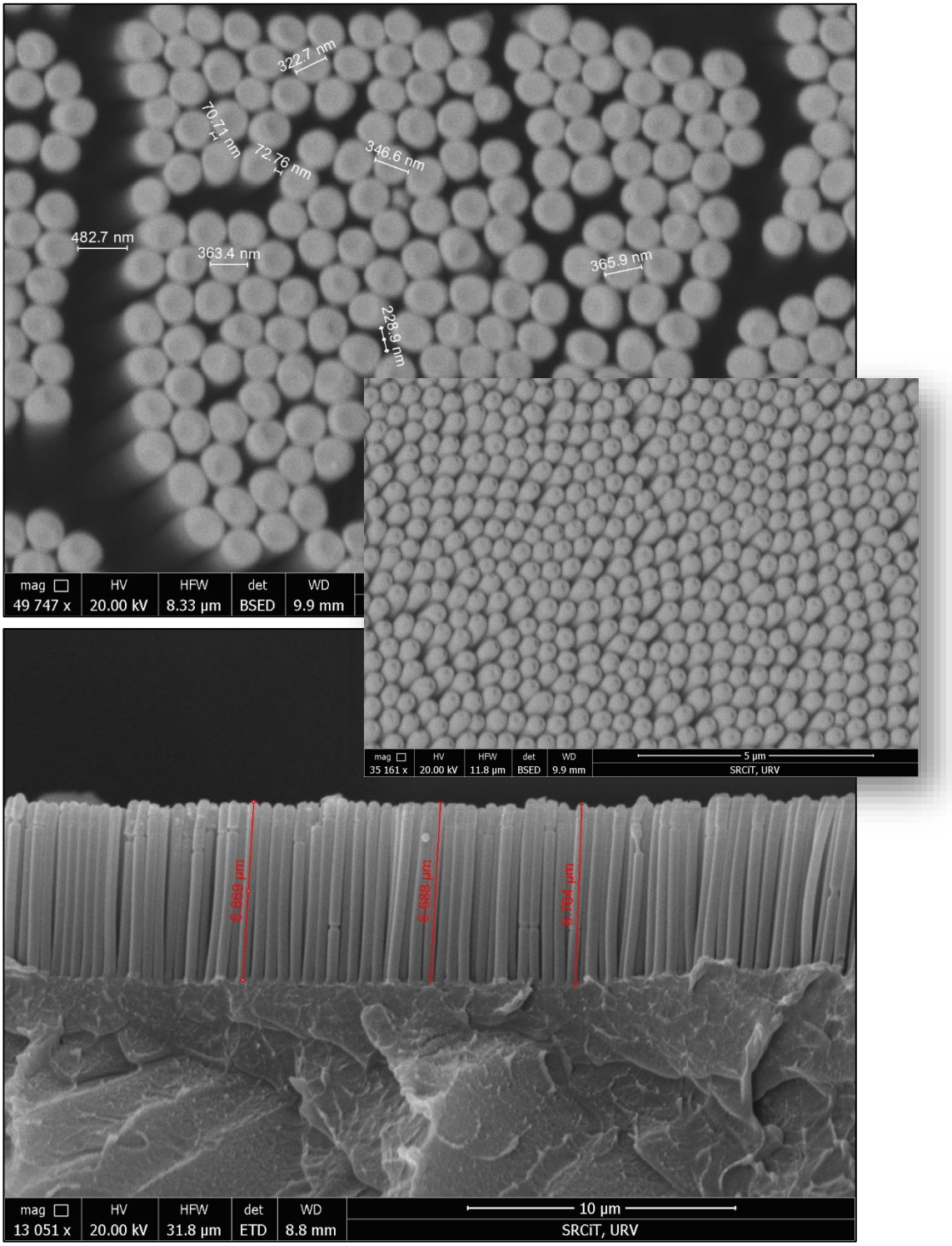

Figure 35: *SEM image of a polymeric replica made of POLYSTYRENE from NAA_7µm(thickness)_350nm(size) template. First image, top view of the microstructures with measurements using BSED mode. Second image, close up top view of the micropillars using BSED mode. Third image, close up cross-section view of the micropillars with measurements using ETD mode.*

BEST POLYSTYRENE replica made from **POROUS ALUMINA TEMPLATE** (250 nm size / 2 µm depth)

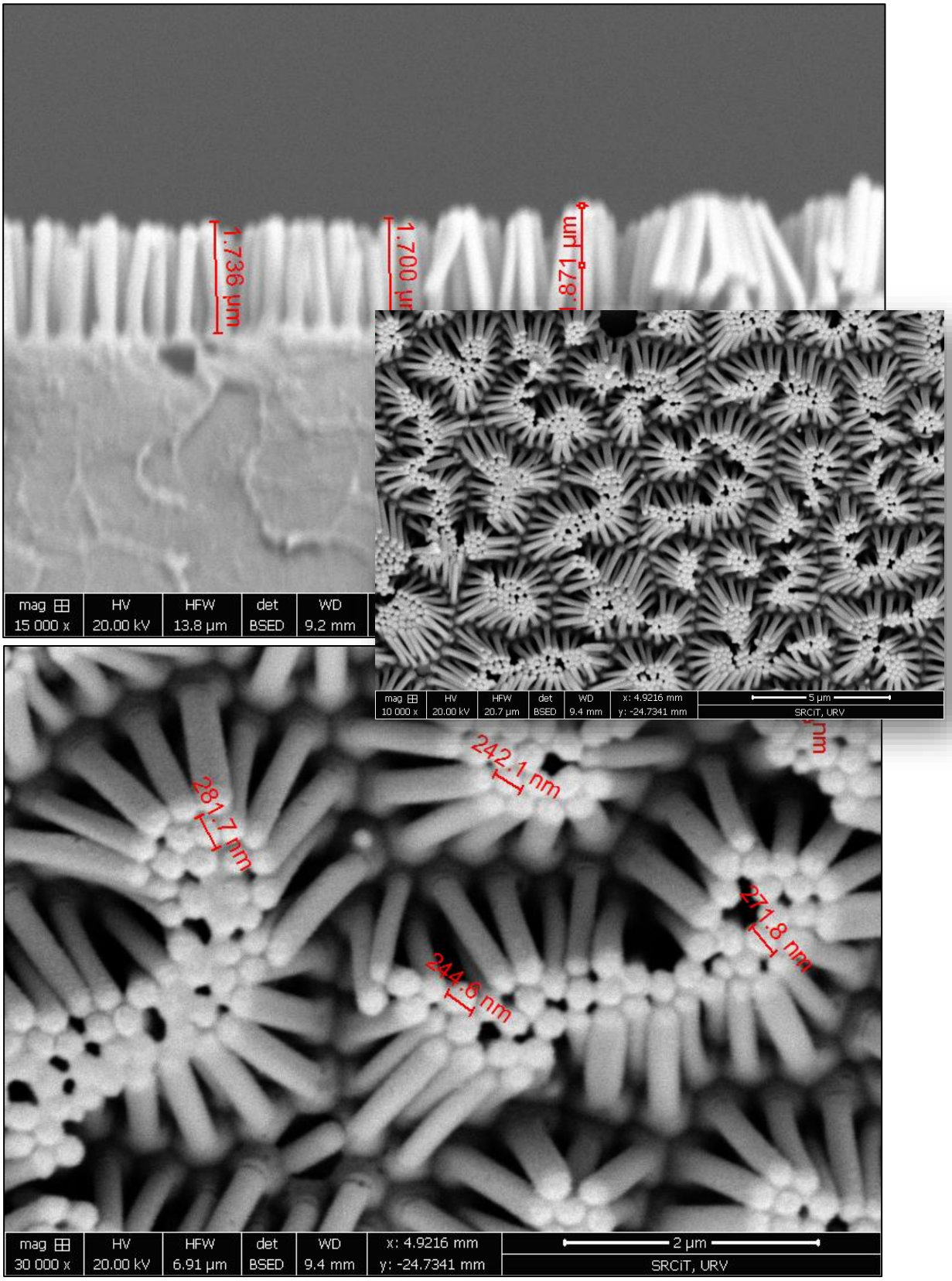

Figure 36: *SEM image of a polymeric replica made of POLYSTYRENE from NAA_7µm(thickness)_250nm(size) template. First image, close up cross-section view with measurements. Second image, general top view of the microstructures. Third image, close up top view of the micropillars with measurements. (BSED mode used in the whole set of images)*

BEST POLYSTYRENE replica made from **macropSi TEMPLATE**

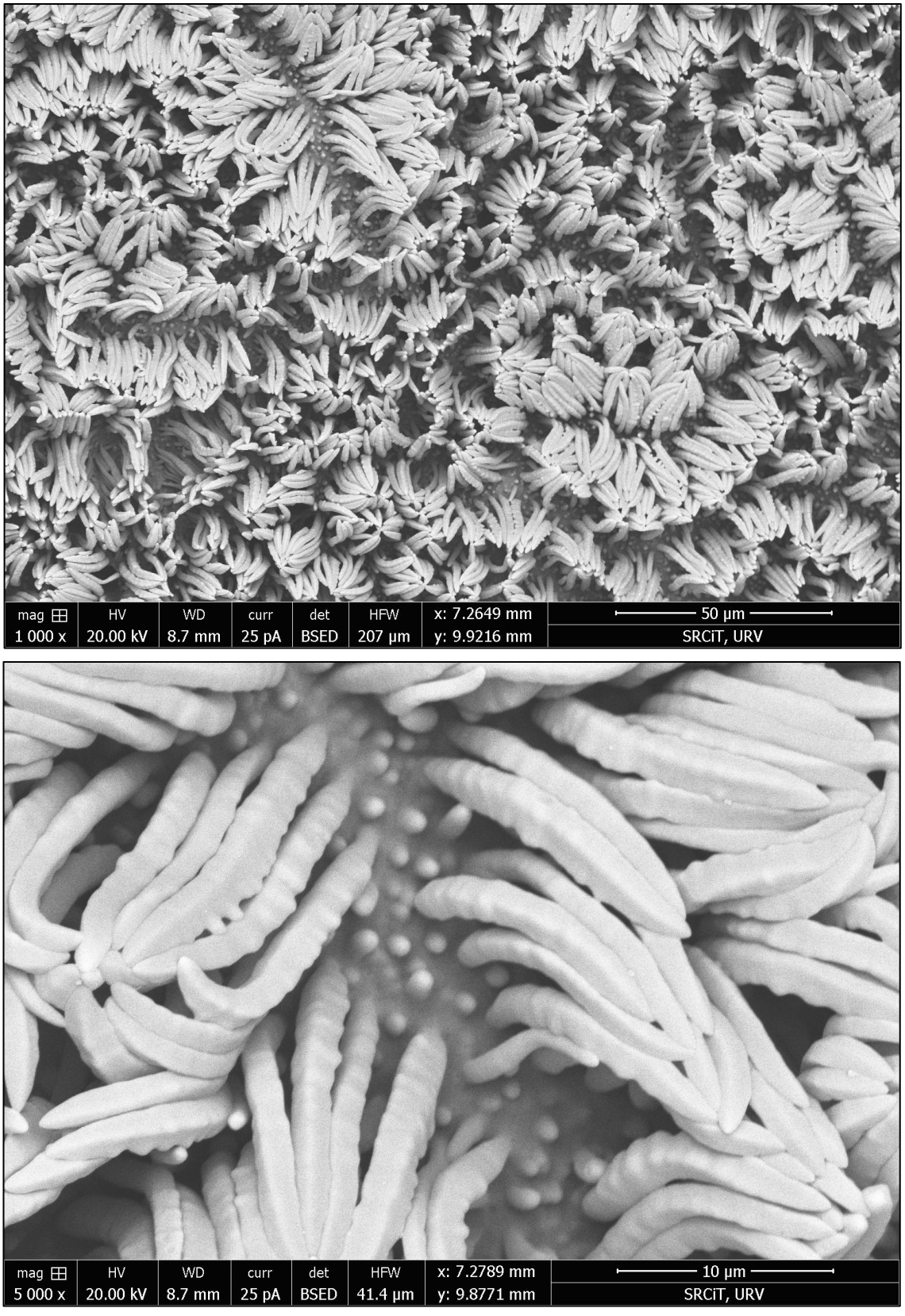

Figure 37: *SEM image of a polymeric replica made of POLYSTYRENE from macropSi template. First image, top view of the microstructures using BSED mode. Second image, close up top view of the micropillars using BSED mode.*

BEST PDMS replica made from **macropSi TEMPLATE**

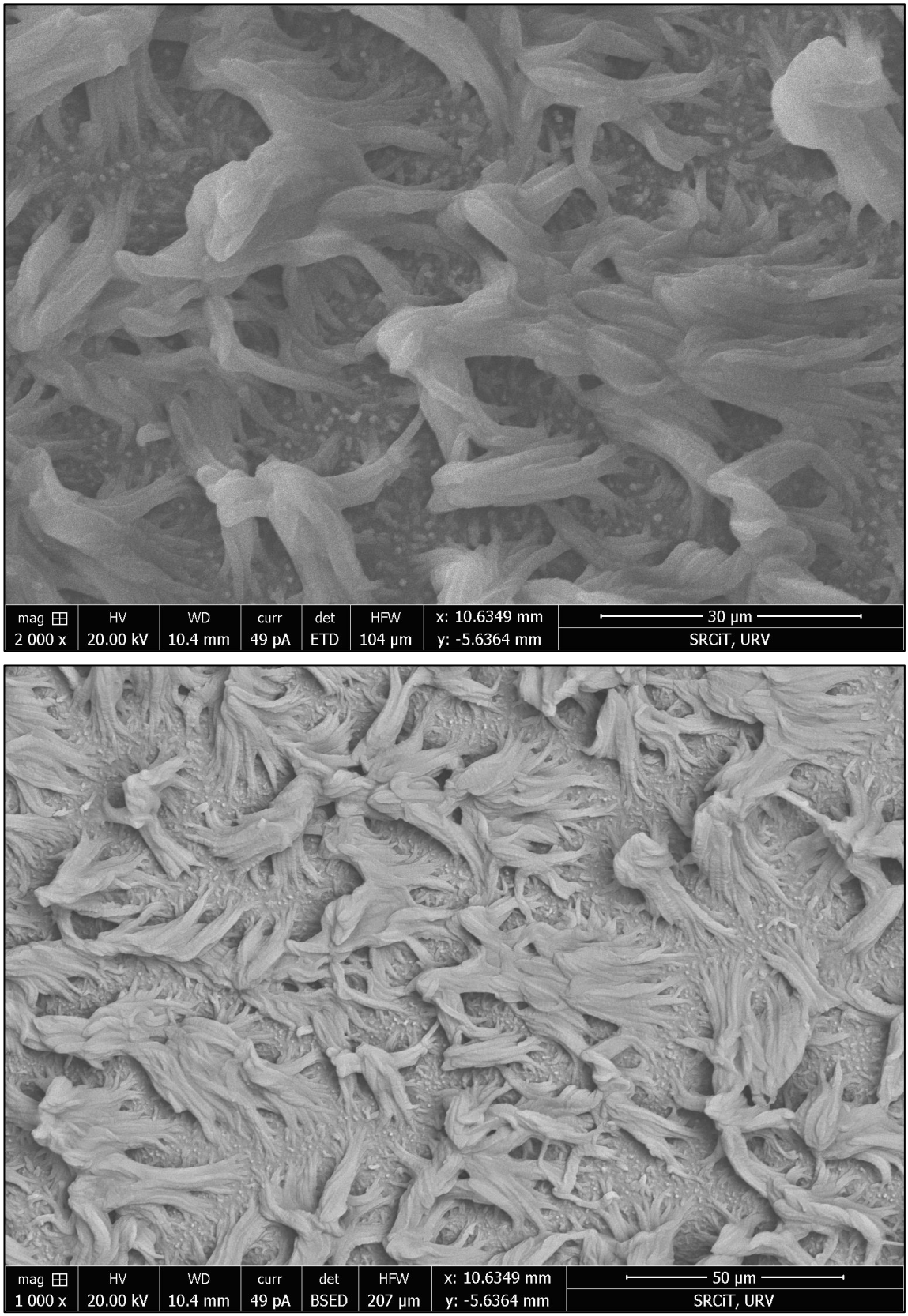

Figure 38: *SEM image of a polymeric replica made of PDMS from macropSi template. Both images show a top view of the micropillars. First one using BSED, second one with ETD mode.*

Before moving on to the discussion, I wanted to clarify that the results we are aiming for, in terms of pore size and pore thickness are 1 µm and 7 µm respectively. In addition, and in order to facilitate reading, from now on whenever reference is made to a sample, the nomenclature 1A, 2A, 3C will be used, being the numerical part the number of the sample and the letter the set to which it belongs (1st set = A, 2nd set = B, 3rd set = C).

SET A DISCUSSION

Table 3 shows the results of pore size and pore thickness for each of the macropSi samples of SET A. In order to have a better idea of how the anodization parameters affect the pore characteristics, we have also decided to order the samples from larger to smaller pore size, and finally from larger to smaller pore thickness.

First of all, let us note that all this set of samples has been subjected to the same conditions during the first anodization (2 mA for 1 h), therefore, we can be sure that the changes observed in the pore characteristics are **exclusively** the result of the way in which the second anodization has been carried out and the parameters used.

We observe in the table how the smallest pore size is shared by samples 2A and 4A, with 1185 ± 0.10 ± 0.09 nm, respectively. While sample 4A was only subjected to a second anodization of 4 mA for 4 min, sample 2A had in addition to the above, an extra anodization of 3 mA for 4 min. As can be seen, it seems that this extra step is not relevant in modifying the surface of the sample, even the pore thickness remains the same in the two samples. The next two samples with a higher pore size are 5A with 1273 ± 0.17 nm and 1A with 1300 ± 0.18 nm. We can observe that sample 1A has not been subjected to a second anodization, and even so, its pore size is not only very similar to that of 5A but also larger, reinforcing the hypothesis that perhaps the role of the second anodization is not entirely related to the widening of the pores. However, the sample with the largest pore size is 3A, which has been subjected to a second anodization of 3 and 4 mA for 2 and 2 minutes, respectively. Even so, we have again that the difference between the **pore sizes** of this set of samples, is **not too significant.**

Table 3: *Set A of macropSi samples with the anodization parameters used together with the averages calculated from all the measures taken in the SEM images for pore size and pore thickness*

	1st Anod Current (mA)	Time 1 (h)	2on Anod Current (mA)	Time 2 (min)	Avg. Pore size (nm)	Avg. Thickness (µm)
Sample 1	2	1	x	x	1300 ± 0,18	8,9 ± 0,40
Sample 2	2	1	3 and 4	4 and 4	1185 ± 0,10	9,4 ± 0,25
Sample 3	2	1	3 and 4	2 and 2	1327 ± 0,18	8,5 ± 0,44
Sample 4	2	1	4	4	1185 ± 0,09	9,4 ± 0,54
Sample 5	2	1	5	4	1273 ± 0,17	23,2 ± 0,18
Ordered by avg. Pore size (high to low)						
	1st Anod Current (mA)	Time 1 (h)	2on Anod Current (mA)	Time 2 (min)	Avg. Pore size (nm)	Avg. Thickness (µm)
Sample 3	2	1	3 and 4	2 and 2	1327 ± 0,18	8,5 ± 0,44
Sample 1	2	1	x	x	1300 ± 0,18	8,9 ± 0,40
Sample 5	2	1	5	4	1273 ± 0,17	23,2 ± 0,18
Sample 2	2	1	3 and 4	4 and 4	1185 ± 0,10	9,4 ± 0,25
Sample 4	2	1	4	4	1185 ± 0,09	9,4 ± 0,54
Ordered by avg. thickness (high to low)						
	1st Anod Current (mA)	Time 1 (h)	2on Anod Current (mA)	Time 2 (min)	Avg. Pore size (nm)	Avg. Thickness (µm)
Sample 5	2	1	5	4	1273 ± 0,17	23,2 ± 0,18
Sample 2	2	1	3 and 4	4 and 4	1185 ± 0,10	9,4 ± 0,25
Sample 4	2	1	4	4	1185 ± 0,09	9,4 ± 0,54
Sample 1	2	1	x	x	1300 ± 0,18	8,9 ± 0,40
Sample 3	2	1	3 and 4	2 and 2	1327 ± 0,18	8,5 ± 0,44

In relation to pore thickness, we can see at a glance how, in this case, the results obtained do **vary significantly** between samples. The sample with the smallest pore thickness coincides with the one that previously had the largest pores size, we are talking

about 3A. Having seen the above, this seems to make sense, since 3A is the sample with the mildest conditions of second anodization, both in current and time, excluding 1A which is the only one that has not been subjected to a second anodization and we would expect that its pore thickness would be less than that of 3A, but this is not the case. We have that 1A has a pore thickness greater than 3A by only a few tenths, 8.5 ± 0.44 µm of 3A vs. 8.9 ± 0.40 µm of 1A. Still, this small difference would not be a compelling fact that would conflict with our hypothesis that the second anodization actively participates in the pore thickness increase. The next two samples ,4A and 2A, have the same pore thickness 9.4 ± 0.54 µm and 9.4 ± 0.25 µm respectively. In spite of this, we can observe in the standard deviation how 2A presents a smaller variation. This would indicate that having undergone a second more aggressive anodization than 4A (it has been subjected to two steps), a better homogeneity of the pores has been obtained. Finally, the sample with the greatest pore thickness (by far) is 5A. We realize that despite not having been subjected to a second two-step anodization, it is the one that presents the most aggressive conditions with the highest current (5 mA) for the longest time (4 minutes). In addition, we also see that it is the sample that presents the smallest standard deviation with ± 0.18 µm. Seeing these results, we can affirm that the second anodization has a very important weight both in the increase of the pore thickness and in the homogeneity of the porous surface.

SET B DISCUSSION

Initially, this set was a failure resulting in flat macropSi templates with practically no pores. This happened because the electrolytic solutions were used in more fabrication rounds than they should have been. In general, the solutions had to be renewed after the fabrication of 4 or 5 templates. With this, new solutions were made and the set was repeated, resulting in what we will discuss below.

Since in SET A we obtained pore thicknesses greater than what we needed (6-7 µm approx.), we decided to experiment also with the parameters of the first anodization, hoping that by reducing these, the thickness of the pores would also be reduced while maintaining a good homogeneity. This is also why in this case, for Table 4, we only took into account the pore thickness since it was the most important parameter for us at that time. Specifically, we thought that, by reducing the anodization time by half, we would obtain pores with half the thickness, which, as we will see below, is totally false.

In this case, Table 4 will show the results obtained from SET B.

Table 4: *Set B of macropSi samples with the anodization parameters used together with the averages calculated from all the measures taken in the SEM images for pore size and pore thickness*

	1st Anod Current (mA)	Time 1 (min)	2on Anod Current (mA)	Time 2 (min)	Avg. Thickness (µm)
Sample 1	2	15	x	x	NO RESULTS
Sample 2	2	30	x	x	1,92 ± 0,40
Sample 3	3	15	x	x	NO RESULTS
Sample 4	3	30	X	X	2,16 ± 0,37
Sample 5	3	15	4	4	1,49 ± 0,07
Sample 6	3	30	4	4	2,19 ± 0,33

Ordered by avg. thickness (high to low)

	1st Anod Current (mA)	Time 1 (min)	2on Anod Current (mA)	Time 2 (min)	Avg. Thickness (µm)
Sample 6	3	30	4	4	2,19 ± 0,33
Sample 4	3	30	x	x	2,16 ± 0,37
Sample 2	2	30	x	x	1,92 ± 0,40
Sample 5	3	15	4	4	1,49 ± 0,07
Sample 1	2	15	x	x	NO RESULTS
Sample 3	3	15	x	x	NO RESULTS

NON-LINEAR RELATION CURRENT/TIME

We can observe how samples 3B and 1B, did not show any result, as can also be seen in Figures 54 and 52 (3B and 1B) attached in the annex section. What is happening here is that a first anodization time of 15 minutes, coupled with the absence also of a second anodization, is NOT sufficient to cause the formation of pores on the silicon surface. On the other hand, we observe how the following sample 5B, does show results despite also having been subjected to only 15 minutes of first anodization, witnessing the birth of small pores of 1.49 ± 0.07 µm. This is due to the fact that, unlike samples 1B and 3B, 5B has undergone a second anodization of 4 mA for 4 minutes, which are also relatively aggressive conditions. With this, we again witness the relevance of the second anodization in pore elongation, in addition to having discovered "threshold" conditions (a second anodization at 4 mA for 4 min induces pore formation after a first anodization of only 15 min). The next two samples (2B and 4B), share the same conditions except for the current value of the first anodization where in 2B it is 2 mA while in 4B it is 3 mA. As for the pore thickness, we have 1.92 ± 0.40 µm for 2B and 2.16 ± 0.37 µm for 4B. These results are fairly even, even so, 4B has those extra tenths due to the fact that its first anodization was performed at 3 mA. Although the second anodization seems to have relevance in the thickness of the pores, this does not mean that the first anodization is also important to a lesser extent, which we witnessed in these two samples. Finally, we have that sample 6B has the highest pore thickness because the first anodization was performed with the highest time and current values (3 mA for 30 min) as well as with the second anodization (4 mA for 4 min).

In general, although we have achieved what was proposed at the beginning of this discussion of reducing the thickness of the pores, the results of this set have not been entirely good, mainly due to the short first anodization time used. As a conclusion of this set, we conclude that a first anodization time longer than 30 min is necessary to obtain good results and that there is not a linear relationship between time and current as we can see in the attached figures taken from the study cited below (Figure 39) [33].

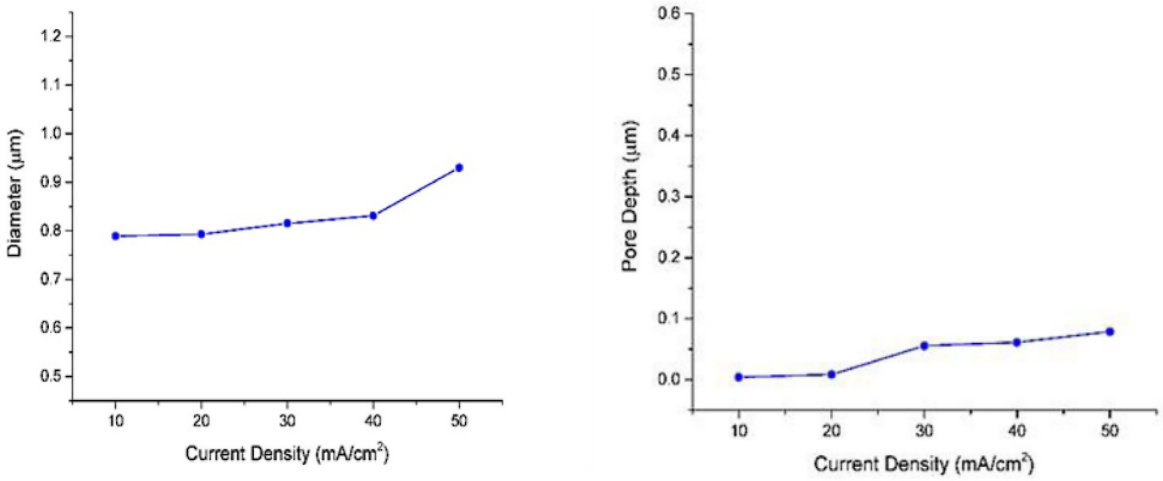

Figure 39: *On the left, relationship between current density and pore diameter of pSi. On the right, relationship between current density and pore depth of pSi.*

SET C DISCUSISON

At this point, we have that in SET A we obtained pores with a thickness too large to the one we want (6-7 µm), while with SET B we fell short and, even in some cases, we did not obtain results at all. That is why the parameters that we will find in this SET C, are halfway between SET A and SET B. Table 5 shows that the time used during the first anodization is more than 30 min (SET B) but less than 1 h (SET A), with the aim of obtaining pore thicknesses between 3 - 6 µm approximately.

We can see how 3C is the sample with the smallest pore thickness, with 1.57 ± 0.14 µm, as it has the shortest first anodization time. What is strange in this case is that 3C has been subjected to a second anodization of 4 mA for 2 min so it should have a thicker pore than 2C, but this is not the case since the latter has a pore depth of 4.82 ± 0.49 µm without having been subjected to a second anodization. Despite this, we observe that 3C has a more homogeneous surface than 2C and 1C despite having a shallower pore depth. Finally, we found a promising sample in 4C. This was subjected to 45 min of anodization at 3 mA and then a 4 mA anodization at 2 min was performed, resulting in a pore thickness of 7.45 ± 0.47 µm, which could be quite consistent and useful in our application.

Table 5: *Set C of macropSi samples with the anodization parameters used together with the averages calculated from all the measure taken in the images for pore size and pore thickness*

	1st Anod Current (mA)	Time 1 (min)	2on Anod Current (mA)	Time 2 (min)	Avg. Thickness (µm)
Sample 1	3	45	x	x	1,94 ± 0,28
Sample 2	3	37	x	x	4,82 ± 0,49
Sample 3	3	37	4	2	1,57 ± 0,14
Sample 4	3	45	4	2	7,45 ± 0,47
Ordered by avg. thickness (high to low)					
	1st Anod Current (mA)	Time 1 (min)	2on Anod Current (mA)	Time 2 (min)	Avg. Thickness (µm)
Sample 4	3	45	4	2	7,45 ± 0,47
Sample 2	3	37	x	x	4,82 ± 0,49
Sample 1	3	45	x	x	1,94 ± 0,28
Sample 3	3	37	4	2	1,57 ± 0,14

POLYMERIC REPLICAS DISCUSSION

The classification of the best results of polymeric replicas will be made according to two criteria:

1. macropSi templates vs pAAO templates
2. Type of polymer (styrene vs polystyrene vs PDMS)

In relation to the two types of templates used, we have found that in our experience, using pAAO templates we are able to obtain much straighter microstructures (pillars), with a good density and homogeneity between their thicknesses, and without showing important problems in terms of rupture or deformation of the microstructures. One of the best results obtained, which reinforces the above, can be found in the figure below (Figure 40). Two polymers were selected for the polymer replica. PS was selected as a rigid polymer and PDMS as a rubber. In addition, in-situ polymerization of styrene inside the template pores was studied.

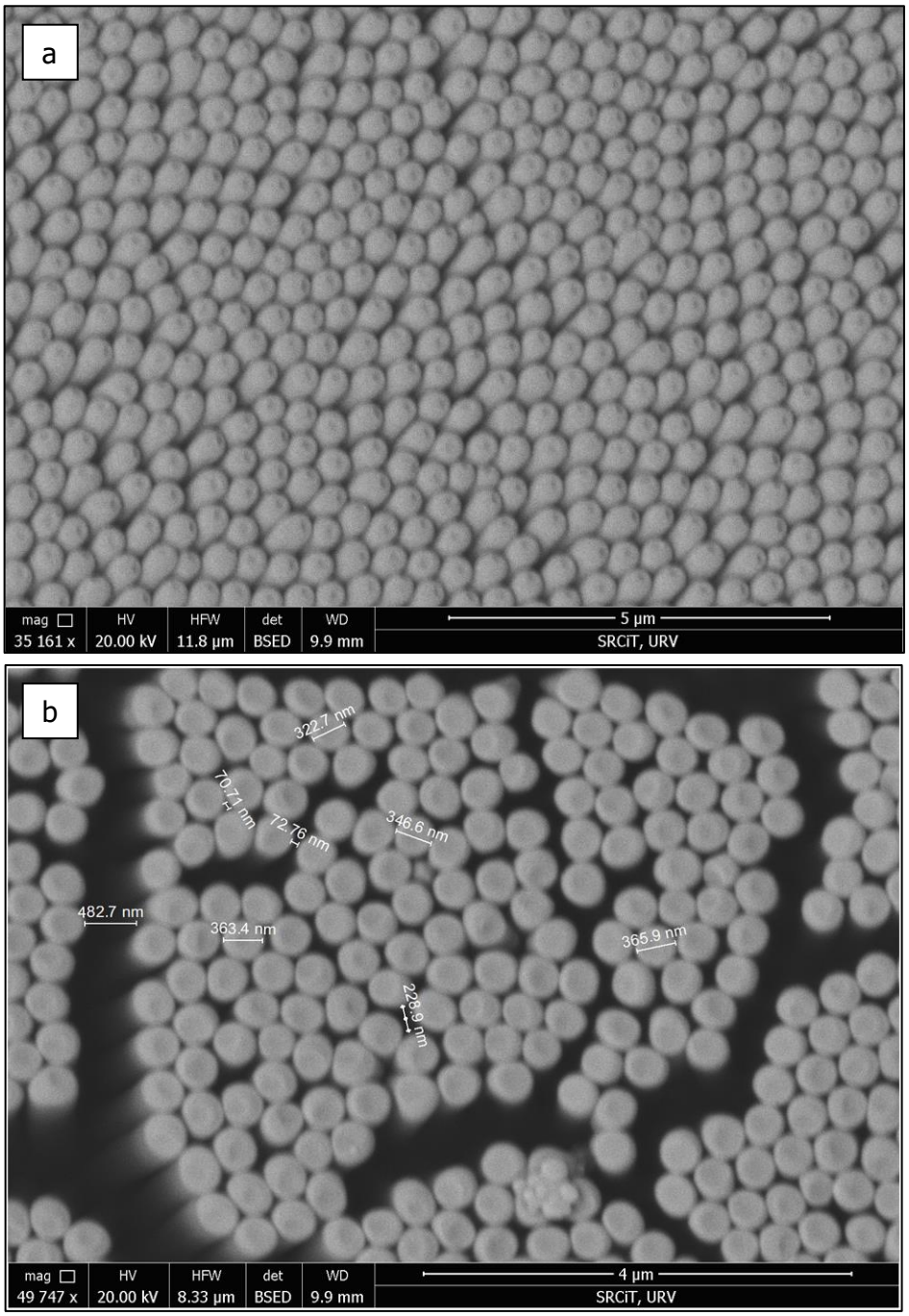

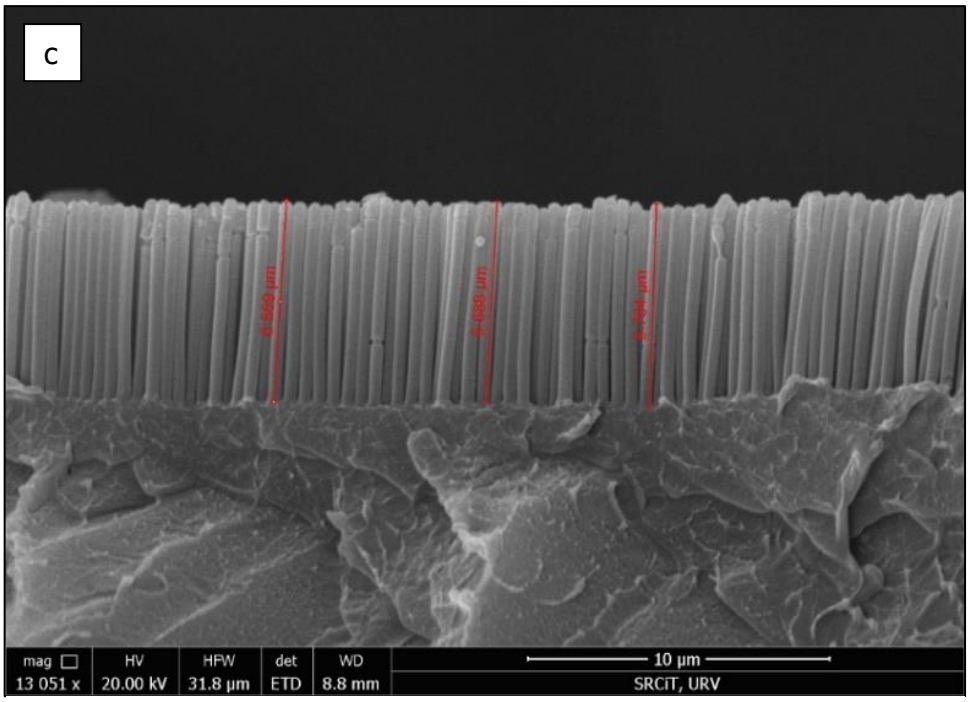

Figure 40: *Polymeric replica made of POLYSTYRENE from pAAO_7 µm(thickness)_350 nm(size) template.* ***a,*** *close up top view.* ***b,*** *general top view with measurements.* ***c,*** *close up of the cross-section with measurements.*

This template of 350 nm pore diameter and 7 µm depth resulted in microstructures of 6.71 ± 0.04 µm thickness, which is well within the target of 6-7 µm that we had. These highly ordered and homogeneous resulting microstructures have been made possible by the high stability of the honeycomb self-ordered porous structure of the pAAO. We can observe a good density of stable and straight pillars, without any collapse of microstructures. What can also be seen in Figure 41.b, is that there are some cracks separating the microstructures into domains. We discovered that this was due to the nature of the pAAO template itself as what we can see in the image, coincided with the pAAO domains created during its fabrication. These cracks can be seen in all the SEM polymeric replica images attached previously such as Figure 34 or Figure 36, made from pAAO templates.

Apart from these cracks, we also see a feature that, for our application in biosensors, can be quite detrimental, and that is the inter-pillar distance. As can be seen in Figure 41.a, seems that a polymeric replica made from a pAAO template presents a rather poor inter-pillar distance. This is very important, since in order to prepare the replica for testing as a biosensor in the future, a homogeneous coating made from gold will be necessary to proceed with the electrochemical techniques. Having this small distance between pillars is expected to be a limitation when trying to get a gold continuous and homogeneous layer. This is why obtaining replicas from macropSi seems to be the best choice, since from our experience and according to the results obtained previously from the optimization of the anodizing parameters, seems that replicas made from macropSi templates can offer a greater distance between pillars, as shown in Figure 41.

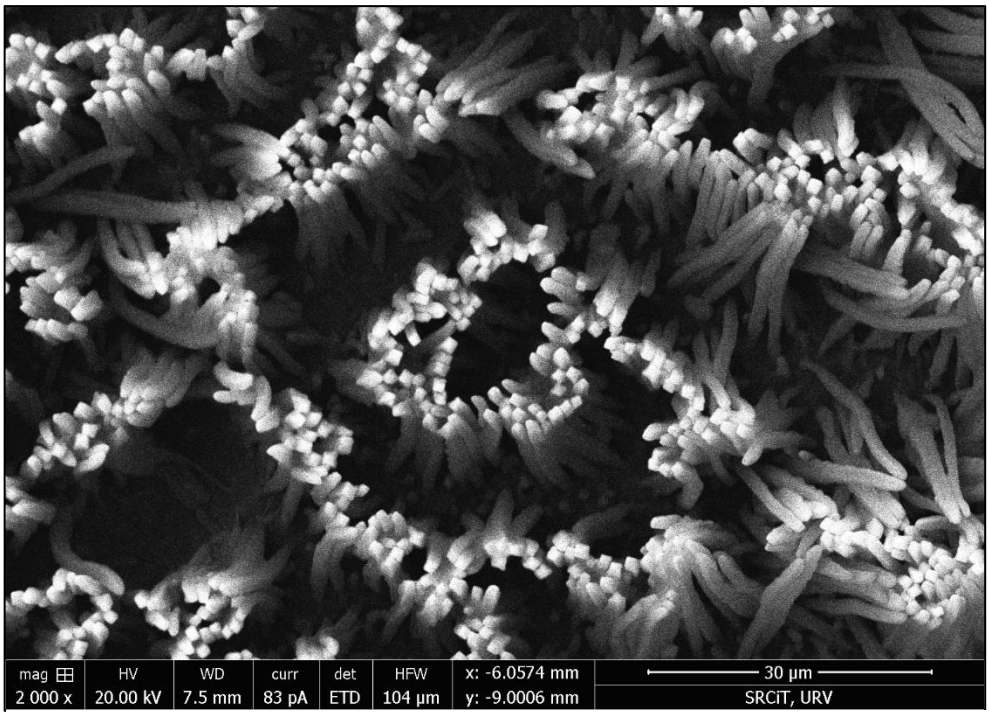

Figure 41: *SEM image of a polymeric replica made of POLYSTYRENE from macropSi template.*

However, the results obtained for polymeric replicas built from macropSi templates were not as good as those of replicas prepared from pAAO templates. In the replica shown in Figure 41, we have as a thickness of these microstructures about 25 µm. It is almost certain that their aspect ratio is posing a problem for the pillars to stay straight, which is why reducing this thickness could help. Another hypothesis to take into account would be the material, in the case of Figure 41 it is polystyrene, a very versatile material that could cause this twisting of the pillars. Perhaps, the use of a more rigid polymer could be used as a base for these microstructures in order to achieve a rigid and stable surface where the growth of straight pillars is possible. This leads us to discuss the results obtained depending on the polymer used.

Starting with styrene, this was the first polymer we decided to use for the manufacture of replicas. As can be seen in Figure 42, the results obtained are very good. The polymer fulfills its function and generates stable and well-shaped structures.

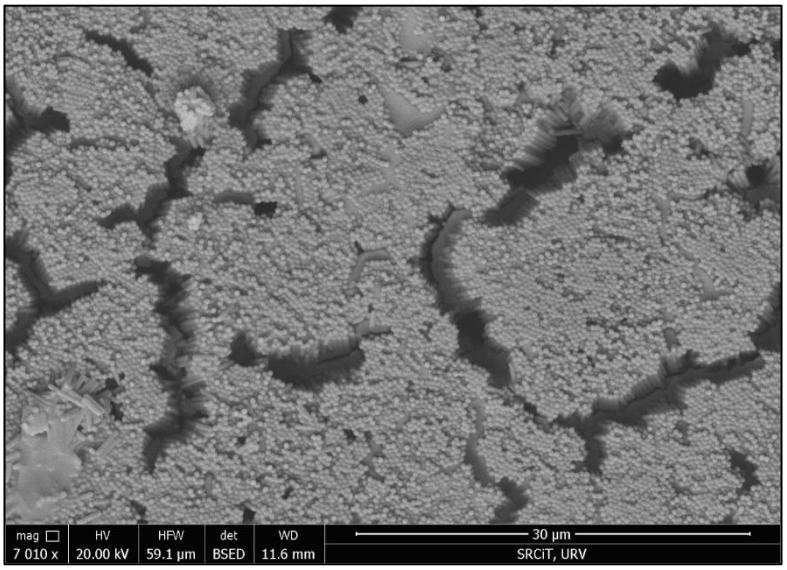

Figure 42: *Polymeric replica made of STYRENE from pAAO_7 µm (thickness)_350 nm (size) template*

In relation to polystyrene results, as we can see in the case of both pAAO and macropSi (Figure 43 and Figure 44), the pillars appear to collapse when using this polymer. While in the case of the macropSi template, the problem may again be due to the aspect ratio of the pillars (they are about 13 µm), in the case of the pAAO, the pillars are only about 2 µm. However, we should remember that previously we commented that this problem of collapsing between structures was due to the domains of the pAAO, so the objective here would be to find a pAAO fabrication methodology that eliminates these domains.

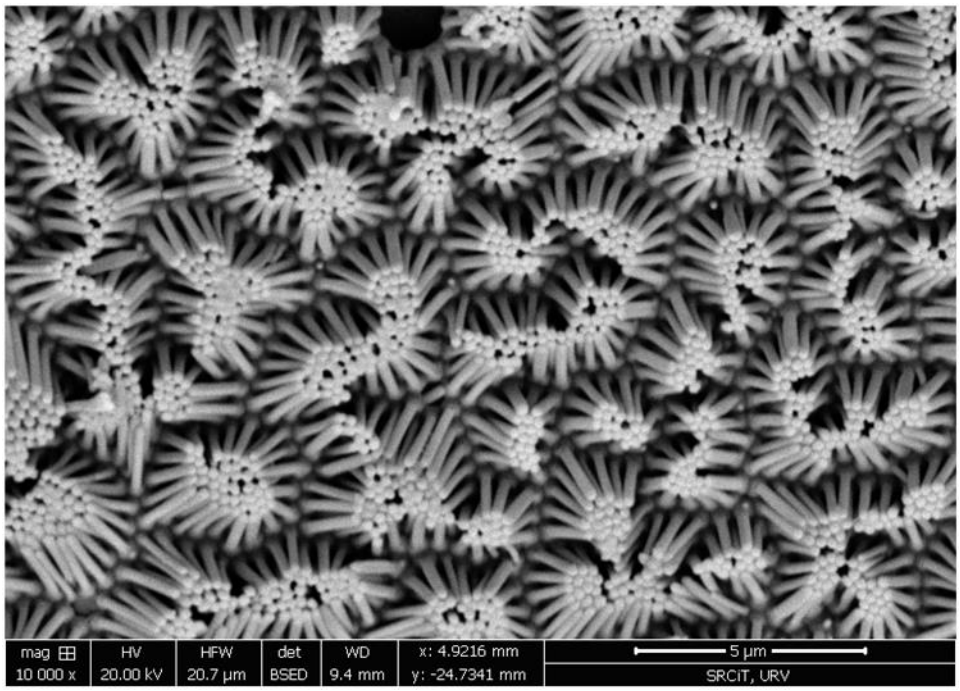

Figure 43: *Polystyrene replica made from porous alumina 250 nm size and 2 µm depth.*

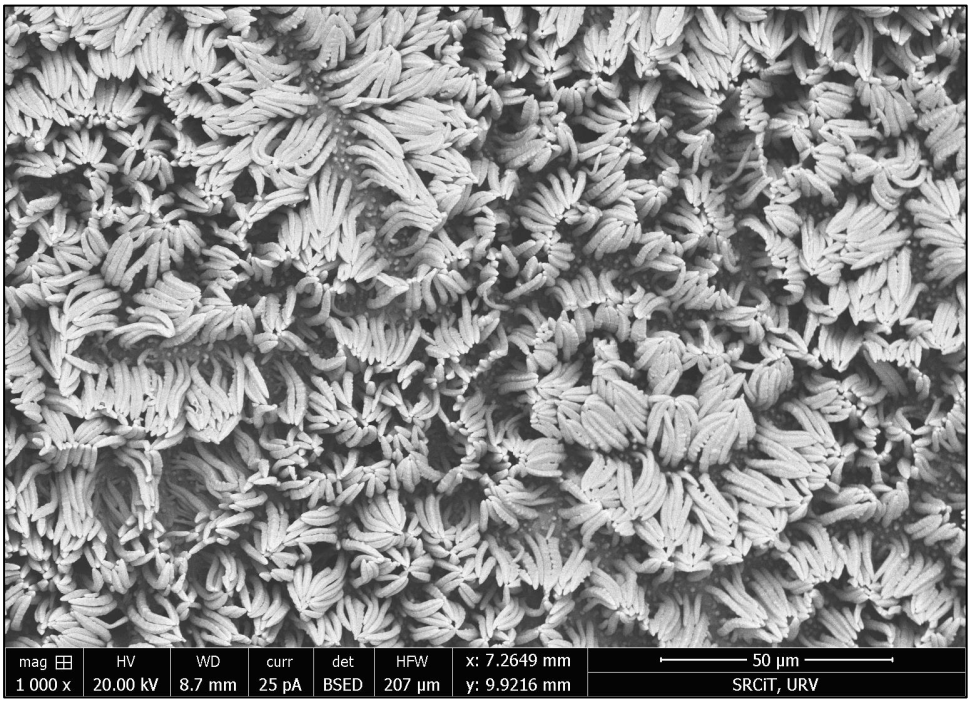

Figure 44: *Polystyrene replicas made from macropSi template*

Apart from this, we also thought that these problems could be due to the high temperatures to which the replica was subjected during the polymerization process in the oven, so we decided to test the fabrication of replicas with PDMS as it is a polymer characterized by its excellent thermal resistance, among many other properties such as its flexibility (it is a rubbery material). As we can see in Figure 45.b, the results were quite strange. Being PDMS, the problem could not be the temperature. We thought that it could be a reaction caused by the dissolution of the template due to the use of a too aggressive solution, but it could not be possible because the rest of the samples did not present this melting problem. After some research, we found a work [31] where the results obtained with PDMS (Figure 45.a), were similar to ours even with thinner pillars (2 μm). As reported there, the problem could be due to the softness of the PDMS.

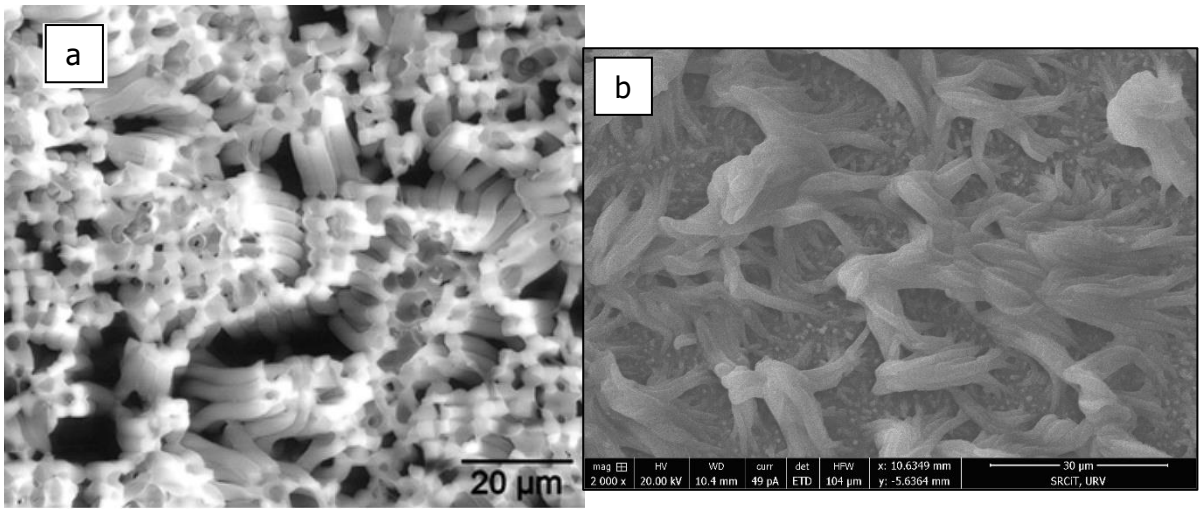

Figure 45: *On the left, PDMS replica from macropSi extracted from reference [31]. On the right, my result of PDMS replica*

5.2 Effectiveness of polymeric replicas for the detection of key biomarkers (Future Work)

Due to the work required to optimize the features of the polymeric replicas to be used in the development of electrochemical biosensors, the detection of key biomarkers could not be dealt with during the course of this project. This step was the one that followed after the obtention of the polymeric replicas. As we have seen, the replicas have been successfully obtained, but due to time constraints, their use for electrochemical sensing could not be explored. Next, polymeric replicas prepared using the optimum fabrication parameters will be prepared and then gold coated to allow them acting as electrodes. If they provide good electrochemical characterization, the next step will be to assess their performance towards the detection of an antibiotic, vancomycin.

6 Conclusion

From all the results discussed above, we can draw the following conclusions:

1. By optimizing the parameters involved in the macropSi anodizing process, we can state the following:

    a. The shorter the time of the second anodization, the larger the pore size will be.

    b. While the first anodization has a strong impact on the pore size, the second anodization has special relevance in providing better pore homogeneity, as well as larger pore thickness values the higher the current and the longer the anodizing time.

    c. First anodization times below 30 min, are not sufficient for the formation of pores on the silicon surface, unless this step is accompanied by a second anodization.

2. Obtaining correct polymeric replicas from the fabrication of pAAO/macropSi templates using the template-assisted method, is possible.

3. In case of polystyrene, both use of polymer solutions, and in-situ polymerization in the templates lead to the formation of pillar structures. However, the use of polymer solution and its addition in a vacuum cell leads to more uniform pillar structures.

4. The PDMS could be successfully used for the replica fabrication of micro-pillars.

5. Taking into account the morphological characteristics of the microstructures of the replicas, we obtain the best results using pAAO templates. Despite this, the replicas made from macropSi may have the right characteristics for their use in biosensing applications, especially because of their good inter-pillar distance.

6. In relation to the type of polymer, good results have been obtained with both styrene and polystyrene. Although we thought that PDMS would be a good choice for our replicas, according to our experiments it is difficult to obtain good results.

7 References

[1] National Institute of Environmental Health Sciences. 2022. Biomarkers. [online] Available at: < > [Accessed 23 August 2022].

[2] M. Dervisevic, M. Alba, L. Esser, N. Tabassum, B. Prieto-Simon, and N. H. Voelcker, "Silicon Micropillar Array-Based Wearable Sweat Glucose Sensor," ACS Applied Materials & Interfaces, vol. 14, no. 1, pp. 2401–2410, Dec. 2021, [Online]. Available: https://pubs.acs.org/doi/full/10.1021/acsami.1c22383 doi: 10.1021/acsami.1c22383.

[3] G. Rajeev, B. Prieto Simon, L. F. Marsal, and N. H. Voelcker, "Advances in Nanoporous Anodic Alumina-Based Biosensors to Detect Biomarkers of Clinical Significance: A Review," Advanced Healthcare Materials, vol. 7, no. 5, p. 1700904, Dec. 2017, doi: 10.1002/adhm.201700904.

[4] J. Kim, A. S. Campbell, B. E.-F. de Ávila, and J. Wang, "Wearable biosensors for healthcare monitoring," Nature Biotechnology, vol. 37, no. 4, pp. 389–406, Feb. 2019, doi: 10.1038/s41587-019-0045-y.

[5] Munje, R. D., Muthukumar, S., Jagannath, B. & Prasad, S. A new paradigm in sweat based wearable diagnostics biosensors using room temperature ionic liquids (RTILs). Sci. Rep. 7, 1950 (2017).

[6] Gao, W. et al. Fully integrated wearable sensor arrays for multiplexed in situ perspiration analysis. Nature 529, 509–514 (2016).

[7] Lee, H. et al. A graphene-based electrochemical device with thermoresponsive microneedles for diabetes monitoring and therapy. Nat. Nanotechnol. 11, 566–572 (2016)

[8] Lee, H. et al. Wearable/disposable sweat-based glucose monitoring device with multistage transdermal drug delivery module. Sci. Adv. 3, e1601314 (2017).

[9] Koh, A. et al. A soft, wearable microfuidic device for the capture, storage, and colorimetric sensing of sweat. Sci. Transl. Med. 8, 366ra165 (2016).

[10] Sekine, Y. et al. A fuorometric skin-interfaced microfuidic device and smartphone imaging module for in situ quantitative analysis of sweat chemistry. Lab Chip 18, 2178–2186 (2018).

[11] "Noviosense | Tear Glucose Sensor." http://noviosense.com/ (accessed Sep. 05, 2022).

[12] "Smart Contact Lens," sites.google.com. https://sites.google.com/site/smartcontactlens/ (accessed Sep. 05, 2022).

[13] Kim, J. et al. Wearable smart sensor systems integrated on soft contact lenses for wireless ocular diagnostics. Nat. Commun. 8, 14997 (2017).

[14] Kim, J. et al. Wearable salivary uric acid mouthguard biosensor with integrated wireless electronics. Biosens. Bioelectron. 74, 1061–1068 (2015).

[15] Mitsubayashi, K. & Arakawa, T. Cavitas sensors: contact lens type sensors & mouthguard sensors. Electroanalysis 28, 1170–1187 (2016)

[16] Tseng, P., Napier, B., Garbarini, L., Kaplan, D. L. & Omenetto, F. G. Functional, RF-trilayer sensors for tooth-mounted, wireless monitoring of the oral cavity and food consumption. Adv. Mater. 30, e1703257 (2018)

[17] Kim, J. et al. Non-invasive mouthguard biosensor for continuous salivary monitoring of metabolites. Analyst 139, 1632–1636 (2014).

[18] L. Ventrelli, L. Marsilio Strambini, and G. Barillaro, "Microneedles for Transdermal Biosensing: Current Picture and Future Direction," Advanced Healthcare Materials, vol. 4, no. 17, pp. 2606–2640, Dec. 2015, doi: 10.1002/adhm.201500450.

[19] M. Dervisevic, M. Alba, B. Prieto-Simon, and N. H. Voelcker, "Skin in the diagnostics game: Wearable biosensor nano- and microsystems for medical diagnostics," Nano Today, vol. 30, p. 100828, Feb. 2020, doi: 10.1016/j.nantod.2019.100828.

[20] W. Jia et al., "Electrochemical Tattoo Biosensors for Real-Time Noninvasive Lactate Monitoring in Human Perspiration," Analytical Chemistry, vol. 85, no. 14, pp. 6553–6560, Jul. 2013, doi: 10.1021/ac401573r.

[21] S. Campuzano, P. Yánez-Sedeño, and J. M. Pingarrón, "Electrochemical bioaffinity sensors for salivary biomarkers detection," TrAC Trends in Analytical Chemistry, vol. 86, pp. 14–24, Jan. 2017, doi: 10.1016/j.trac.2016.10.002.

[22] Kim et al., "Non-invasive mouthguard biosensor for continuous salivary monitoring of metabolites," The Analyst, vol. 139, no. 7, pp. 1632–1636, 2014, doi: 10.1039/c3an02359a.

[23] "Introduction to Porous Silicon," sailorgroup.ucsd.edu. https://sailorgroup.ucsd.edu/research/porous_Si_intro.html#:~:text=Porous%20silicon%20is%20a%20nanostructured%20material%20prepared%20by (accessed Aug. 28, 2022).

[24] K. Guo et al., "Porous Silicon Nanostructures as Effective Faradaic Electrochemical Sensing Platforms," Advanced Functional Materials, vol. 29, no. 24, p. 1809206, Apr. 2019, doi: 10.1002/adfm.201809206.

[25] P. Oller, "Nanosensors for therapeutic drug monitoring," Thesis, Universitat Rovira i Virgili, 2021.

[26] F. Karbassian, "Porous Silicon", in Porosity - Process, Technologies and Applications. London, United Kingdom: IntechOpen, 2018 [Online]. Available: https://www.intechopen.com/chapters/58683 doi: 10.5772/intechopen.72910

[27] R. Chhasatia, M. J. Sweetman, B. Prieto-Simon, and N. H. Voelcker, "Performance optimisation of porous silicon rugate filter biosensor for the detection of insulin," Sensors and Actuators B: Chemical, vol. 273, pp. 1313–1322, Nov. 2018, doi: 10.1016/j.snb.2018.07.021.

[28] Wikipedia Contributors, "Scanning electron microscope," Wikipedia, Jan. 08, 2019.

[29] "Q150T Plus - Turbomolecular pumped coater," Quorum Technologies Ltd. https://www.quorumtech.com/q150t-turbo-pumped-sputter-coatercarbon-coater/ (accessed Sep. 02, 2022).

[30] N. Elgrishi, K. J. Rountree, B. D. McCarthy, E. S. Rountree, T. T. Eisenhart, and J. L. Dempsey, "A Practical Beginner's Guide to Cyclic Voltammetry," Journal of Chemical Education, vol. 95, no. 2, pp. 197–206, Nov. 2017, doi: 10.1021/acs.jchemed.7b00361.

[31] R. Palacios, "FABRICATION AND CHARACTERIZATION OF POLYMER MICRO- AND NANOSTRUCTURES BY TEMPLATE-BASED METHOD," Thesis, Universitat Rovira i Virgili.

[32] D. Verma, Ed., "Bridging the gap between science and industry with technologies towards point-of care devices."

[33] B. Pratama et al., "Formation of porous silicon on N-type Si (100) and Si (111) substrates by electrochemical anodization method," Materials Today: Proceedings, vol. 44, pp. 3426–3429, Jan. 2021, doi: 10.1016/j.matpr.2021.02.832.

[34] Y. Y. Li et al., "Polymer Replicas of Photonic Porous Silicon for Sensing and Drug Delivery Applications," Science, vol. 299, no. 5615, pp. 2045–2047, Mar. 2003, doi: 10.1126/science.1081298.

[35] "Piranha solution," Wikipedia, Aug. 14, 2022. https://en.wikipedia.org/wiki/Piranha_solution (accessed Sep. 06, 2022).

[36] "Aluminum Anodizing | Full service Anodizing at amazing prices," Wisconsinmetaltech.com, Aug. 17, 2019. https://wisconsinmetaltech.com/aluminum-anodizing/

[37] H. Masuda and K. Fukuda, "Ordered Metal Nanohole Arrays Made by a Two-Step Replication of Honeycomb Structures of Anodic Alumina," Science, vol. 268, no. 5216, pp. 1466–1468, Jun. 1995, doi: 10.1126/science.268.5216.1466.

[38] "Anodic aluminium oxide," Wikipedia, Sep. 05, 2022. https://en.wikipedia.org/wiki/Anodic_aluminium_oxide#:~:text=Porous%20AAO%20is%20formed%20by%20electrochemical%20oxidation%20%28anodization%29 (accessed Sep. 06, 2022).

[39] "Electropolishing as a Pretreatment for Anodizing," www.pfonline.com. https://www.pfonline.com/articles/electropolishing-as-a-pretreatment-for-anodizing (accessed Sep. 06, 2022).

[40] R. Kazemi-Darsanaki, A. Azizzadeh, M. Nourbakhsh, G. Raeisi, and M. AzizollahiAliabadi, "Biosensors: Functions and Applications," Journal of Biology and Today's World, vol. 2, no. 1, 2013, doi: 10.15412/j.jbtw.01020105.

[41] "Interstitial Fluid and Lymph Formation and Transport: Physiological Regulation and Roles in Inflammation and Cancer | Physiological Reviews," Physiological Reviews, 2020. http://refhub.elsevier.com/S1748-0132(19)30314-7/sbref0095 (accessed Sep. 06, 2022).

[42] Z. Sonner et al., "The microfluidics of the eccrine sweat gland, including biomarker partitioning, transport, and biosensing implications," Biomicrofluidics, vol. 9, no. 3, p. 031301, May 2015, doi: 10.1063/1.4921039.

[43] S. Emaminejad et al., "Autonomous sweat extraction and analysis applied to cystic fibrosis and glucose monitoring using a fully integrated wearable platform," Proceedings of the National Academy of Sciences, vol. 114, no. 18, pp. 4625–4630, Apr. 2017, doi: 10.1073/pnas.1701740114.

[44] H.V.H. Scallan, R.J. Korthuis, The Interstitium, Capillary Fluid Exchange: Regulation, Functions, and Pathology, Morgan & Claypool Life Sciences, San Rafael (CA), 2010.

[45] Baca, J. T., Finegold, D. N. & Asher, S. A. Tear glucose analysis for the noninvasive detection and monitoring of diabetes mellitus. Ocul. Surf. 5, 280–293 (2007).

[46] Mishima, S., Gasset, A., Klyce, S. D. Jr. & Baum, J. L. Determination of tear volume and tear fow. Invest. Ophthalmol. 5, 264–276 (1966).

[47] "Square Wave Voltammetry (SWV)," Pine Research Instrumentation Store, Apr. 20, 2020. https://pineresearch.com/shop/kb/software/methods-and-techniques/voltammetric-methods/square-wave-voltammetry/ (accessed Sep. 06, 2022).

[48] O. Ikkala and G. ten Brinke, "Functional Materials Based on Self-Assembly of Polymeric Supramolecules," Science, vol. 295, no. 5564, pp. 2407–2409, Mar. 2002, doi: 10.1126/science.1067794.

[49] M. Bognitzki et al., "Nanostructured Fibers via Electrospinning," Advanced Materials, vol. 13, no. 1, pp. 70–72, Jan. 2001, doi: 3.0.co;2-h">10.1002/1521-4095(200101)13:1<70::aid-adma70>3.0.co;2-h.

[50] Kang, Y.H., Oh, S.S., Kim, Y.S. and Choi, C.G. (2010) Fabrication of Antireflection Nanostructures by Hybrid Nano-Patterning Lithography. Microelectronic Engineering, 87, 125-128.https://doi.org/10.1016/j.mee.2009.06.006

[51] "Electrochemical Impedance Spectroscopy (EIS)," PalmSens. https://www.palmsens.com/knowledgebase-article/electrochemical-impedance-spectroscopy eis/#:~:text=%20Electrochemical%20Impedance%20Spectroscopy%20%28EIS%29 20%201%20Electrochemical (accessed Sep. 06, 2022).

8 Annex

SET A

Sample 1: 1st anodization at 2 mA – 1 h

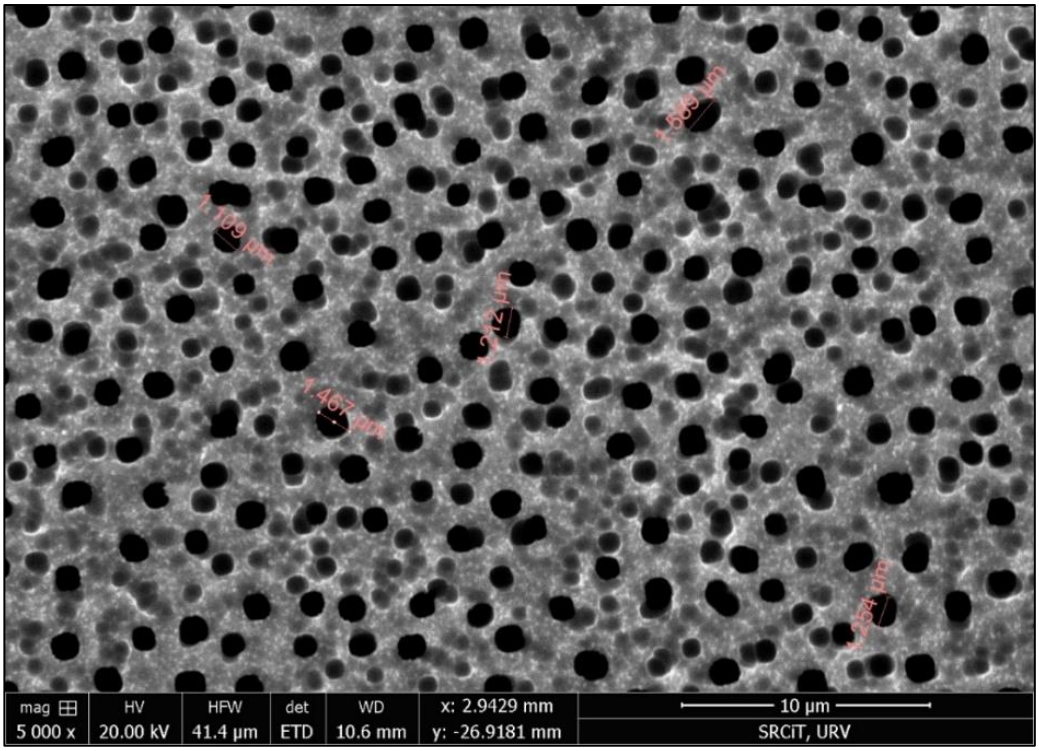

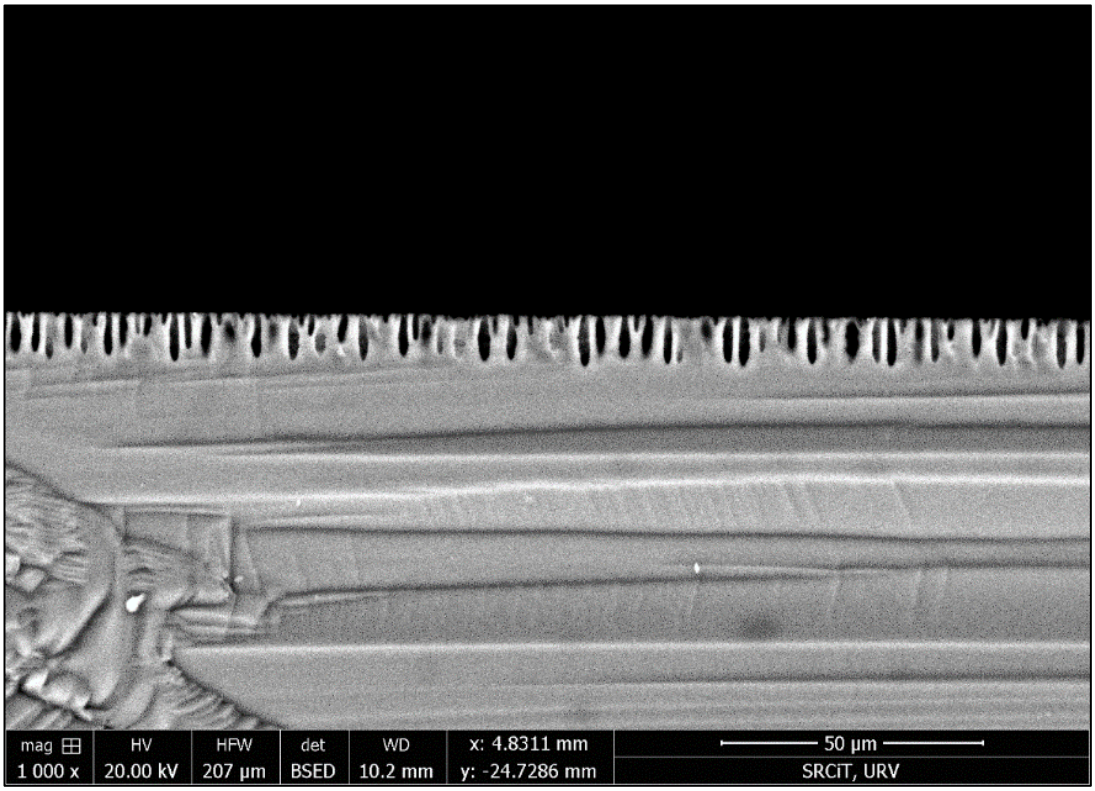

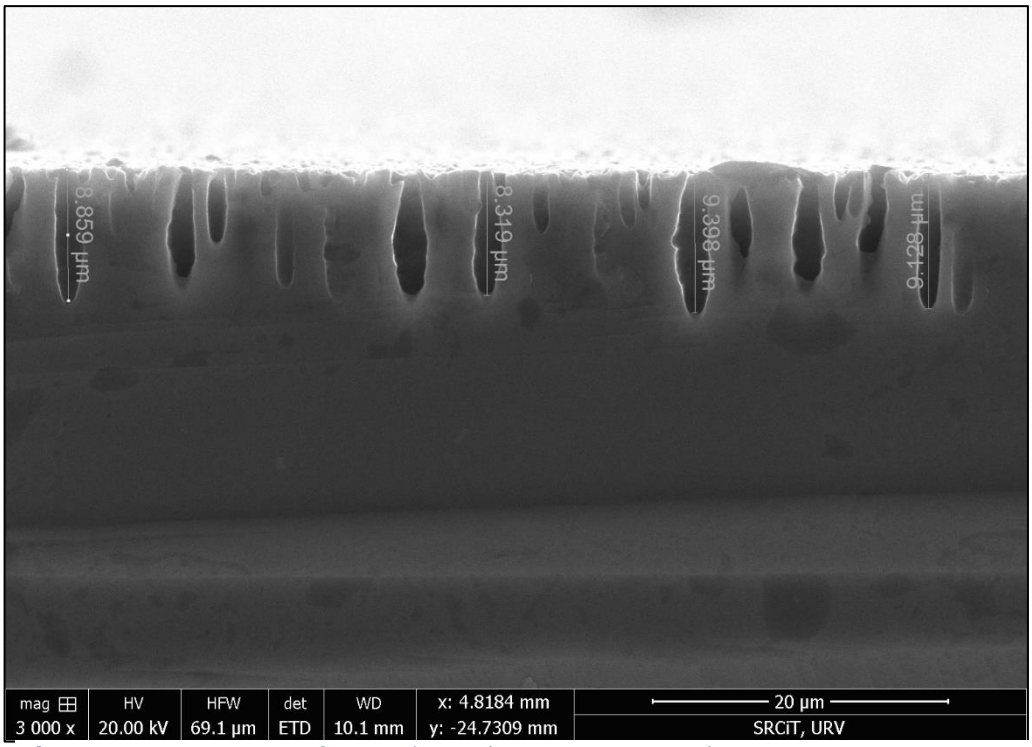

Figure 46: *SEM images of Set A / Sample 1 macropSi template. First image, top view with measurements using ETD. Second image, general cross-section view using BSED. Third image, close up view of the cross-section with measurements using ETD.*

Sample 2: 1st anodization at 2 mA – 1 h
2nd anodization at 3 mA – 4 min then 4 mA – 4 min

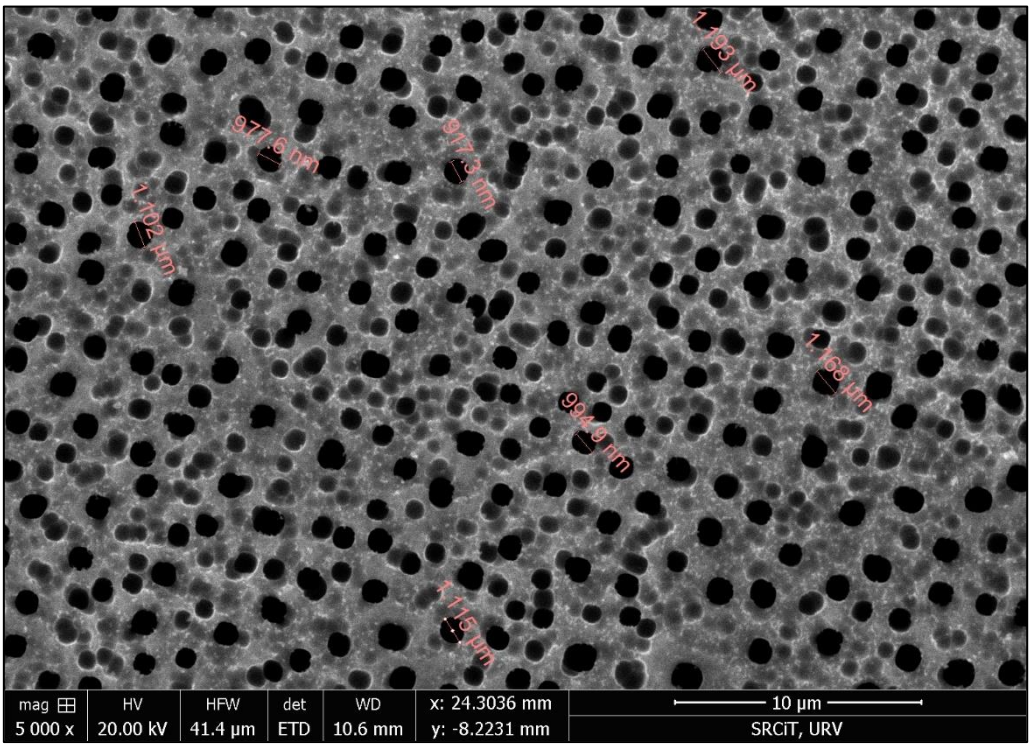

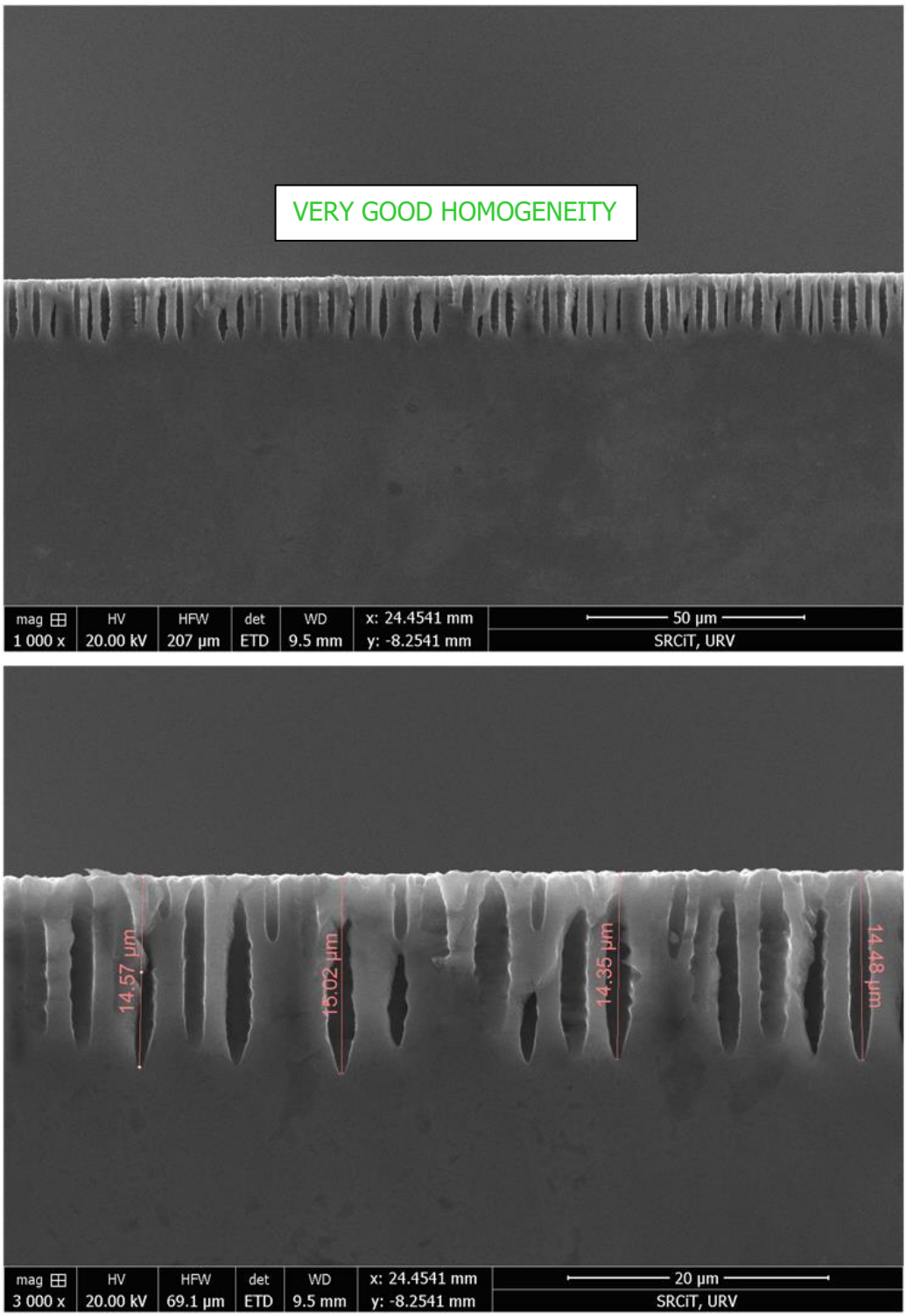

Figure 47: *SEM images of Set A / Sample 2 macropSi template. First image, top view with measurements using ETD. Second image, general cross-section view using ETD. Third image, close up view of the cross-section with measurements using ETD.*

Sample 3: 1st anodization at 2 mA – 1 h
2nd anodization at 3 mA – 2 min then 4 mA – 2 min

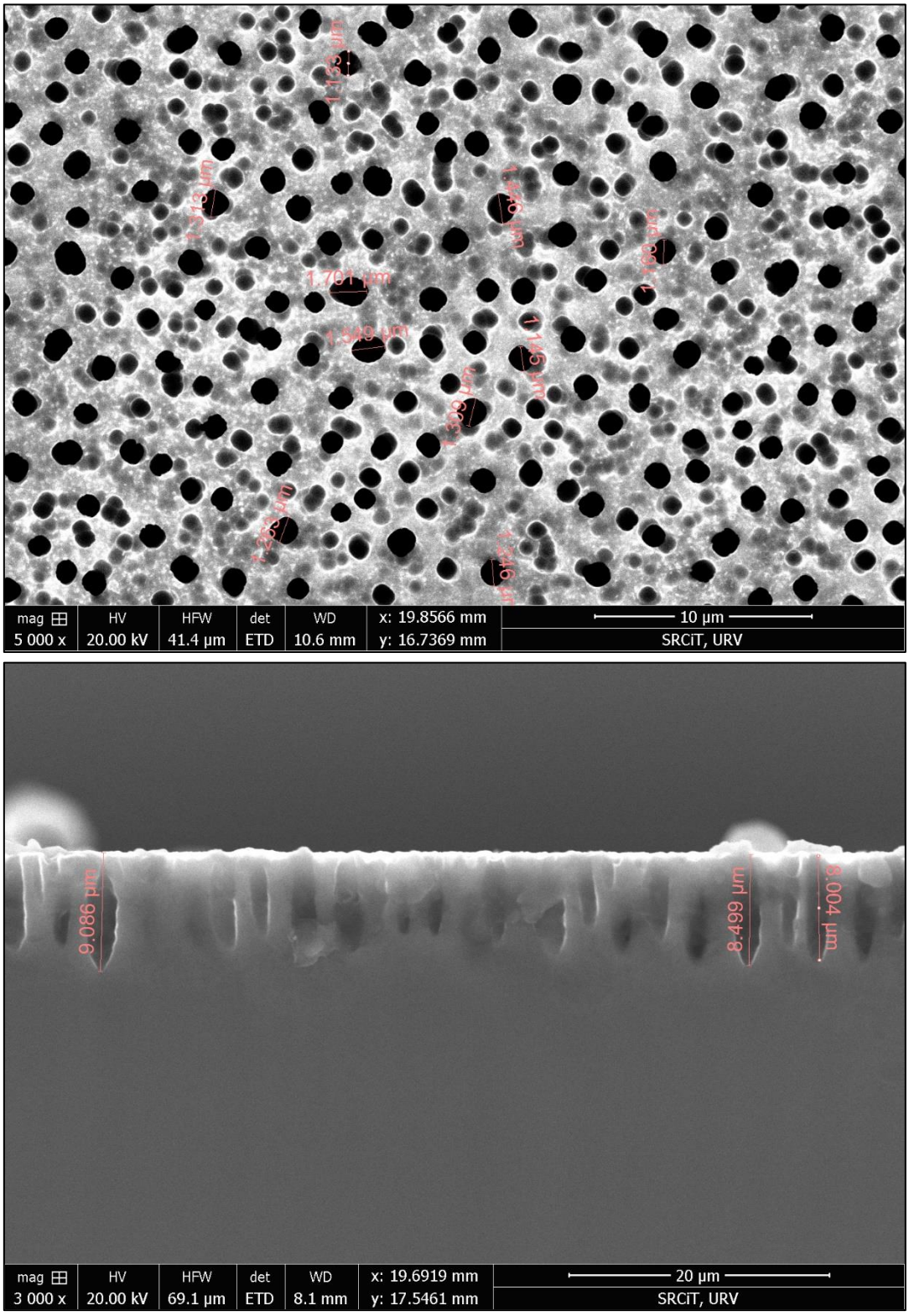

Figure 48: *SEM images of Set A/ Sample 3 macropSi template. First image, top view with measurements using ETD. Second image, close up view of the cross-section with measurements using ETD.*

Sample 4: 1st anodization at 2 mA – 1 h
2nd anodization at 4 mA – 4 min

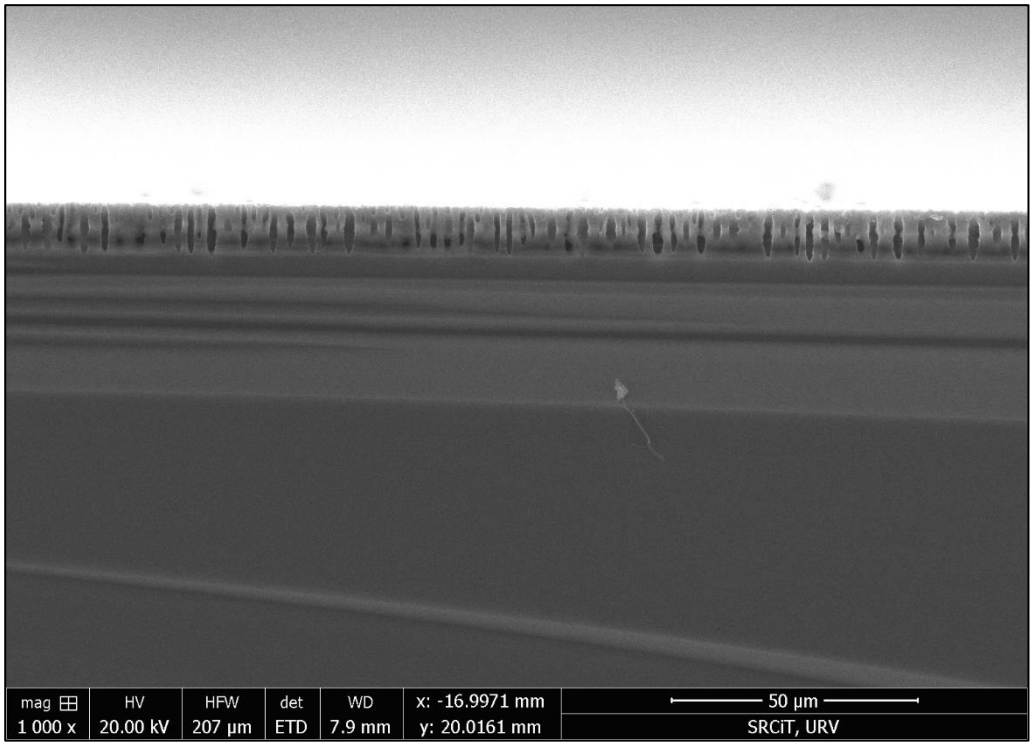

Figure 49: *SEM images of Set A / Sample 4 macropSi template. General cross-section view using ETD mode.*

Sample 5: 1st anodization at 2 mA – 1 h
2nd anodization at 5 mA – 4 min

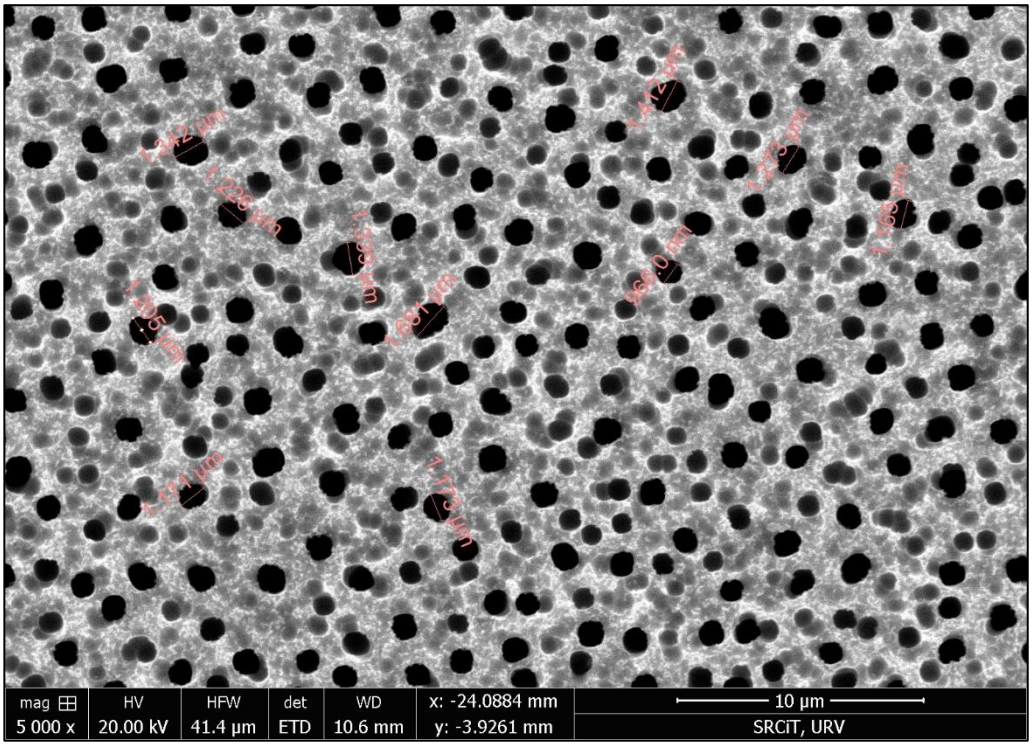

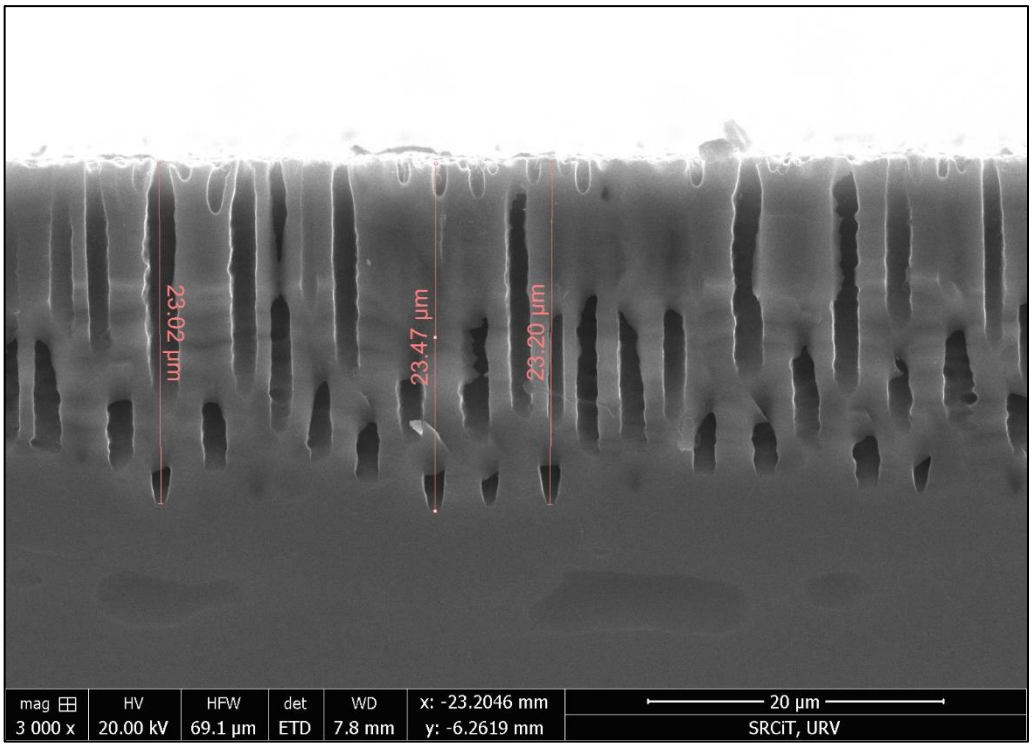

Figure 50: *SEM images of Set A / Sample 5 macropSi template. First image, top view with measurements using ETD. Second image, close up view of the cross-section with measurements using ETD.*

SET B

Sample 1: 1st anodization at 2 mA – 15 min

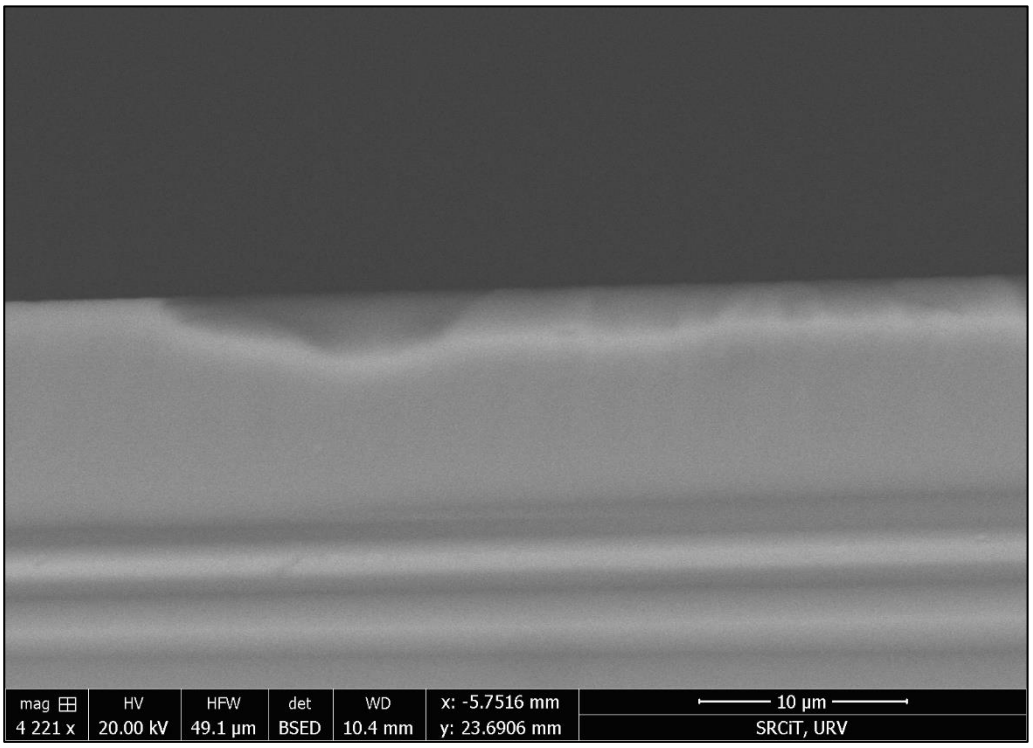

Figure 51: *SEM image of Set B / Sample 1 macropSi template. Cross-section view using BSED*

Sample 2: 1st anodization at 2 mA – 30 min

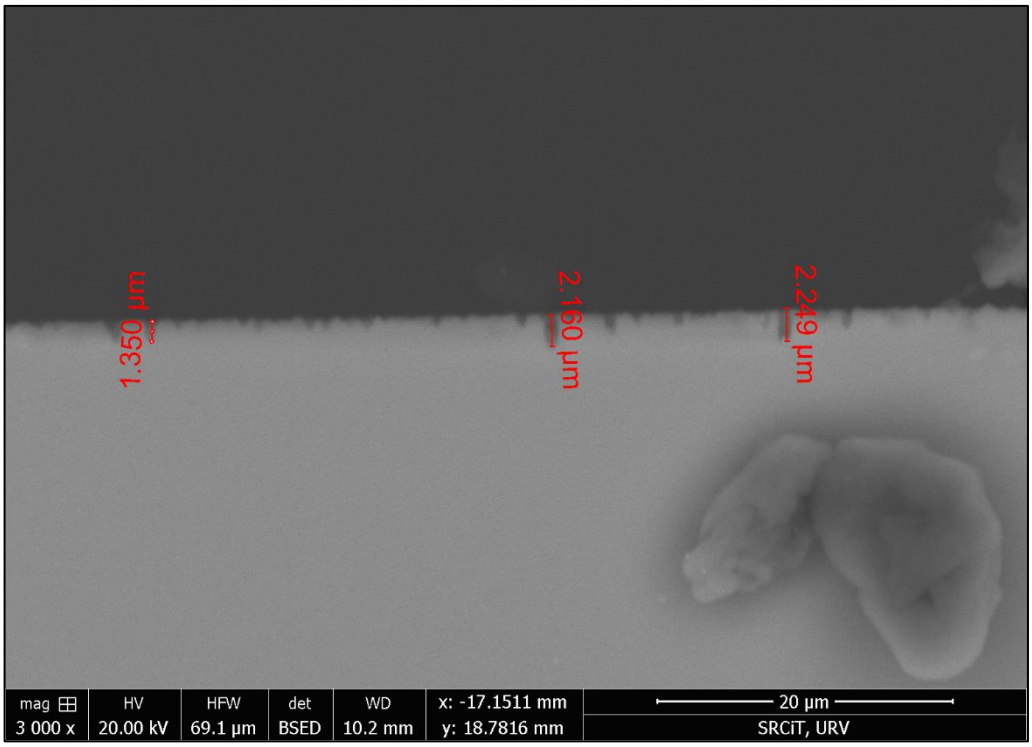

Figure 52: *SEM image of Set B / Sample 2 macropSi template. Cross-section view with measurements using BSED*

Sample 3: 1st anodization at 3 mA – 15 min

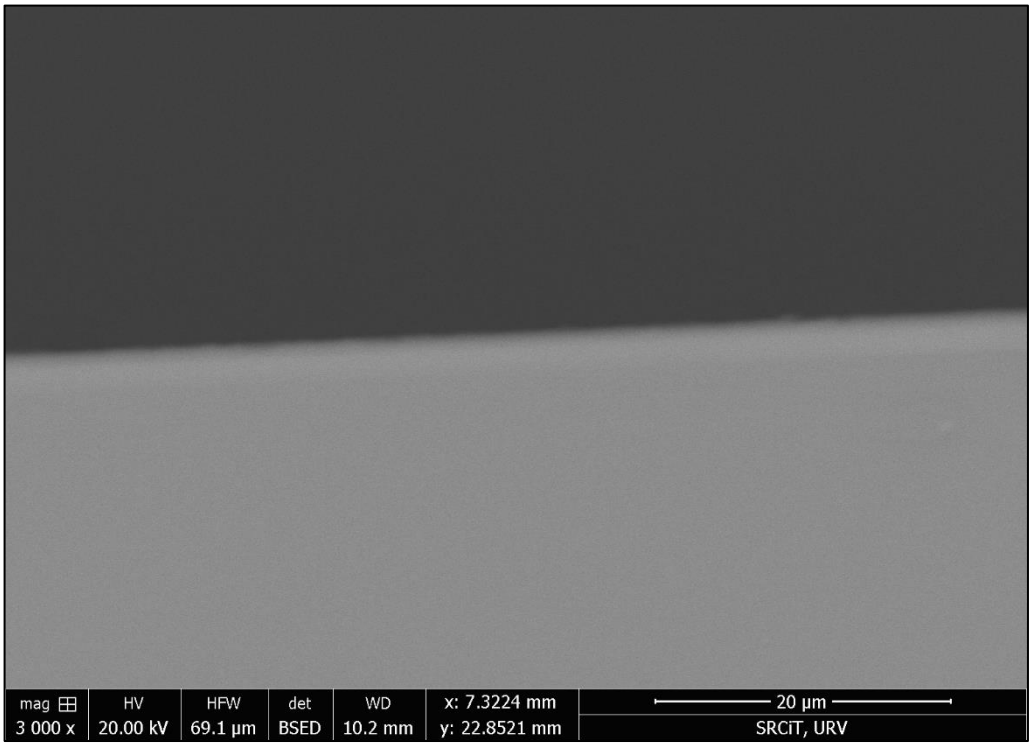

Figure 53: *SEM image of Set B / Sample 3 macropSi template. Cross-section view using BSED*

Sample 4: 1st anodization at 3 mA – 30 min

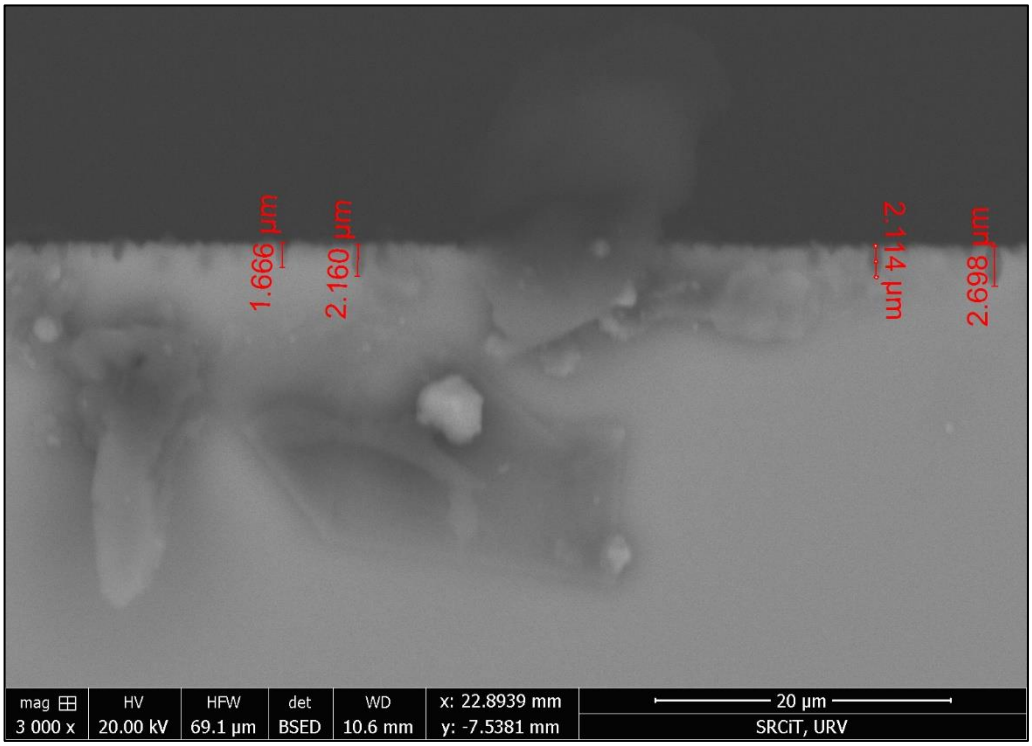

Figure 54: *SEM image of Set B / Sample 4 macropSi template. Cross-section view with measurements using BSED*

Sample 5: 1st anodization at 3 mA – 15 min
2nd anodization at 4 mA – 4 min

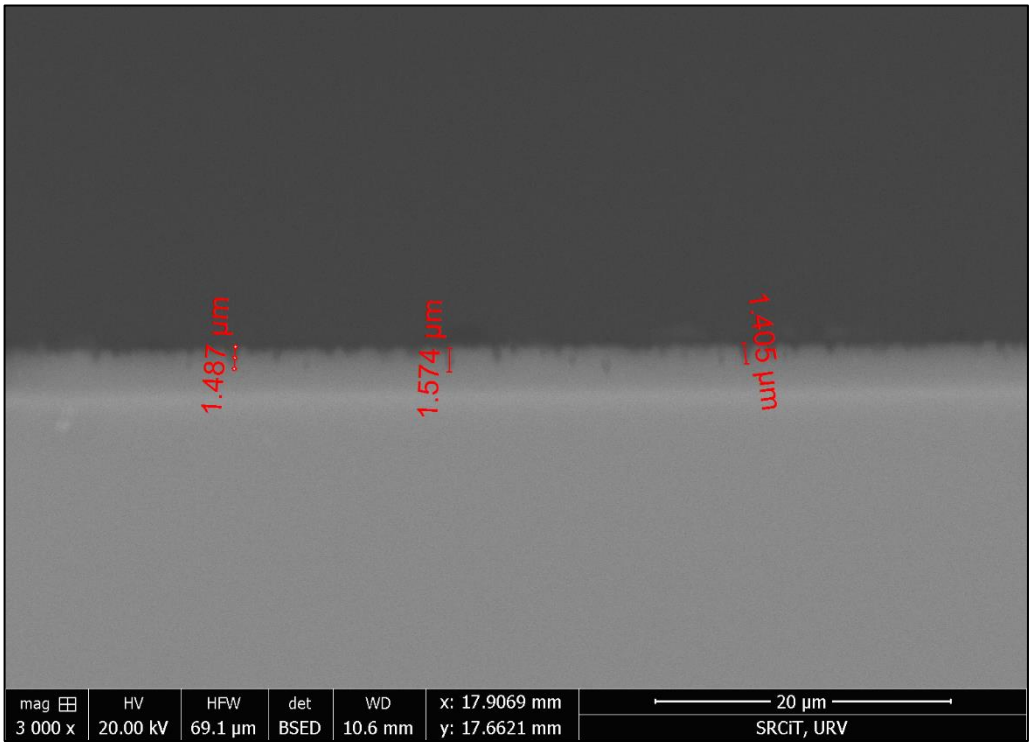

Figure 55: *SEM image of Set B / Sample 5 macropSi template. Cross-section view with measurements using BSED*

Sample 7: 1st anodization at 3 mA – 1 h

2nd anodization at 4 mA – 10 min

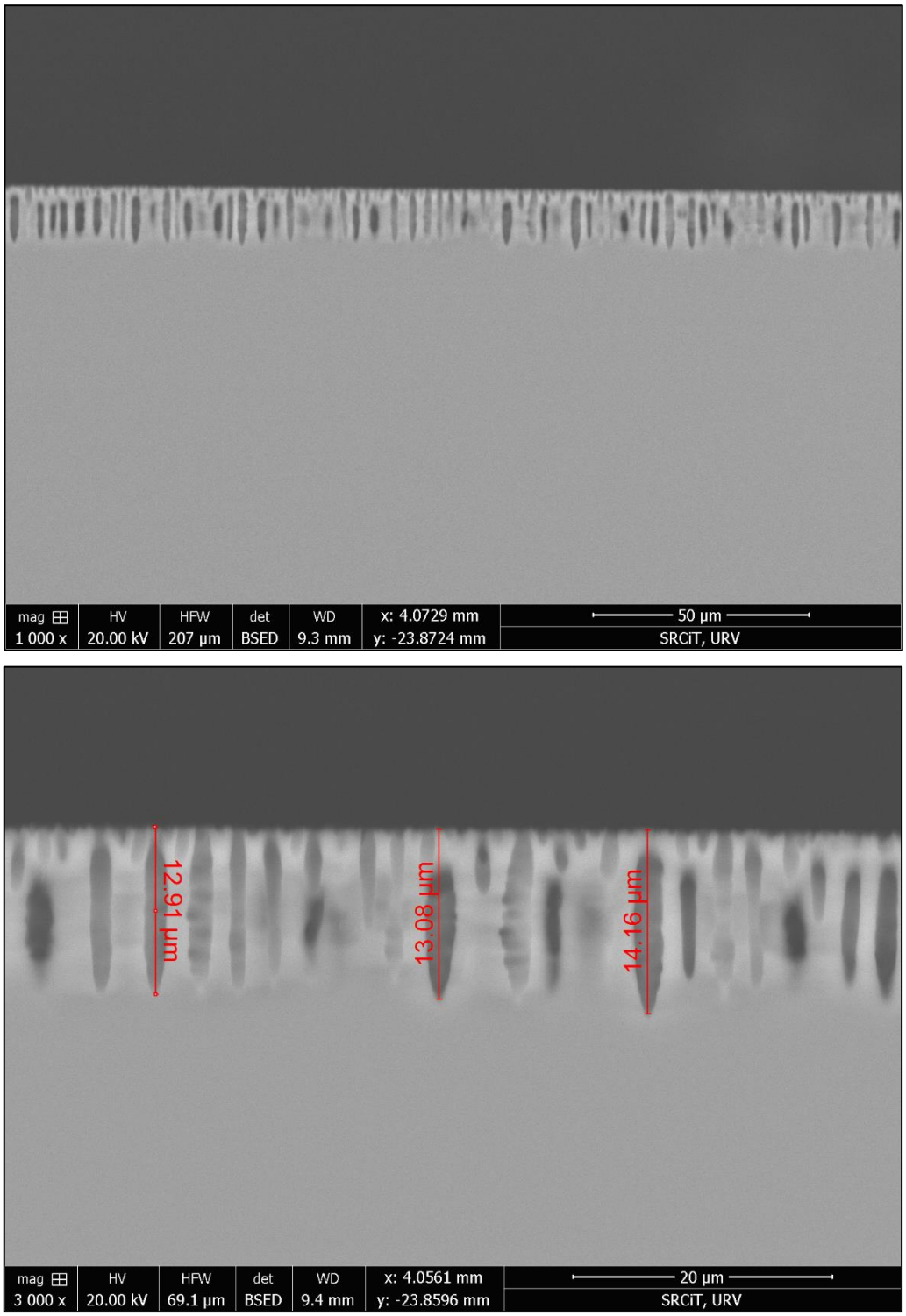

Figure 56: *SEM image of EXTRA Sample 7 macropSi template. First image, general cross-section view using BSED. Second image, close up view of the cross-section with measurements using BSED.*

SET C

Sample 1: 1st anodization at 3 mA – 45 min

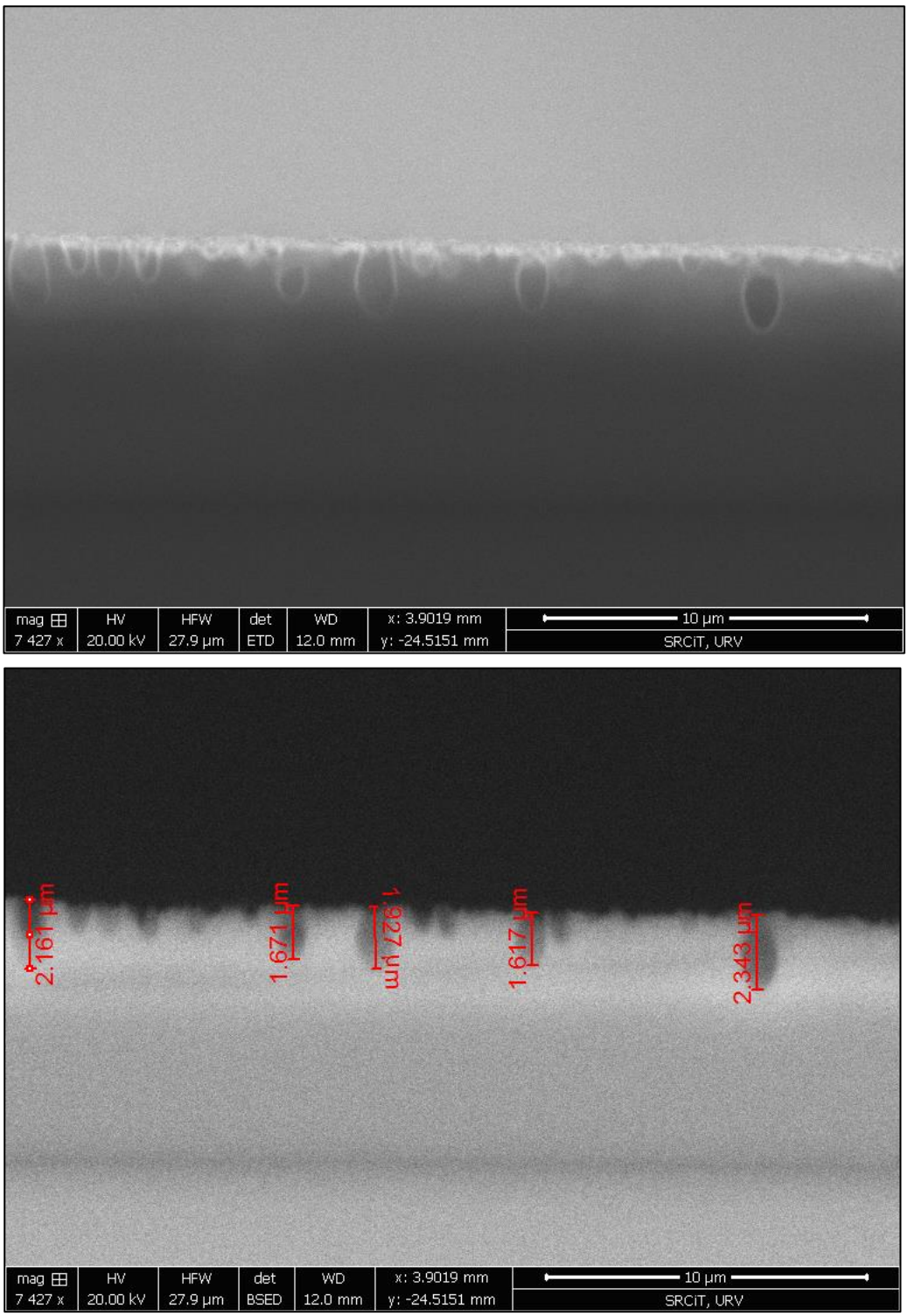

Figure 57: *SEM image of Set C / Sample 1 macropSi template. First image, general cross-section view using ETD. Second image, close up view of the cross-section with measurements using BSED.*

Sample 2: 1st anodization at 3 mA – 37 min

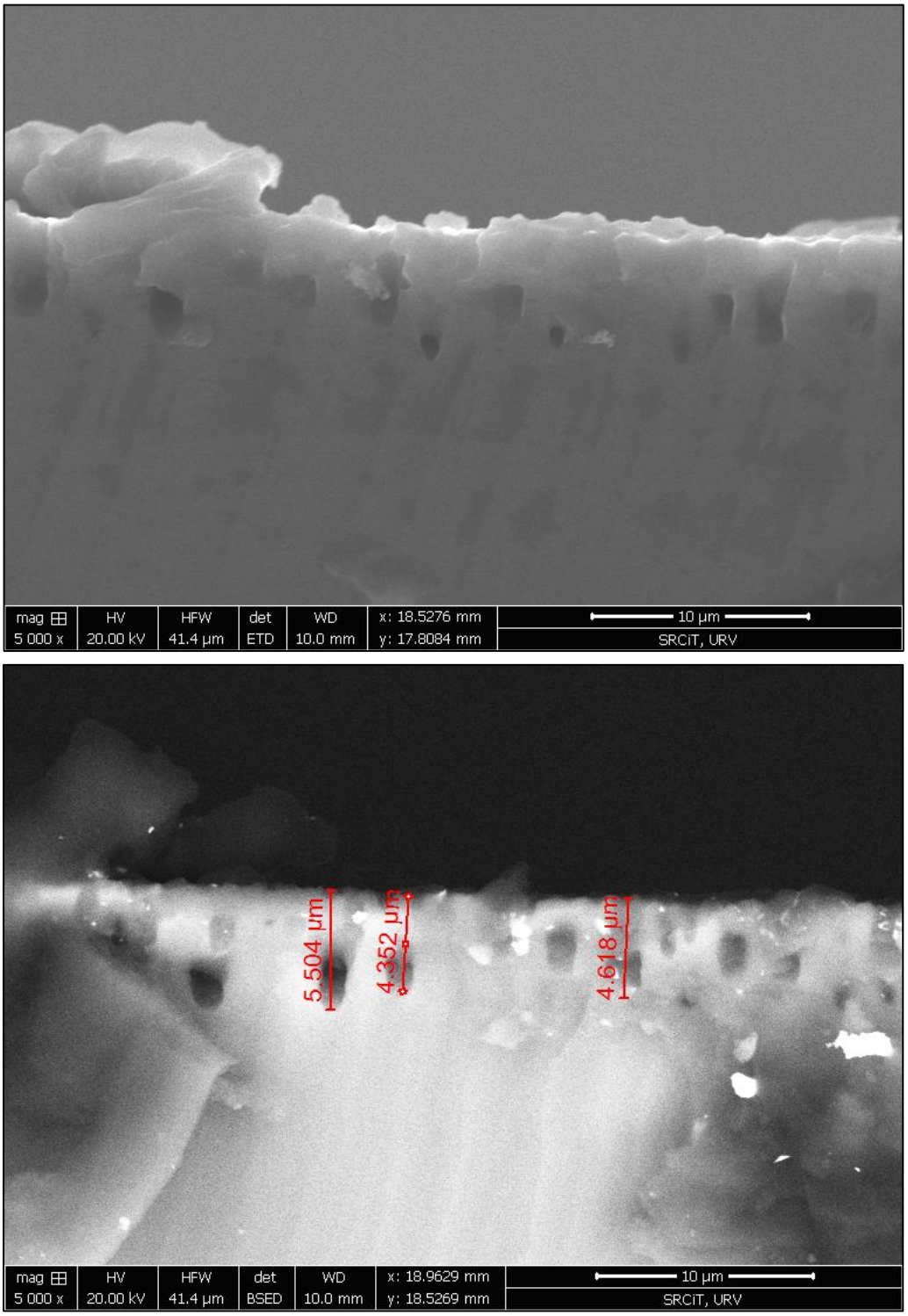

Figure 58: *SEM image of Set C / Sample 2 macropSi template. First image, general cross-section view using ETD. Second image, close up view of the cross-section with measurements using BSED.*

Sample 3: 1st anodization at 3 mA – 37 min
2nd anodization at 4 mA – 2 min

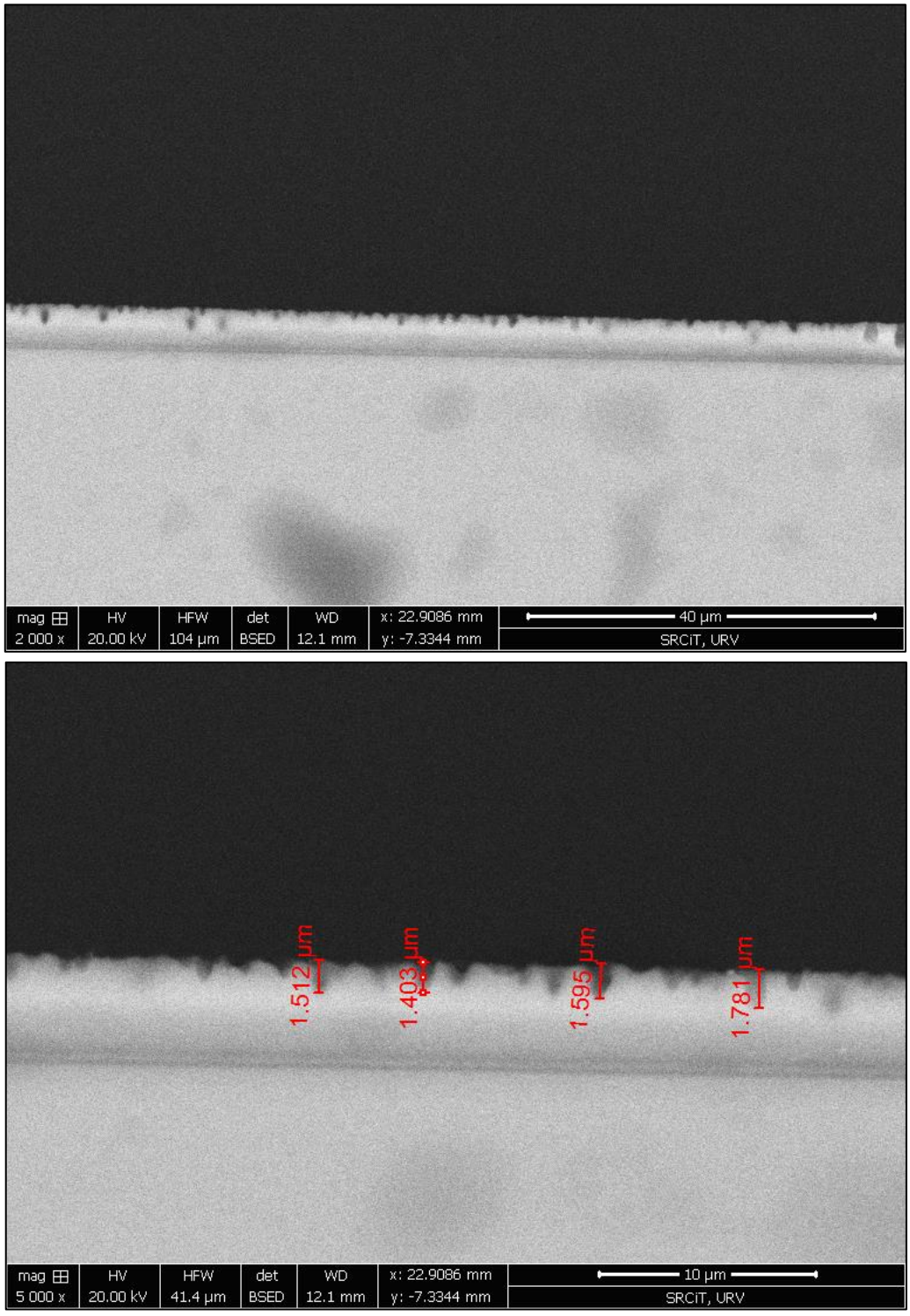

Figure 59: *SEM image of Set C / Sample 3 macropSi template. First image, general cross-section view using BSED. Second image, close up view of the cross-section with measurements using BSED.*

REPLICA RESULTS

Replica on NAA_350nm – POLYSTYRENE (Removal of Al2O2 at room Tª)

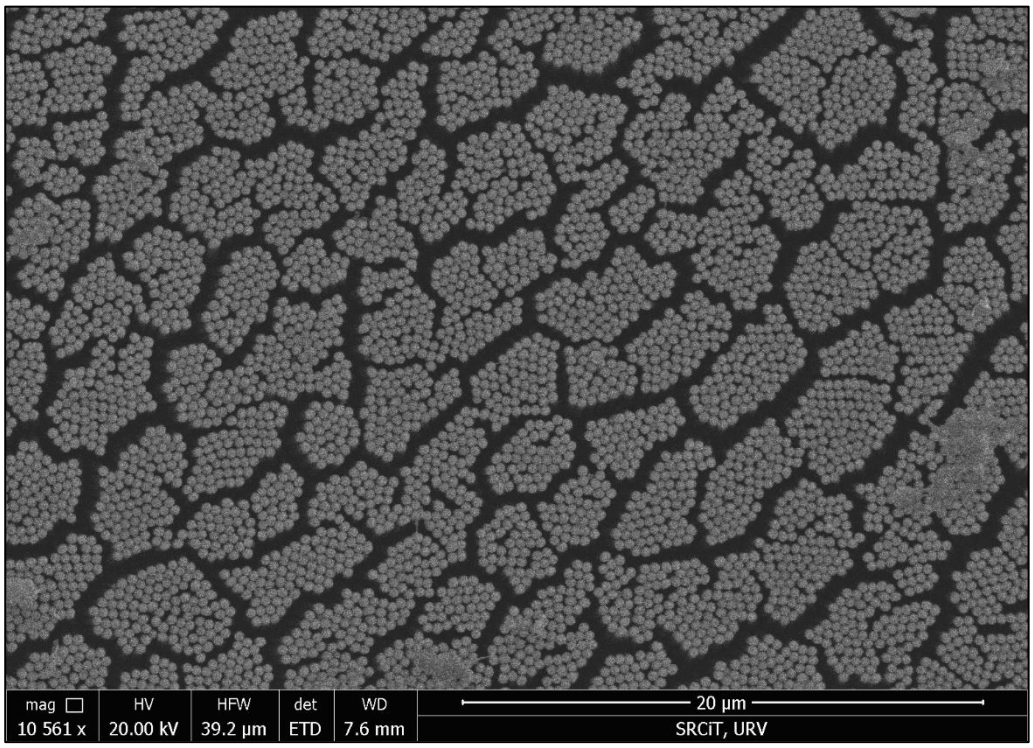

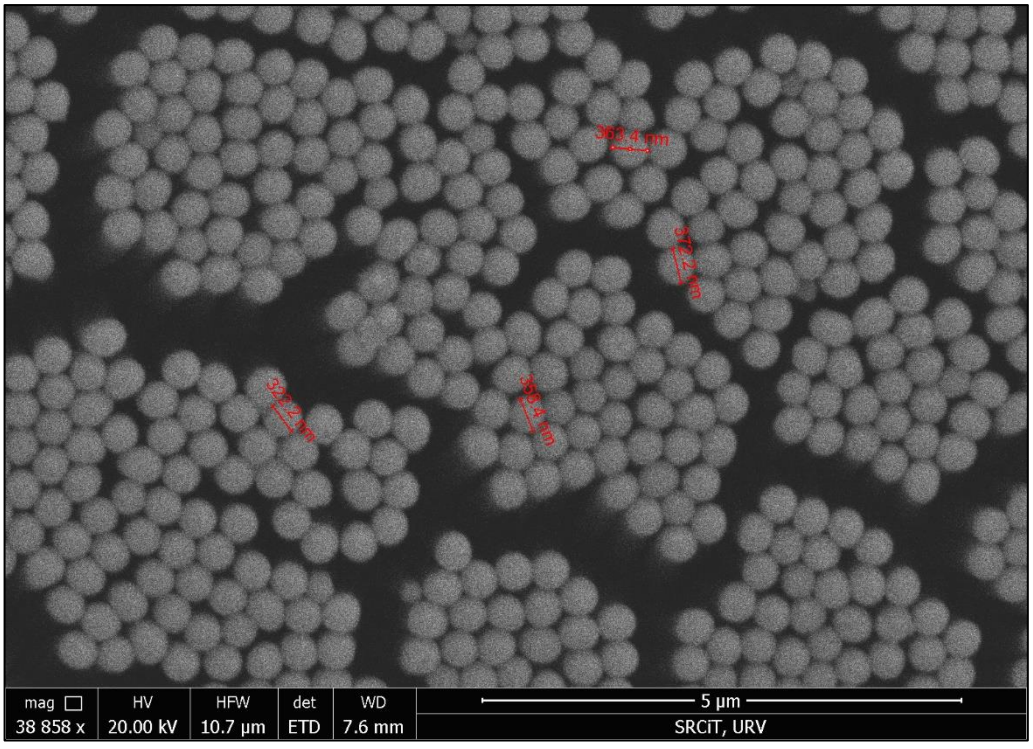

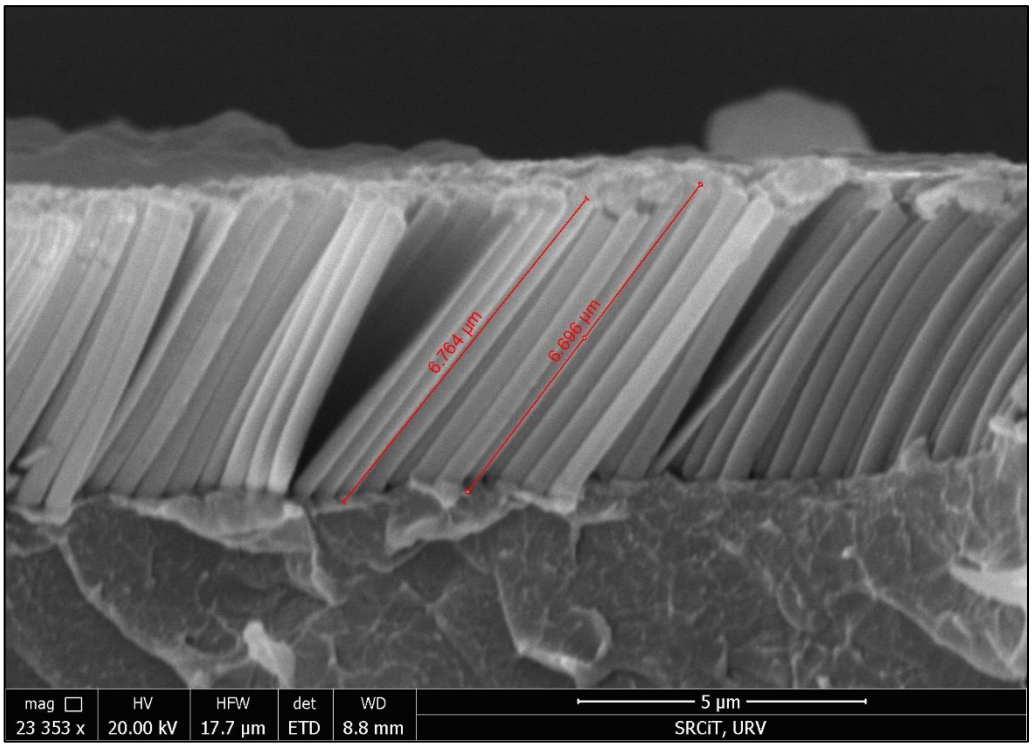

Figure 60: *SEM image of a polymeric replica made of STYRENE from NAA_7um(thickness)_350nm(size) template. First image, general top view of the microstructures using ETD. Second image, close up top view of the micropillars with measurements using ETD. Third image, close up cross-section view of the micropillars with measurements using ETD.*

Replica on NAA_250nm – POLYSTYRENE

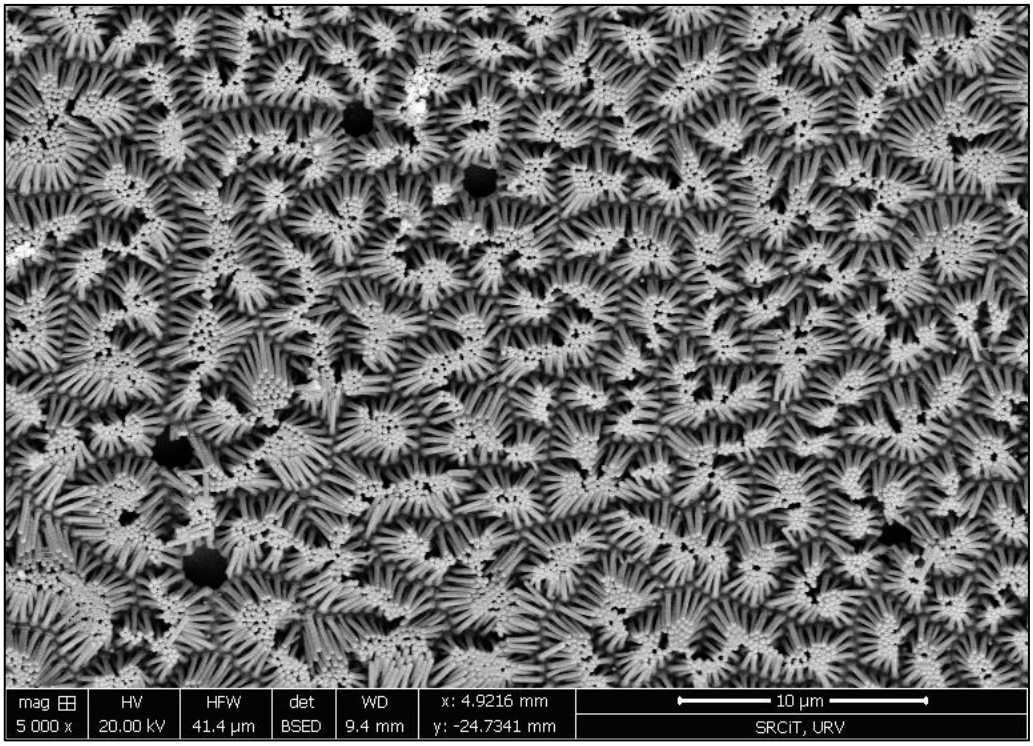

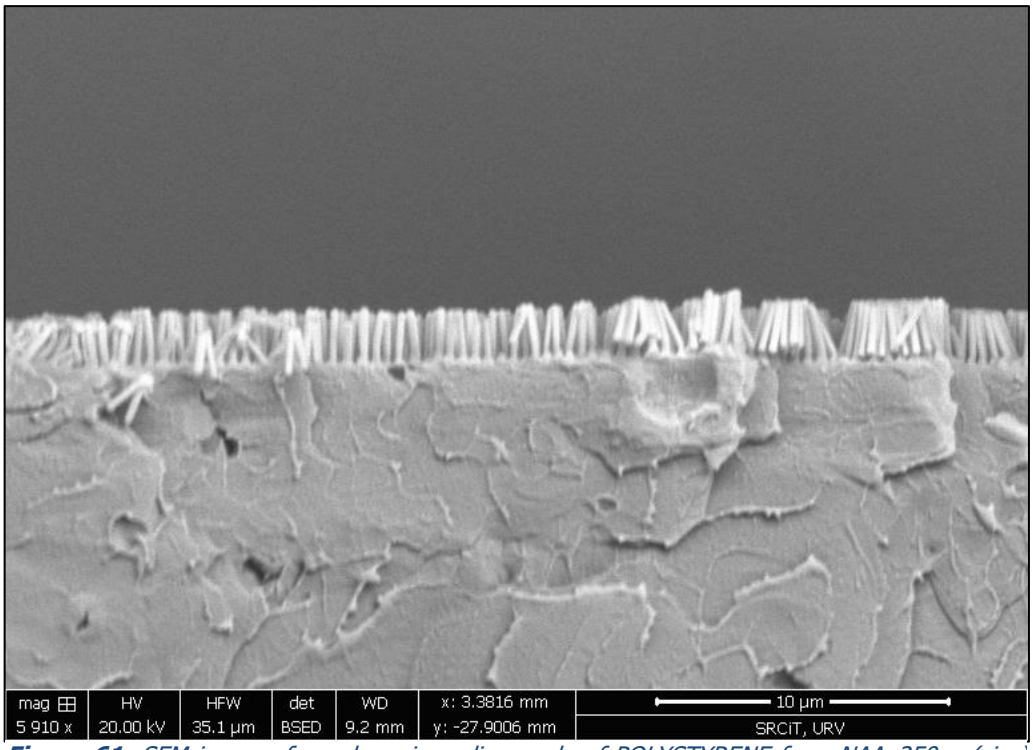

Figure 61: *SEM image of a polymeric replica made of POLYSTYRENE from NAA_250nm(size) template. First image, general top view of the micropillars array using BSED. Second image, close up cross-section view of the micropillars using BSED.*

Macroporous Si – POLYSTYRENE

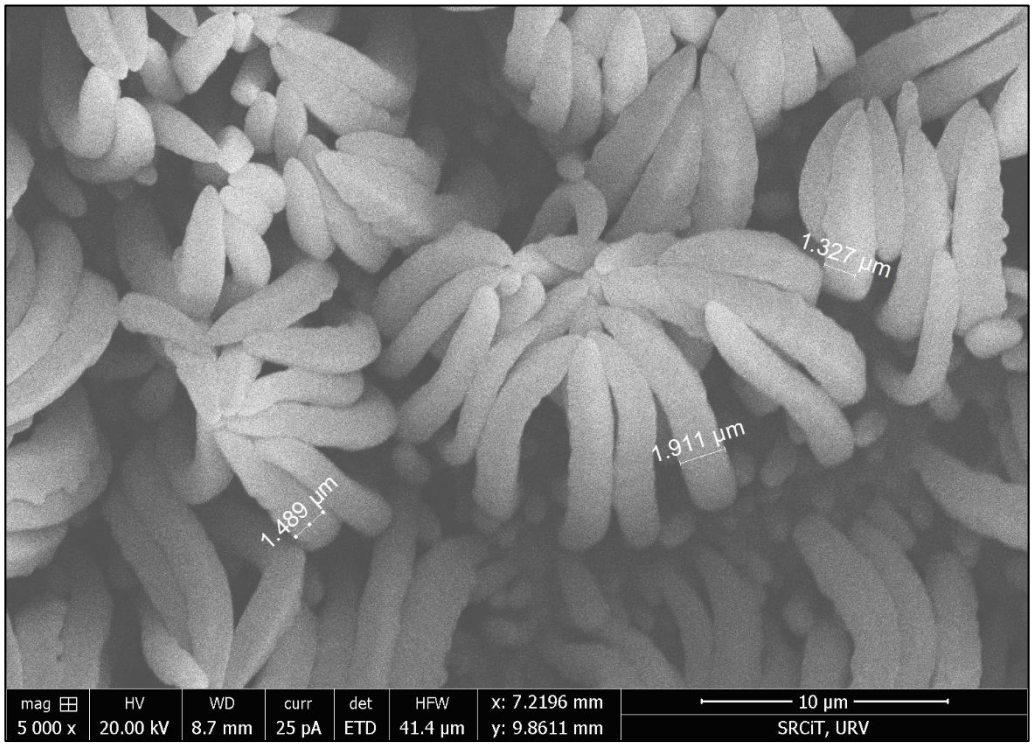

Figure 62: *SEM image of a polymeric replica made of POLYSTYRENE from macropSi template. Close up top view of the micropillars with measurements using ETD.*

Macroporous Si – POLYSTYRENE (Room T[a])

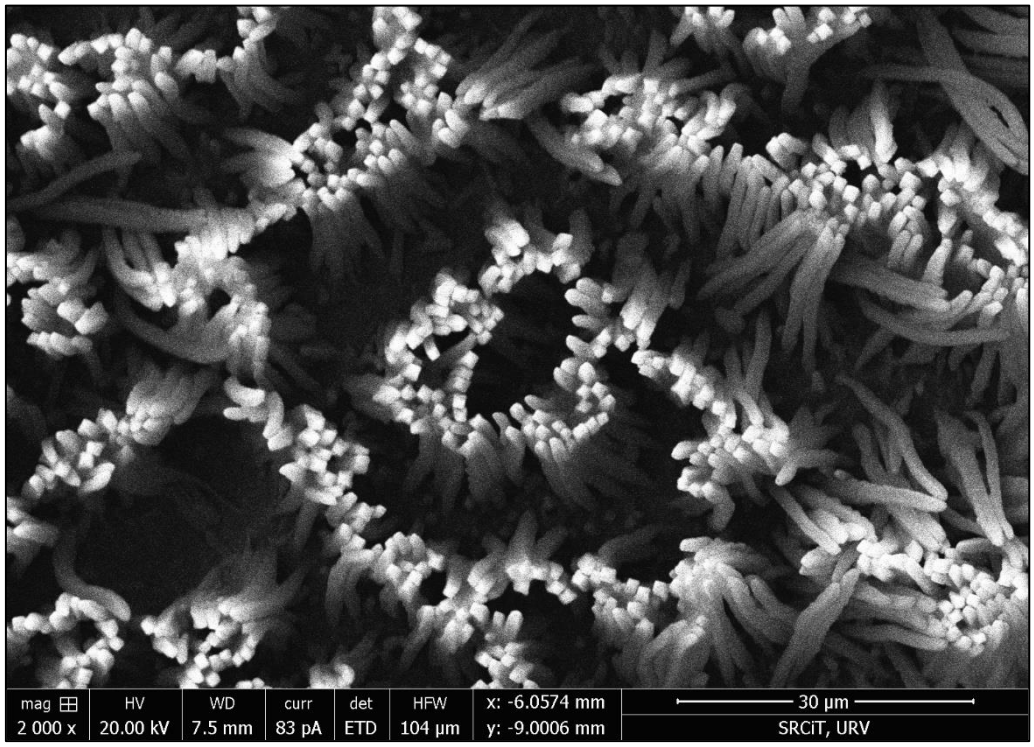

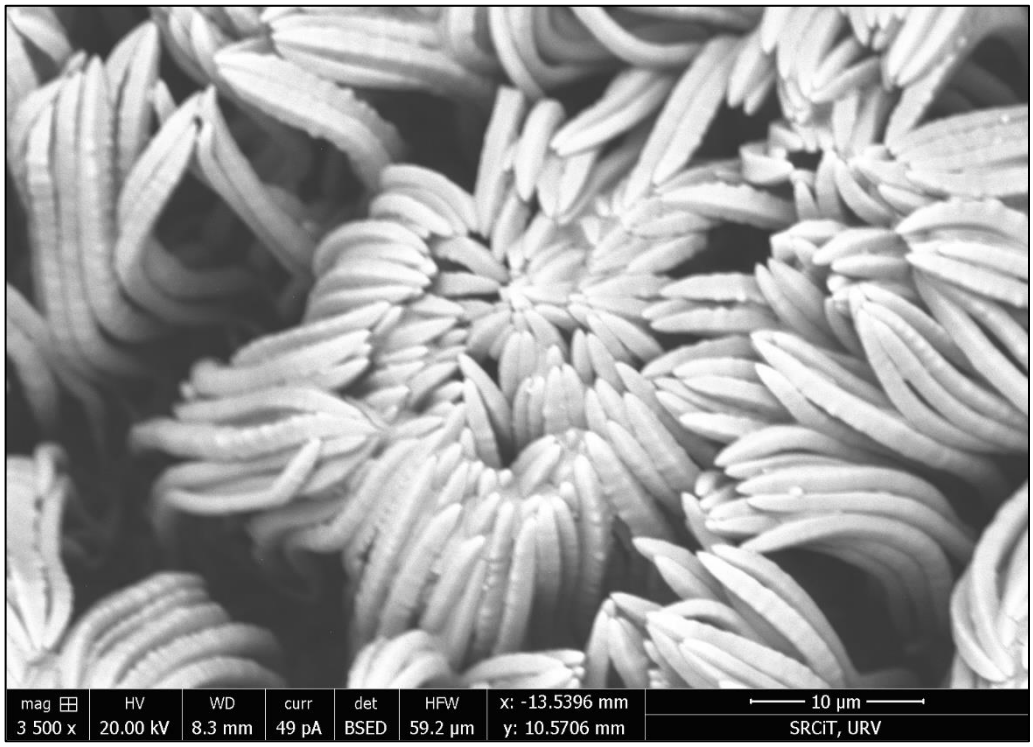

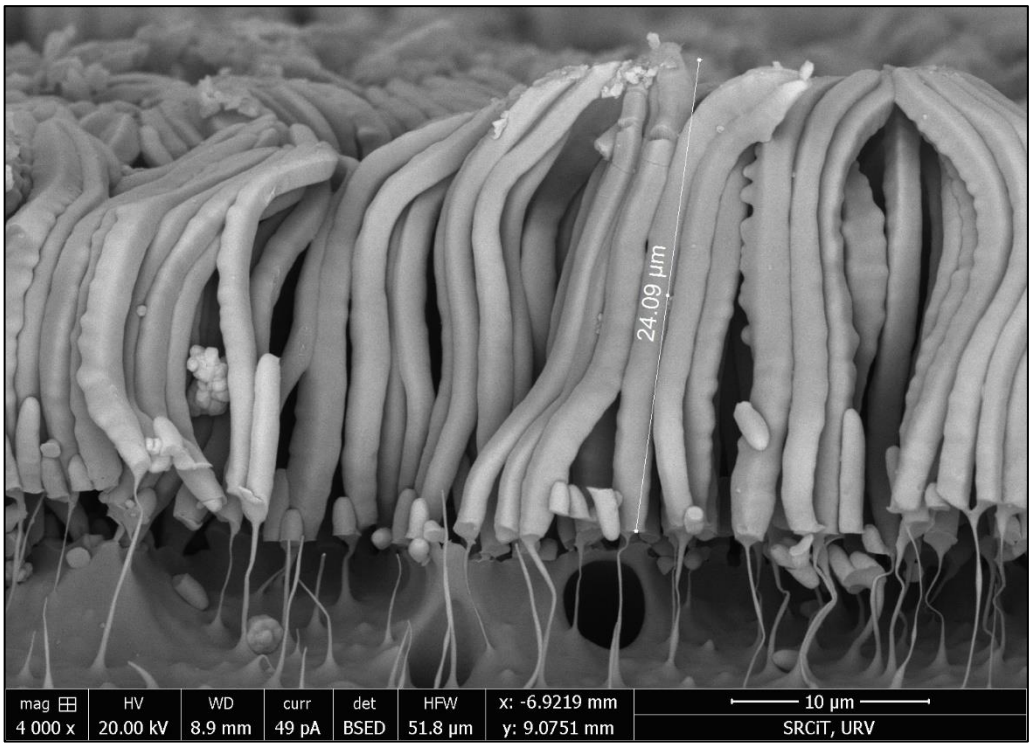

Figure 63: *SEM image of a polymeric replica made of POLYSTYRENE from macropSi template. First image, general top view of the microstructures using ETD. Second image, close up top view of the micropillars using BSED. Third image, close up cross-section view with measurements using BSED.*